ANALYSIS AND CHARACTERIZATION OF CONSUMER PRODUCTS

BY FTIR, RAMAN, CHEMOMETRICS, AND TWO DIMENSIONAL

ATR-FTIR CORRELATION SPECTROSCOPY

by

JUN ZHANG

A Dissertation submitted to the

Graduate School-New Brunswick

Rutgers, the State University of New Jersey

In partial fulfillment of the requirements

For the degree of

Doctor of Philosophy

Graduate Program in Chemistry and Chemical Biology

Written under the direction of

Professor Eugene S. Hall

And approved by

_____

_____

_____

_____

New Brunswick, New Jersey

May, 2009

ABSTRACT OF THE DISSERTATION

Analysis and Characterization of Consumer Products by FTIR, Raman,

Chemometrics, and Two Dimensional ATR-FTIR Correlation Spectroscopy

By Jun Zhang

Dissertation Director:

Dr. Gene Hall

My research focused on two projects using Fourier Transform Infrared (FTIR), Micro-Raman spectroscopy, Chemometrics (Principle Component Analysis, PCA), and two-dimensional (2D) ATR-FTIR correlation spectroscopic techniques.

Project one involves method development and validation for the simultaneous determination of dimethicone and cyclomethicone in skin protectant ointments by FTIR. A unique FTIR method that utilizes two absorbance bands (1260 cm^{-1} and 808 cm^{-1}) to determine the concentrations of dimethicone and cyclomethicone using two simultaneous equations was first time developed. The absorbances at two fixed wave numbers 1258.50 cm^{-1} and 800.00 cm^{-1} were used to calculate the concentrations of dimethicone and cyclomethicone. A series of comprehensive method validation experiments were designed and carried out. The simultaneous equation approach employed in the method was shown to be linear, accurate, precise, and specific.

Project two is to characterize fish oil supplements using ATR-FTIR, Micro-Raman, Principle Components Analysis, and 2D ATR-FTIR Correlation Spectroscopy. Most of the fish oil supplements claim active ingredient EPA and DHA on the labels, but the actual chemical forms (ethyl ester or triglyceride) are not indicated. A fast qualitative ATR-FTIR method was developed to distinguish between the ethyl ester and the

triglyceride forms of fatty acids using the carbonyl band position. Chemometrics

approach - Principal Component Analysis (PCA) was used to classify fish oil

supplements successfully by grouping the FTIR and Raman spectra. PCA was also

demonstrated as a powerful tool to screen fish oil supplements and identify the products

that may be made by the same manufacturers with the same quality, but sold with

different prices. A fish oil FTIR spectral library was also created for rapid searching and

product comparison. In addition, an ATR-FTIR standard addition method was evaluated

for quantitative analysis of active ingredients EPA and DHA esters in fish oil products.

Lastly, two-dimensional FTIR correlation spectroscopy was first time used as a new

technique to study temperature dependent spectral characteristics of fatty acids such as

EPA and DHA esters to provide further spectral information of these polyunsaturated

omega-3 fatty acids.

Acknowledgement

I would like to sincerely thank Dr. Gene Hall for having me as his student and for his continues guidance, support, kindness, and always being there for discussions and ideas during the course of my graduate research.

I would like also to thank Dr. Jing Li and Dr. Ralf Warmuth, for serving on my thesis committee and for their interest in my projects, their suggestions for my research work, and support throughout this process. Thank Dr. Ed Castner who served as a member of my proposal defense committee.

I am deeply grateful to Dr. Ken Karaisz, who is my J&J colleague and supervisor, for discussing with me on the projects and for his suggestions and continues encouragement during my graduate study and for serving on my thesis committee.

Many thanks to my J&J colleagues Dr. Jane Cai and Dr. Ming Bai for their understanding and great support during my graduate study. Special thanks to my previous J&J colleague Dr. Jian Chen for his constant encouragement.

Finally, I would like express my sincere appreciation to my husband Dr. Zhuying Wang, my daughter Betty Wang, and my son Benjamin Wang for their constant understanding and support during the past years when I spent countless family time (weekends and nights) on my graduate study.

Table of Contents

List of Tables

List of Illustrations

xiii

xiv

Chapter 1: Analytical Techniques Overview

1.1 Fourier Transform Infrared (FTIR) Spectroscopy

1.1.1 Theory of Infrared Absorption

Infrared spectroscopy utilizes the fact that molecules have specific frequencies at which they rotate or vibrate corresponding to discrete energy levels (vibrational modes). The far-infrared, approximately 400-10 cm^{-1}, has low energy and may be used for rotational spectroscopy. The mid-infrared, the region of most interest for chemical analysis, which corresponds to changes in vibrational energies within molecules approximately 4000-400 cm^{-1} may be used to study the fundamental vibrations and associated rotational-vibrational structure. The higher energy near-IR, approximately 13300-4000 cm^{-1}, can excite overtone or harmonic vibrations. Figure 1-1 shows an energy level diagram of the transitions that are responsible for IR absorption.
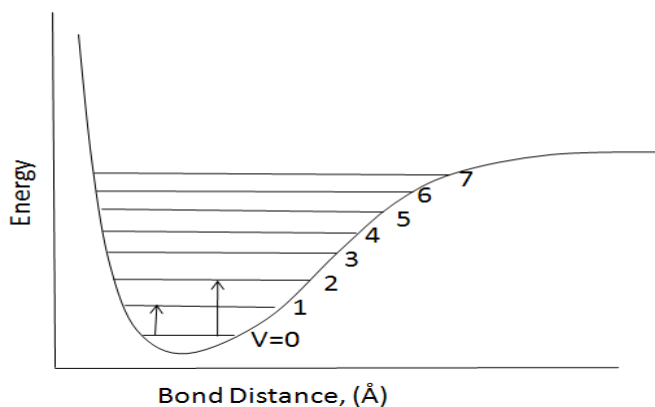
Figure 1-1   Vibrational energy diagram (Morse potential energy surface)

These specific resonant frequencies are determined by the shape of the molecular potential energy surface, the masses of the atoms and, eventually by the associated vibration coupling. In order for a vibrational mode in a molecule to be IR active, it must

be associated with changes in the permanent dipole moment. Equation (1-1) shows that the dipole moment μ is related to the bond distance r, and Equation (1-2) shows that the IR energy transition probability R is related to a change in dipole moment ($\partial\mu/\partial r$).

$$\mu = \mu_o + (r - r_e)(\frac{\partial\mu}{\partial r})_o + \frac{1}{2}(r - r_e)^2(\frac{\partial^2\mu}{\partial^2 r})_o + ... \qquad (1\text{-}1)$$

$$R = \int \Psi_i [\ \mu_0 + (r\text{-}r_e)\ (\partial\mu/\partial r)_0\ ]\ \Psi_i\, d\tau \qquad (1\text{-}2)$$

The number of predicted vibrational modes in a molecule with N atoms can be determined by 3N-6 for non-linear molecules and 3N-5 for linear molecules. Under experimental conditions, the number of observed absorption bands will be more or less and will depend on the instrumentation and the physical properties of the molecule and its state of matter. Simple diatomic molecules have only one bond, which may stretch. More complex molecules have many bonds, and vibrations can be conjugated, leading to infrared absorptions at characteristic frequencies that may be related to chemical groups. For example, the atoms in a CH_2 group, commonly found in organic compounds can vibrate in six different ways: symmetrical and antisymmetrical stretching, scissoring, rocking, wagging and twisting as shown in Figure 1-2.
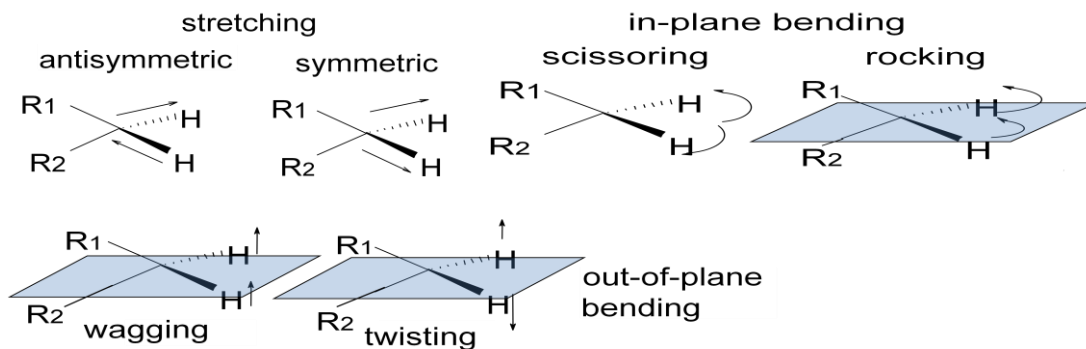
Figure 1-2   Six different vibrations of CH_2 group

The infrared spectrum of a sample is collected by passing a beam of infrared light through the sample. Examination of the transmitted light reveals how much energy was absorbed at each wavelength. Analysis of these absorption characteristics reveals details about the molecular structure of the sample. This technique works almost exclusively on samples with covalent bonds. Simple spectra are obtained from samples with few IR active bonds and high levels of purity. More complex molecular structures lead to more absorption bands and more complex spectra. Thus, IR spectroscopy is an important and popular tool for structural elucidation and compound identification.

1.1.2   Development of FTIR

The development of FTIR would have been impossible without the use of the Michelson interferometer (The instrument used to interfere the waves together is called an interferometer) which was invented by Albert Abraham Michelson in 1880 [1]. Unfortunately, the time consuming calculation needed to convert an interferogram into a spectrum made the usage of an interferometer to obtain spectra impractical. The invention of computers and advances in how computers perform mathematical operations made Fourier transform IR a reality. The major advance in this area was made by J.W.Cooley and J.W. Tukey, who invented Fast Fourier Transform (FFT, Cooley-Tukey Algorithm)[2-3]. This algorithm quickly performs Fourier transforms on a computer and the marriage of the FFT algorithm and minicomputers was the breakthrough that made FTIR possible.

The first commercially available FTIRs were manufactured by Digilab, a company of Block Engineering in Cambridge, Massachusetts in 1960s [4]. These instruments made feasible acquiring high resolution data in a short period of times, and

established the advantages of FTIR over previous means of obtaining IR spectra. Since the 1960s many other companies have begun manufacturing and selling FTIRs in United States. Nicolet Instruments was introduced in mid-1970, and quickly became one of the largest FTIR manufactures. Perkin-Elmer FTIR instrumentation was introduced to market in the early 1980s, and these FTIRs were amongst the first to be used in quality control labs due to their low cost, and opened up a whole new market for FTIR.

The advantages of FTIR quickly gave rise to adaptation of attenuated total reflectance (ATR) [5] and diffuse reflectance (DRIFTS) [6] for the rapid and reproducibility analysis of liquids and solids. A major advance in the kinds of samples that can be analyzed by FTIR occurred with the introduction of the FTIR microscopy in the early 1980s[7]. This allows the IR spectra of the samples as small as 10 microns in diameter to be obtained.

The current status of FTIR technology is very exciting. A new GC-FTIR interface using cryogenic trapping[8] has pushed the minimum amount of material an FTIR can detect to less than 100 picograms. Development of dynamic alignment and step scanning interferometers allow microsecond kinetic studies, photoacoustic depth profiling, and two-dimensional IR spectroscopy to be performed. Finally, the number of applications of the more established techniques is constantly growing, making FTIR more and more useful.

1.1.3 Sampling and Instrumentation

Infrared spectra can be obtained by different sampling techniques. Liquid samples can be sandwiched between two plates of a high purity salt (commonly sodium chloride, sometime other salts such as potassium bromide or calcium fluoride are also

used). The plates are transparent to the infrared light and will not introduce any

interference onto the spectra. Some salt plates are soluble in water, and so the sample

and washing reagents must be anhydrous (without water). For solid samples, the

common way is to grind a quantity of the sample with a purified salt (usually potassium

bromide) finely. This powder mixture is then crushed in a mechanical die press to form a

translucent pellet through which the beam of the spectrometer can pass. Gaseous samples

require little preparation beyond purification, but a sample cell with a long path length

(typically 5-10 cm) is normally needed, as gases show relatively weak absorbances.

Spectra obtained from different sample preparation methods will look slightly different

from each other due to the different physical states the sample is in.

Figure 1-3 shows a typical FTIR spectrometer. It consists of a source,

Interferometer (beamsplitter and two mirrors), sample compartment, and a detector. The

IR light is guided through an Interferometer. After passing through the sample, where

some energy is absorbed and some is transmitted. The transmitted portion reaches the

detector, which records the total intensity. The measured signal is the interferogram.

This signal is digitized and processed using a computer by performing a mathematical

Fourier Transform on this signal results in a spectrum. The final spectrum can be

presented as transmittance (%T) or absorbance, the computer easily performs this

conversion.

Source   Interferometer   Sample   Detector   Computer
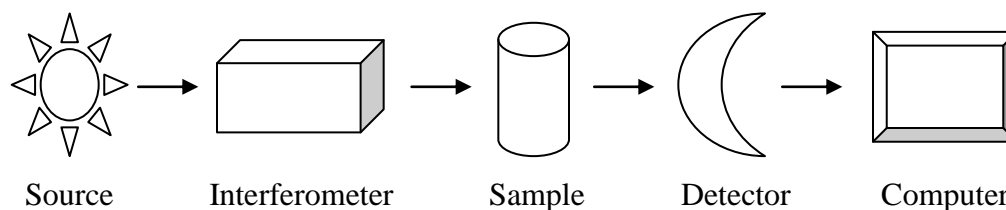
Figure 1-3   Diagram of a typical FTIR instrumentation

Another commonly used sampling technique is attenuated total reflectance (ATR) where solid and liquid samples can be analyzed without sample preparation. In ATR, the IR beam contacts the sample by a diamond or other crystal (germanium, etc.) with a high index of refraction and penetrates the sample a few microns depending on the refractive index of the sample. The depth of penetration (d_p) can be determined using the following equation (1-3):

$$d_p = \frac{\lambda}{2\pi n_p (\sin^2 \theta - n_{sp}^2)^{1/2}} \qquad (1-3)$$

where n_{sp} and n_p are the ratio of the refractive indices of the sample vs the support and the support respectively. Theta is the angle of incidence and λ is the wavelength. For ZnSe and a polymer sample, depth is 2.0 mm at 1,000 cm^{-1}.

ATR uses a property of total internal reflection called the evanescent wave. A beam of infrared light is passed through the ATR crystal in such a way that it reflects at least once off the internal surface in contact with the sample. This reflection forms the evanescent wave which extends into the sample. The beam is then collected by a detector as it exits the crystal. Figure 1-4 shows how the infrared beam interacted with the ATR and sample.

IR instruments are now small, and can be transported, even for use in field trials. With increasing technology in computer filtering and manipulation of the results, samples in solution can now be measured accurately (water produces a broad absorbance across the range of interest, and thus renders the spectra unreadable without this computer treatment). Some instruments will also automatically tell you what substance is being measured from a database of thousands of reference spectra.
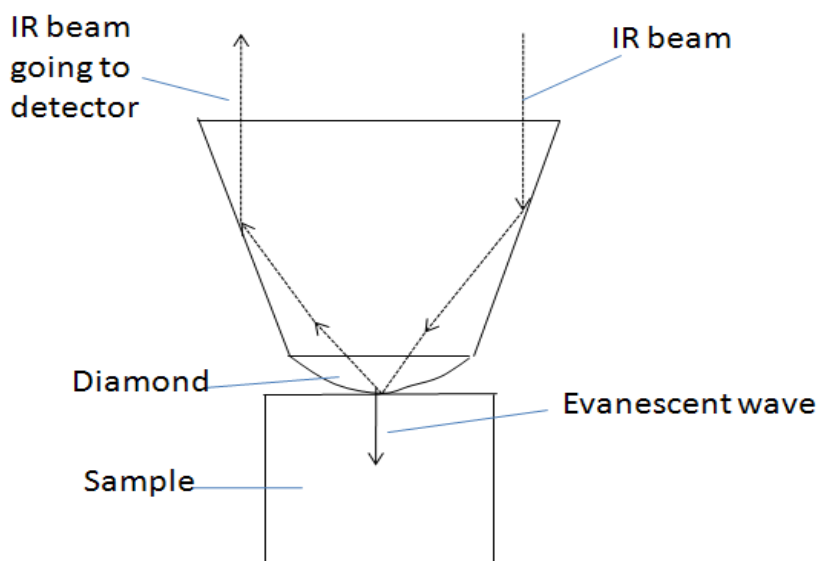
Figure 1-4   IR beam interaction with ATR and sample

1.1.4 Application of FTIR

Infrared spectroscopy is widely used in both academic research and industry as a simple and reliable technique for measurement, quality control and dynamic analysis. It has been highly successful for applications in both organic and inorganic chemistry. Infrared spectroscopy has been utilized in various fields such as:

- Forensic analysis[9-10] including analyzing textile fibers, paint chips, dye, rubber, drugs, photocopy and laser printer toners , etc. in forensic samples.

- Biological sample analysis[11-12] such as study of structures of biological tissues, plant, human skin, and blood cell, etc., and protein structure analysis[13].

- Polymer properties, structures, characterization, film and material studies, etc.[14-15]

- Lubricants analysis[16] and Semiconductor[19] such as silicon, aluminum arsenide, etc.

- Food analysis[17-18] such as edible oils, fruit juices, and meat, etc. studies.

1.2   Two-Dimentional Infrared (2D-IR) Spectroscopy

1.2.1   Introduction of Generalized 2D Correlation Spectroscopy

The success of 2D NMR motivated the desire to extend this powerful concept into other optical spectroscopy applications. However, it was very difficult to implement the experimental approach based on multiple pulses in optical wavelengths, which has been so successfully employed in 2D NMR using radio frequency excitations. The characteristic time scale of molecular vibration observed in IR absorption spectroscopy is on the order of picosecond, compared to the micro to millisecond ranges usually encountered in NMR. Nowadays, it has become possible to conduct certain experiments based on ultrafast femosecond optical pulse in a fashion analogous to pulse-based 2D NMR experiments. However, optical 2D spectroscopy using a conventional commercial spectrometer might not be quite feasible if one is forced to employ the same approach used in NMR.

A conceptual breakthrough in the development of practical optical 2D spectroscopy was first proposed by Noda in 1986[20 - 22]. Later the concept evolved into the so-called generalized 2D correlation spectroscopy that has become a powerful tool for the detailed analysis of various spectral data[23]. The 2D experiments in optical spectroscopy can be carried out with a conventional spectrometer by introducing a relatively slow external perturbation applied to the system of interest. When a certain perturbation (such as temperature, pressure, concentration, stress, electrical field, etc) is applied to a sample, various chemical constituents of the system are selectively excited or transformed. The perturbation-induced changes, such as excitation and subsequent relaxation toward the equilibrium, can be monitored with electromagnetic probes such as

an IR beam or laser (Raman) to generate so-called dynamic spectra. The intensity

changes, band shifts, and changes in the band shapes are typical spectral variations

observed under external perturbation. In a typical 2D experiment, a series of

perturbation-induced dynamic spectra are collected in some sequential order. Such a set

of spectra may be readily manipulated mathematically, with the use of a simple scheme

of correlation analysis, to yield desired 2D correlation spectra[24 - 25]. Figure 1-5 shows the

basic scheme for a 2D correlation experiment based on external perturbation.

External Perturbation
Such as thermal, chemical, optical, electrical, etc.

Electro-magnetic
Probe (IR, Raman,
UV, etc) → System → Dynamic spectra → Correlation analysis → 2D correlation spectra
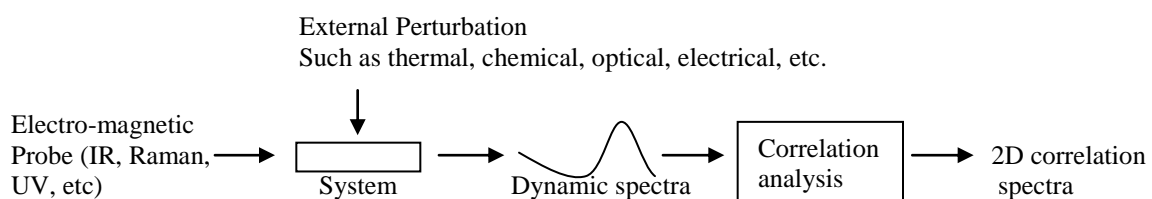
Figure 1-5   Basic diagram for a 2D correlation experiment

1.2.2   *Generalized 2D Correlation Analysis*

2D correlation is nothing but a quantitative comparison of spectral intensity

variations observed at two different spectral variables over some fixed perturbation

interval. To construct generalized 2D correlation spectra, a set of dynamic spectra must

be calculated first. Then, two kinds of correlation spectra, namely synchronous and

asynchronous spectra, are generated from the dynamic spectra. Detailed mathematical

procedure to generate 2D correlation spectra was provided in references 23 and 26. Only

essence of the procedure is described here.

For a spectral intensity variation $y(v, t)$ observed as a function of a spectral

variable v during an interval of some additional variable t between T_{min} and T_{max}, the

dynamic spectrum $\tilde{y}(v, t)$ is defined as:

$$\tilde{y}(v, t) = \begin{cases} y(v, t) - \check{y}(v) & \text{for } T_{min} \leq t \leq T_{max} \\ 0 & \text{otherwise} \end{cases} \quad (1\text{-}4)$$

where $\check{y}$ is the reference spectrum of the system. The selection of a reference spectrum is

not strict, but in most of cases, $\check{y}(v)$ is the averaged spectrum defined by the following

equation:

$$\check{y}(v) = \frac{1}{T_{max} - T_{min}} \int_{Tmin}^{Tmax} y(v, t)\, dt \quad (1\text{-}5)$$

A formal definition of the generalized 2D correlation spectrum $X(v_1, v_2)$ is given by:

$$X(v_1, v_2) = \Phi(v_1, v_2) + i\Psi(v_1, v_2) = \frac{1}{\pi(Tmax - Tmin)} \int_0^\infty \hat{Y}1(\omega).\hat{Y}2(\omega)d\omega \quad (1\text{-}6)$$

where the two orthogonal components $\Phi(v_1, v_2)$ and $\Psi(v_1, v_2)$ are the synchronous and

asynchronous 2D correlation intensity, respectively. The synchronous 2D correlation

intensity $\Phi(v_1, v_2)$ represents the overall similarity between two separate spectral intensity

variations measured at different spectral variables when an external perturbation is

applied. The asynchronous 2D correlation intensity $\Psi(v_1, v_2)$, on the other hand, is

regarded as a measure of dissimilarity of the spectral intensity variations. The term

$\hat{Y}_1(\omega)$ is the Fourier transform of the spectral intensity $\tilde{y}(v_1, t)$ observed at some spectral

variable v_1 and likewise, $\hat{Y}_2(\omega)$ is the Fourier transform of the spectral intensity $\tilde{y}(v_2, t)$

observed at some spectral variable v_2.
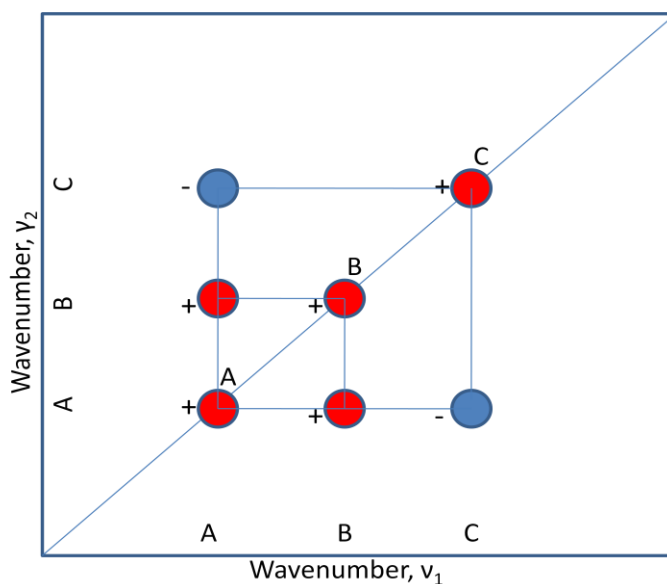
Figure 1-6   Contour map of a synchronous 2D correlation spectrum

Figure 1-6 shows a diagram example of a synchronous 2D correlation spectrum plotted as a contour map. A synchronous spectrum is a symmetric spectrum with respect to a diagonal line corresponding to coordinates $v_1 = v_2$. Correlation peaks show at both diagonal and off-diagonal positions. The intensity of peaks located at diagonal positions corresponds mathematically to the autocorrelation function of spectral intensity variations observed during a perturbation interval. The diagonal peaks are then referred to as *autopeaks*. The magnitude of an autopeak intensity, which is always positive (marked in red color), represents the overall extent of spectral intensity variation. Any regions of a spectrum which change intensity to a great level under a given perturbation will show strong autopeaks, while those remaining near constant develop few or no autopeaks. In the example spectrum shown in Figure 1-6, there are three positive (red color) autopeaks located at the coordinates A, B, and C.

Cross peaks located at the off-diagonal positions of a synchronous 2D spectrum

represent concurrent or coincidental changes of spectral intensities observed at two

different spectral variables, v_1 and v_2. Such a synchronized change suggests the

possible existence of a coupled or related origin of the spectral intensity variations.

While the sign of autopeaks is always positive, the sign of cross peaks can be either

positive (in red color) or negative (in blue color). The sign of synchronous cross peaks

becomes positive if the spectral intensities at the two spectral variables corresponding to

the coordinates of the cross peak are either increasing or decreasing together as functions

of the external variable during the observation interval. On the other hand, a negative

sign of cross peaks indicates that one of the spectral intensities is increasing while the

other is decreasing. In the example spectrum Figure 1-6, the sign of cross peaks at

coordinates A and B is positive, indicating that the spectral intensities at both bands A

and B increase (or decrease) together. The sign of cross peaks at coordinates A and C is

negative, indicating that intensity at one band is increasing while the other one is

decreasing.
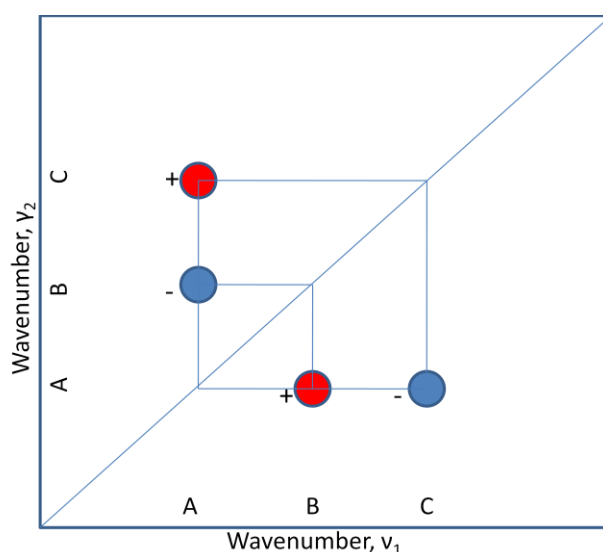
Figure 1-7   Contour map of an asynchronous 2D correlation spectrum

Figure 1-7 shows an example of an asynchronous 2D correlation spectrum. The intensity of an asynchronous spectrum represents sequential, or successive, changes of spectral intensities measured at v_1 and v_2. Unlike a synchronous spectrum, the asynchronous spectrum has no autopeaks, consisting solely of cross peaks located at off-diagonal positions. In Figure 1-7, asynchronous correlation is observed for band pairs A and B (positive), A and C (negative). From the cross peaks, it is possible to draw two asynchronous correlation squares.

An asynchronous cross peak develops only if the intensities of two bands change out of phase (i.e., delayed or accelerated) with each other. This feature is particularly useful in differentiating overlapped bands arising from spectral signals of different origins. For example, different spectral intensity contributions from individual components of a mixture, chemical functional groups experiencing different effects from some external perturbation. Even if bands are located close to each other at some cases, as long as the pattern of sequential variations of spectral intensities are substantially different, asynchronous cross peaks will develop between their spectral coordinates. The sign of asynchronous cross peaks can be either negative (in blue color) or positive (in red color). The sign of an asynchronous cross peak becomes positive if the intensity change at v_1 occurs predominantly before v_2 in the sequential order of t. It becomes negative if the change occurs after v_2. This rule, however, is reversed if $\Phi(v_1, v_2) < 0$. The example spectrum in Figure 1-7 indicates that the intensity changes (either increase or decrease) at band A occurs after the changes at band B, and the intensity changes at band A occurs before the intensity changes at band C (since the synchronous correlation between bands A and C is negative, i.e. $\Phi(v_1, v_2) < 0$) .

It is obvious that the 2D correlation spectrum consists of much sharper and better resolved peaks than the corresponding 1D spectrum. The enhancement of resolution is a direct outcome of spreading highly overlapped peaks along the second dimension. The appearance of positive and negative cross peaks located at the off-diagonal positions of a 2D spectrum indicates various forms of correlation features among spectral bands. Correlation among bands that belong to, for instance, the same chemical group, or groups interacting strongly, can be well investigated by 2D spectra.

1.2.3   Applications of 2D Correlation Spectroscopy

Nowadays, 2D correlation spectroscopy is used in various field including analytical and physical chemistry, material, biological, medical, food and agriculture science and technology, and chemical industries. The technique is establishing itself as a powerful general tool for the analysis of spectroscopic data. It is applied to investigations of inter and intramolecular interactions[27-30], denaturation of protein[31-32], melting behavior of polymers[33], chemical reactions[34-35], electrochemistry[36], adsorption[37], photochemistry[38], rheology[39], and many more[40].

1.3   Raman Spectroscopy

1.3.1   Theory of Raman Spectroscopy

Raman spectroscopy is a spectroscopic technique based on inelastic scattering of monochromatic light, usually from a laser source. Inelastic scattering means that the frequency of photos in monochromatic light changes upon interaction with sample. Photos of the laser light are absorbed by the sample and then reemitted. Frequency of the reemitted photons is shifted up or down in comparison with the original monochromatic

frequency, which is called the Raman effect. For the spontaneous Raman effect, the molecule will be excited from the ground state to a virtual energy state, and relax into a vibrational excited state, which generates Stokes Raman scattering. If the molecule was already in an elevated vibrational energy state, the Raman scattering is then called anti-Stokes Raman scattering. Rayleigh scattering corresponds to the photons scattered at the frequency of the initial radiation, whereas the Raman radiation is shifted in frequency from the frequency of the incident radiation by the vibrational energy that is gained or lost in the molecule. Figure 1-8 shows the energy level diagram of how Raman scattering produces Raman spectra.
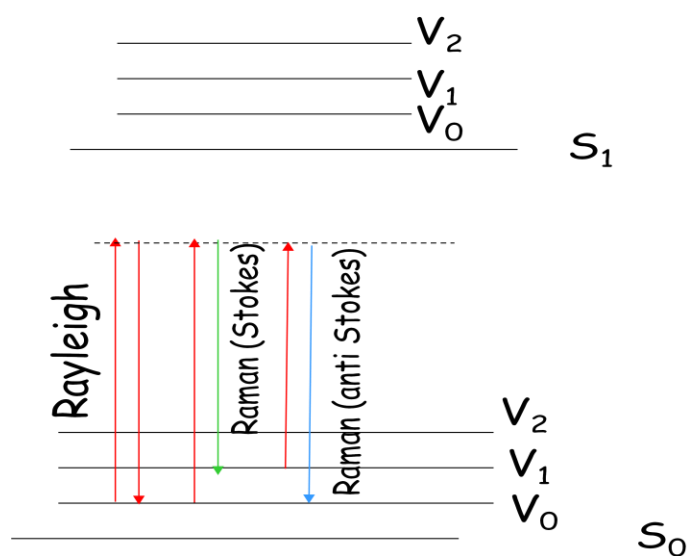
Figure 1-8   Energy level diagram showing the states involved in Raman signal

If a molecule is placed in the electric field of electromagnetic radiation then the electrons and photons will experience oppositely directed forces exerted by the electric field. As a result, the electrons are displaced relative to the protons and the resulting polarized molecule has an induced dipole moment caused by the external electromagnetic radiation. The induced dipole moment P is given by:

$$P = \alpha E = \alpha E_0 \cos 2\pi\nu t$$

$$= \alpha_0 E_0 \cos 2\pi\nu t + (\partial\alpha/\partial q)_0 \, q_0 E_0 \cos 2\pi\nu t \cos 2\pi\nu_i t$$

$$= \alpha_0 E_0 \cos 2\pi\nu t$$

$$+ \frac{1}{2}(\partial\alpha/\partial q)_0 \, q_0 E_0 \{ \cos [2\pi(\nu+\nu_i) \, t] + \cos [2\pi(\nu-\nu_i) \, t] \} \qquad (1\text{-}7)$$

According to classical theory, the first term describes an oscillating dipole which radiates light of frequency ν (Rayleigh scattering). The second term gives Raman scattering of frequencies $\nu + \nu_i$ (anti-Stokes) and $\nu - \nu_i$ (Stokes). If there is no change in polarizability, the second term disappears. Therefore, there must be a change in polarizability during the vibration in order for Raman scattering to occur. The amount of the polarizability change will determine the Raman scattering intensity, whereas the Raman shift is equal to the vibrational level that is involved. The scattered light intensity (vibrational transition m to n) is given by:

$$I_{n\leftarrow m} \propto N(\nu_0 \pm \nu_{mn})^4 \sum_{i,j} \left| (\alpha_i)_{mn} E_j \right|^2 \qquad (1\text{-}8)$$

where N is number of molecules, ν_0 is incident light frequency, ν_{mn} is vibration frequency, $(\alpha_i)_{mn}$ is polarizability, and E is electric field strength.

Different vibrational modes include: symmetrical stretch, asymmetrical stretch, bending, and twisting. Raman spectroscopy is ideal for organic and inorganic compounds that contain symmetrical bonds such as C=C. Raman and IR are complimentary vibrational spectroscopic techniques. If a vibrational mode is strong in the IR due to a large change in dipole moment, then it is weak in Raman because a small change in the polarizability . If a vibrational mode is strong in the Raman due to a large

change in the polarizability, then it is weak in the IR because of a small change in the dipole moment. By using the two analytical techniques, detailed information of the molecular structure of a molecule can be elucidated.

1.3.2   Development of Raman Spectroscopy

The Raman effect was named after one of its discoverers, the Indian scientist C. V. Raman who observed the effect by means of sunlight in 1928[41] together with K. S. Krishnan and independently by Russian scientist Grigory Landsberg and Leonid Mandelstam. Raman won the Nobel Prize in Physics in 1930 for this discovery accomplished using sunlight, a narrow band photographic filter to create monochromatic light and a "crossed" filter to block this monochromatic light. He found that light of changed frequency passed through the "crossed" filter.

Systematic pioneering theory of Raman effect was developed by George Placzek in 1930-1934[42]. Subsequently the mercury arc became the principal light source, first with photographic detection and then with spectrophotometric detection.

The development of lasers in the 1960's spurred interest in the Raman technique but acceptance was mainly limited to research laboratories. The old style of instrumentation was based on dispersive grating systems which require skilled operators just to collect simple spectra. These system need to be constantly maintained and calibrated since the wavelength scale will drift with changing ambient conditions — such processes as reliable subtractions and library searches were unthinkable.

In addition to these difficulties, Raman spectroscopy was also afflicted by fluorescence. Fluorescence is a strong light emission from the sample which interferes with — and often completely swamps — the weak Raman signal. However, the chance

of an unknown sample exhibiting fluorescence is strongly dependent on the wavelength of the laser used for excitation. Dispersive Raman usually employs visible laser radiation. Typical laser wavelengths are 780 nm, 633 nm, 532 nm, and 473 nm, although others are common. The intensity of Raman scatter is proportional to $1/\lambda^4$, so there is a strong enhancement as the excitation laser wavelength becomes shorter.

In 1986, near-infrared excitation and a commercial interferometer-based FT-IR spectrometer were combined to record a Raman spectrum. This has lead to a number of advantages. Near-infrared laser excitation (around 1 micron wavelength) greatly reduces the number of samples prone to fluorescence and allows higher laser powers to be used without photo decomposition.

Following the demonstration of FT Raman spectroscopy in 1986, the use of Nd:YAG lasers operating at 1064 nm has been generalized to decrease the fluorescence level. Optoelectronic devices have progressed dramatically in the past decade as a consequence of major achievements in solid-state technology. As a result diode lasers are now available from the visible to the infrared that have been demonstrated to work properly in Raman instruments in combination with suitable filter sets.

FT-Raman's interferometric data collection produces throughput and multiplex advantages similar to its counterpart, FT-IR spectroscopy. This can dramatically increase the speed of data collection and makes sample alignment trivial. Accurate spectral libraries and quantitative analysis are available for FT-Raman.

Micro-Raman spectroscopy has evolved rapidly from 1966 when it was revealed that the intensity of Raman light should be independent of sample volume and should remain essentially constant with decreasing sample size down to the dimension

determined by the diffraction limit, and hence the wavelength, of the laser excitation. With routine limits of detection in the nanogram range and high molecular selectivity, micro-Raman spectroscopy has now become a major analytical technique of application in both industry and research. Confocal optical designs and imaging capabilities have further extended the power of this approach. In nanotechnology, a Raman Microscope can be used to analyze nanowires to better understand the composition of the structures.

1.3.3   Sampling and Instrumentation

The Raman spectra can be obtained directly on solids, liquids, powders, tablets, slurries, gels, and suspensions etc. without further sample preparations. There is no problem for aqueous solution analysis, which is a major advantage for Raman analysis. There are two main types of Raman spectrometers: dispersive Raman and FT-Raman spectrometers. Dispersive Raman uses visible lasers such as 785 nm, 632.8 nm, and 532 nm. Dispersion occurs by grating or prism, and detector is a multi-element Silicon CCD (charged Coupled Device) array. FT-Raman uses NIR laser (predominantly 1064 nm), spectrum is encoded by interferometer, and the detector is a single element InGaAs or Ge. Figure 1-9 shows a diagram of a dispersive Raman spectrometer.
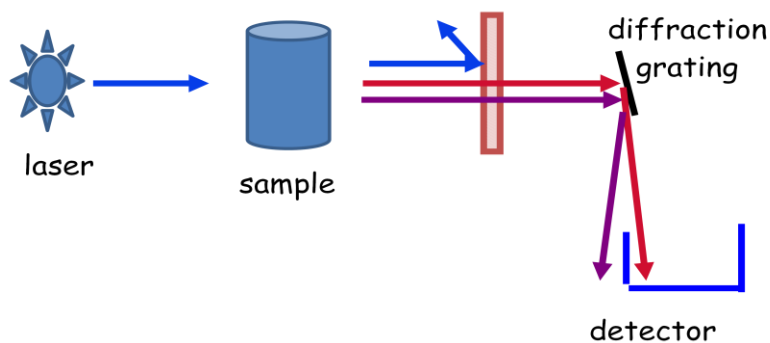
Figure 1-9   Diagram of a dispersive Raman spectrometer

1.3.4   Applications of Raman Spectroscopy

Raman technique was initially used to examine inorganics, it grew extensively in polymer analysis. Recently there has been a growth in pharmaceutical applications, while other applications have been successfully established in semiconductors, art, archaeology and biotech areas. There have also been advances in forensic and process analysis. Raman Spectroscopy is a very good tool for the examination of inorganic materials or those containing inorganic components. Raman spectroscopy can identify both the purity and physical form of elemental carbon, germanium, sulphur, and silicon. Particulates in urban dust[43] have been identified and characterized with Raman technique. By examining the Raman spectra of paintings[44] and archaeologically artfacts such as pottery[45] the age of the work can be determined. A publication[46] devoted 10 chapters to the analysis of polymers with Raman spectroscopy. Polymers have been studied for identification, structure, composition, cure and degree of polymerization in the solid, melt, film, and emulsion, etc. In a recent review[47], different applications of Raman spectroscopy in the field of process analytical of pharmaceutical solid dosage forms are summarized. Applications of Raman spectroscopy on biological sample analysis and diagnosis and its use for medical applications were critically reviewed[48]. Raman method is also very useful in the forensic science[49]. Advances in dispersive optical elements have allowed Raman imaging to become a stand-alone instruments capable of acquiring images with high spatial and spectral resolution[50]. In summary, comparing to many other analytical techniques Raman spectroscopy is reviewed by many as a niche technique, and its applications are fast growing.

1.4   Chemometrics – Principle Components Analysis (PCA)

1.4.1   Introduction to Chemometrics

A data collection task, whether in science, business or engineering, usually involves many measurements made on many samples. Such multivariate data has traditionally been analyzed using one or two variables at a time. However, this way misses the point to discover the relationships among all samples and variables efficiently. Chemometrics [51-52] is the field of extracting information from multivariate chemical data using statistics and mathematics tools and is a growing field with pertinent applications in analytical chemistry[53-54]. Chemometrics can study and model data gained from complex chemical systems, improve the accuracy of current data interpretation methods, and provide an easier and more efficient way to perform the vast calculations that result from the analyses of large data sets.

Chemometrics has developed over the last two decades from a rather theoretical subject to one that is applied in a wide range of sciences. It became organized as a discipline in the 1980s. Early applications were primarily to analytical chemical data sets, often quite simple in nature, for example a set of UV/visible mixture spectra. In the 1990s the application of Chemometrics started expanding, with emphasis on certain industries specially the pharmaceutical industry. A new and exciting stage has emerged from the late 1990s, involving very complex data sets, due to the capacity of analytical instruments to acquire large amounts of data rapidly and the developments of software that can perform fast mathematical calculation.

Chemometrics is typically used for one or more of three main purposes:

- To explore patterns of relationship in data

Patterns of association exist in many data sets, but the relationships between samples can be difficult to discover when the data matrix exceeds three or more features. Exploratory data analysis can reveal hidden patterns in complex data by reducing the information to a more understandable form. Such a chemometric analysis can explain possible outliers and indicate whether there are patterns or trends in the data. Exploratory algorithms such as principal component analysis (PCA) and hierarchical cluster analysis (HCA) are designed to reduce large complex data sets into a series of optimized and interpretable view. These views emphasize the natural groupings in the data and show which variables most strongly influence those patterns.

- To track properties of materials on a continuous basis

In many applications, it is expensive, time consuming or difficult to measure a property of interest directly. Such cases require the analyst to predict something of interest based on related properties that are easier to measure. Chemometric regression analysis is to develop a calibration model which correlates the information in the set of known measurements to the desired property. The mathematic algorithms for performing regression include partial least squares (PLS) and principal component regression (PCR). Because the regression algorithms used are based in factor analysis, the entire group of known measurements is considered simultaneously, and information about correlations among the variables is automatically built into the calibration model. Chemometric regression lends itself practically to on-line monitoring and process control industry, where fast and inexpensive systems are needed to test, predict and make decisions about product quality.

- To prepare and use multivariate classification models

Many applications require that samples be assigned to predefined categories, or "classes". This may involve determining whether a sample is good or bad, or predicting an unknown sample as belonging to one of several distinct groups. A classification model is used to predict a sample's class by comparing the sample to a previously analyzed experience set, in which categories are already known. K-nearest neighbor (KNN) and soft independent modeling of class analogy (SIMCA) are primary chemometric approaches. When these techniques are used to create a classification model, the answers provided are more reliable and include the ability to reveal unusual samples in the data.

1.4.2 *Principle Components Analysis (PCA)*

PCA is probably the most widespread multivariate statistical technique used in Chemometrics, and because of the importance of multivariate measurement in chemistry, it is regarded by many as the technique that most significantly changed the chemist's view of data analysis. PCA is used in all forms of analysis - from neuroscience to computer graphics - because it is a simple, non-parametric method of extracting relevant information from confusing data sets. With minimal additional effort PCA provides a roadmap for how to reduce a complex data set to a lower dimension to reveal the sometimes hidden, simplified dynamics that often underlie it.

PCA is mathematically manipulation of data matrix that transforms original measurement variables into new uncorrelated variables called principal components (PCs). For an original data matrix X, the PCA transformation may take the form:

$$X = T\,P \qquad\qquad\qquad (1\text{-}9)$$

where *T* are called the *scores*, and P are *loadings*. Scores and loadings are the characteristics of principal components. Usually the *scores* relate to the objects or samples and the *loadings* relate to the variables or measurements (e.g. the spectra). The principal components are generated from linear combination of original measurement variables as follows:

$$Sc_{i,pc} = b_{pc,i} \times X_{i,1} + b_{pc,2} \times X_{i,2} + .. + b_{pc,k} \times X_{i,k}$$

(1-10)

where *Sc* – scores; *i* – observation; *pc* – principal component; *b* – loading (-1 to 1); and k – variable.

The original variables (e.g. 100) are reduced to a number of significant PCs (e.g. 3 or 4) each of which is orthogonal to each other. Figure 1-10 shows a diagram of PC-coordinate system. The first Principal component (PC1) covers as much of the variation in the data as possible. The second principal component (PC2) is orthogonal to the first and covers as much of the remaining variation as possible, and so on. By plotting the principal components, one can view interrelationships between different variables, and detect and interpret sample patterns, groupings, similarities or differences.
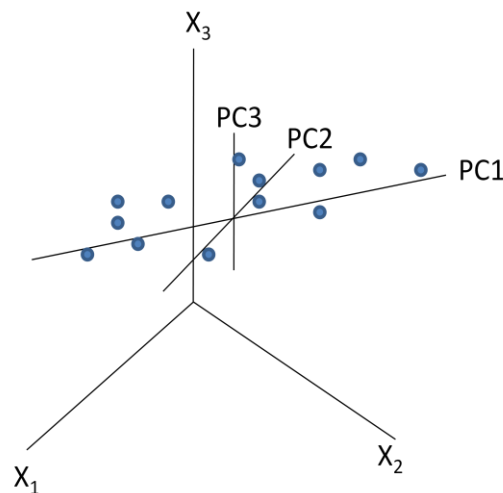
Figure 1-10   Diagram of PC-coordinate data system

The detail theory of PCA mathematic transform is beyond the scope of this thesis. But it is important to understand how to apply PCA. The following case study will demonstrate an example of the applications of PCA.

1.4.3 Case Study[55]

In this case study five physical constants are measured for 27 different elements, namely melting point (m.p), boiling point (b.p), density, oxidation number and electronegativity, to form a 27x5 matrix, whose rows correspond to elements and whose columns to constants. The data are presented in Table 1-1. The aims are to see which elements group together and also which physical constants are responsible for the grouping.

Figure 1-11 illustrates the PCA scores plot for this case study to determine where the main groups are. The plot shows that the halides cluster together at the top left, and the inert gases in the bottom left. The metals are primarily clustered according to their groups in periodic table. This suggests that there are definitive patterns in the data which can be summarized graphically using PCs.

The loading plot for this study is shown in Figure 1-12. The melting point, boiling point and density seem closely clustered. This suggested that these three parameters measure something very similar, as the higher the melting point, the higher the boiling point in most cases. The density (at room temperature) should have some relationship to m.p and b.p. The eletronegativity is in quite a different place, and this suggests it follows entirely different trends.

By reviewing the scores and loadings plots, it is clear that the more dense, high melting point, elements are on the right in the scores plot, and the more electronegative

elements at the top end, so one can look at which variable influences which object by looking at both plots.

Table 1-1   Case study

Element	Group	m.p (K)	b.p (K)	Density (mg/cm^3)	Oxidation number	Electronegativity
Li	1	453.69	1615	534	1	0.98
Na	1	371	1156	970	1	0.93
K	1	336.5	1032	860	1	0.82
Rb	1	312.5	961	1530	1	0.82
Cs	1	301.6	944	1870	1	0.79
Be	2	1550	3243	1800	2	1.57
Mg	2	924	1380	1741	2	1
Ca	2	1120	1760	1540	2	1
Sr	2	1042	1657	2600	2	0.95
F	3	53.5	85	1.7	-1	3.98
Cl	3	172.1	238.5	3.2	-1	3.16
Br	3	265.9	331.9	3100	-1	2.96
I	3	386.6	457.4	4940	-1	2.66
He	4	0.9	4.2	0.2	0	0
Ne	4	24.5	27.2	0.8	0	0
Ar	4	83.7	87.4	1.7	0	0
Kr	4	116.5	120.8	3.5	0	0
Xe	4	161.2	166	5.5	0	0
Zn	5	692.6	1180	7140	2	1.6
Co	5	1765	3170	8900	3	1.8
Cu	5	1356	2868	8930	2	1.9
Fe	5	1808	3300	7870	2	1.8
Mn	5	1517	2370	7440	2	1.5
Ni	5	1726	3005	8900	2	1.8
Bi	6	544.4	1837	9780	3	2.02
Pb	6	600.61	2022	11340	2	1.8
Tl	6	577	1746	11850	3	1.62
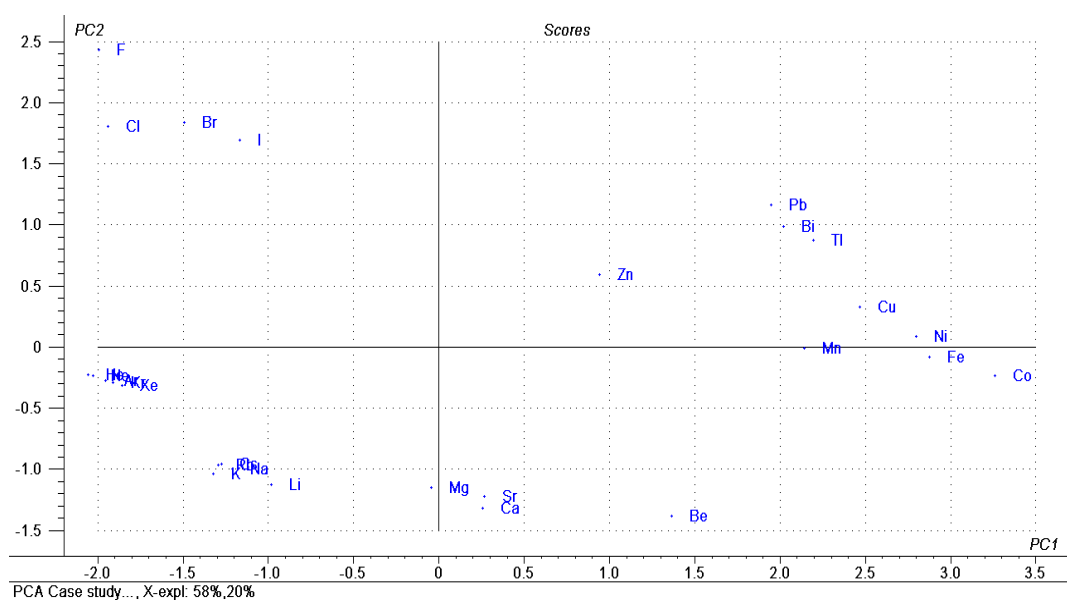
Figure 1-11   Scores plot of the first two PCs for the case study
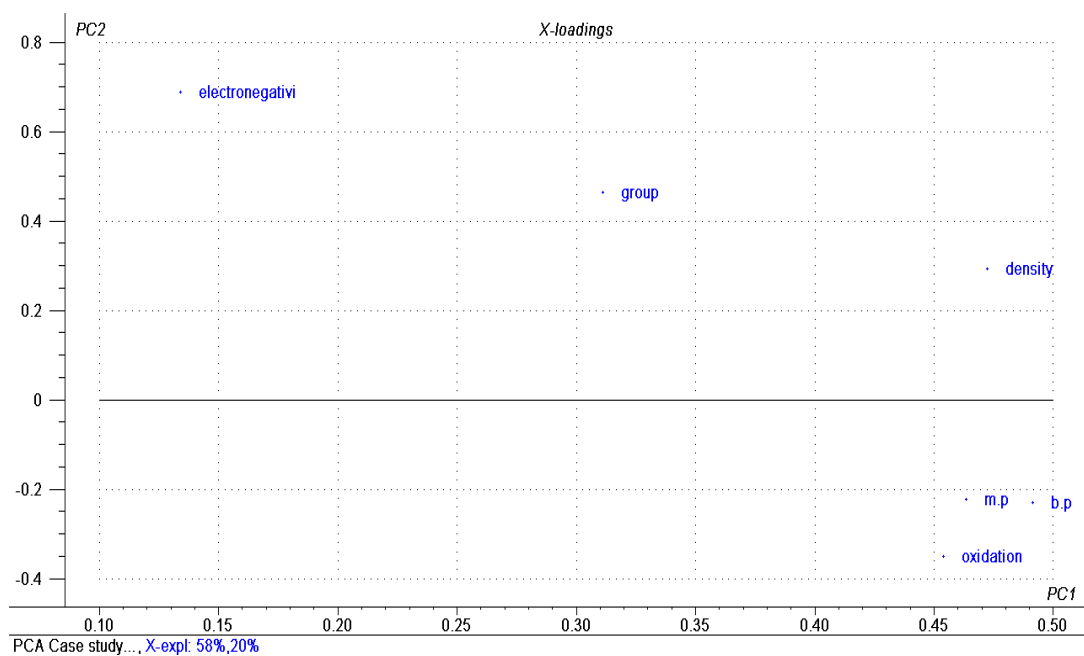
Figure 1-12   Loading plot of the first two PCs for the case study

1.5   Outline of Research Projects in This Thesis

My thesis focuses on two projects. Project one involves a unique method development and validation for the simultaneous determination of dimethicone and cyclodimethicone in skin protectant ointments using FTIR. Project two is to develop analytical methods to rapidly screen and analyze fish oil supplement products on the market using ATR-FTIR, Micro-Raman, PCA, and to characterize temperature dependent IR spectra of the active components omega-3 fatty acids such as ethyl and triglyceride of eicosapentaenoic acid (EPA) using 2D IR correlation analysis.

Chapter 1 References

1. D. M. Livingston, *The Master of Light: A Biography of Albert A. Michelson*, biography by Michelson's daughter, 1973.

2. J.W. Cooley, and J.W. Tukey, *Math. Comput.* 19, 297–301 (1965).

3. J.W. Cooley, P.W. Lewis, and P.D. Welch, *IEEE Trans. on Audio and Electroacoustics* 15 (2), 76–79 (1967).

4. J. Comerford, and A. Hind, Varian RT-IR spectrometers, The history of Varian FT-IR spectrometers, at www.varianinc.com.

5. Harrick, N.J., *Internal Reflection Spectroscopy*. John Wiley & Sons Inc, 342. 1967.

6. M. P. Fuller and P. R. Griffiths, *Anal. Chem.*, 1906 (1978).

7. M. Viktorin, S. Firth, et al., *LaborPraxis*, 13(9), 752, 754, 755-6 (1989).

8. D. Johnson, J. Powell, K. Krishnan, *Proceedings of SPIE-The International Society for Optical Engineering*, 2089 (9TH INTERNATIONAL CONFERENCE ON FOURIER TRANSFORM SPECTROSCOPY), 322-3 (1993).

9. C. Roux, P. Maynard, M. Dawson, *Chemistry in Australia*, 66(2), 1-15 (1999).
10. C. Ricci, K.L. Chan, A. Kazarian, et al., *Applied Spectroscopy*, 60(9), 1013-1021 (2006).

11. Z. Movasaghi, S. Rehman, I. Rehman, *Applied Spectroscopy Reviews*, 43(2), 134-179 (2008).

12. M. P. Fuller, R.J. Rosenthal, *Practical Spectroscopy*, 6(Infrared Microspectrosc.), 153-78 (1988).

13. M. Van De Weert, J.A. Hering, P. Haris, *Biotechnology: Pharmaceutical Aspects*, 3(Methods for Structural Analysis of Protein Pharmaceuticals), 131-166 (2005).

14. N. Mandal, S. Chakraborty, R. Ameta, S. Bandyopadhyay, S. Dasgupta, et al., *Rubber World*, 235(3), 36-40 (2006).

15. H.W. Siesler, *Advances in Chemistry Series*, 236(Structure-Property Relations in Polymers), 41-87 (1993).

16. Anon. USA. *IP.com Journal*, 5(8A), 18 (2005).

17. J. Sedman, F.R. Van De Voort, A. Ismail, et al., *New Techniques and Applications in Lipid Analysis*, 283-324 (1997).

18. S. Bureau, M. Reich, C. Marfisi, J.M. Audergon, G. Albagnac, *Acta Horticulturae*, 717 (Proceedings of the XIIIth International Symposium on Apricot Breeding and Culture), 347-349 (2006).

19. **K.L.** Hanley, R.K.H. Lowry, *American Laboratory* (Shelton, Connecticut), 30(6), 28-31 (1998).

20. I. Noda, Bull. *Am. Phys. Soc.*, 31, 520 (1986).

21. I. Noda, *J. Am. Chem Soc.*, 111, 8116 (1989).

22. I. Noda, *Appl. Spectroscopy*, 44, 550 (1990).

23. I. Noda, *Appl. Spectroscopy*, 47, 1329 (1993).

24. I.Noda, Y.liu, Y. Ozaki, and M.A. Czarnecki, *J. Phys.Chem.*, 99, 3068 (1995).

25. Y.liu, Y. Ozaki, and I. Noda, *J. Phys. Chem.*, 100, 7326 (1996).

26. I. Noda, *Appl. Spectroscopy*, 54, 994 (2000).

27. I. Noda, Y.liu, Y. Ozaki, and M.A. Czarnecki, *J. Phys.Chem.*, 99, 3068 (1995).

28. Y. Ozaki, Y. Liu, and I. Noda, *Appl.Spectrosc.*, 51, 526 (1997).

29. Y.liu, Y. Ozaki, and I. Noda, *J. Phys. Chem.*, 100, 7326 (1996).

30. Y. Ozaki, Y. Liu, and I. Noda, *Macromolecules*, 30, 2391 (1997).

31. H. Fabian, H. H. Mantsch, and C. P. Schultz, *Proc. Natl Acad. Sci.* USA, 96, 13153 (1999).

32. F. Ismoyo, Y. Wang, and A. A. Ismail, *Appl. Spectrosc.*, 54, 930 (2000).

33. G. Tian, Q. Wu, S. Sun, I. Noda, and G. Q. Chen, *Appl. Spectrosc.*, 55, 888 (2001).

34. Y. Wu, K. Murayama, and Y. Ozaki, *J. Phys. Chem. B*, 105, 6251-6259 (2001).

35. T. Amari and Y. Ozaki, *Macromolecules*, 35, 8020-8028 (2002).

36. Y. Kim, Y. M. Jung, S. B. Kim, and S. M. Park, *Analytical Chemistry,* 76(17), 5236-5240 (2004).

37. Z. Zhong, G. Wang, and M. L. Geng, *Journal of Molecular Structure,* 799(1-3), 204-210 (2006).

38. B. Chae, S. W. Lee, M. Ree, Y. M. Jung, and S. B. Kim, *Langmuir*, 19(3), 687-695 (2003).

39. H. Wang, R. Palmer, J. Schoonover, and D. K. Graff, *AIP Conference Proceedings* 503(Two-Dimensional Correlation Spectroscopy), 31-40 (2000).

40. I. Noda, *Journal of Molecular Structure,* 799, 2-15 (2006).

41. C.V. Raman and K.S. Krishnan, *Nature*, 121, 501 (1928).

42. Placzek G.: "Rayleigh Streeung und Raman Effekt", In: Hdb. Der Radiologie, Vol. VI., 2, p. 209, 1934.

43. P. Dhamelincourt, F. Wallart, M. LeClerq, A.T. N'Guyon and D.O. landon, *Anal. Chem.,* 51, 414A (1979).

44. F.R. Perez, H.G.M. Edwards, A. Rivas and L. Drummond, *J. Raman Spectrosc*., 30, 301 (1999).

45. J. Zuo, C. Xu, C. Wang and Z. Yushi, *J. Raman Spectrosc*., 30, 1053 (1999).

46. J. Chalmers and P.Griffiths, *handbook of Vibrational Spectroscopy*, vol. 4, John Wiley & Sons, Inc., New York, 2001.

47. **J.** Rantanen, *Journal of Pharmacy and Pharmacology* , 59 (2), 171-177, 2007.
48. L. Moreira, L.Silveira, F.V.Santos, J. Lyon, et al., *Spectroscopy* (Amsterdam, Netherlands, 22(1), 1-19 (2008).

49. N. Macleod, P. Matousek, *Pharmaceutical Research,* 25(10), 2205-2215 (2008).
50. D. Pappas, B. Smith, J. Winefordner, *Applied Spectroscopy Reviews*, 35(1 & 2), 1-23 (2000).

51. H. Martens, T. Næs, *Multivariate Calibration,* 2nd ed.; John Wiley & Sons: New York, 1991.

52. D. Massart, B.G.M. Vandegonste, L. M. C. Buydens, et al., J. *Handbook of Chemometrics and Qualimetrics;* Elsevier: Amsterdam, 1997.

53. F. Vogt, M. Tacke, M. Jakusch, B. Mizaikoff, *Anal. Chim. Acta.***,** *422,* 187–198 (2000).

54. F. Vogt, H. Steiner, K. Booksh, B. Mizaikoff, *Appl. Spectrosc.***,** *58,* 683–692 (2004).

55. R.G. Brereton, *Applied Chemometrics for Scientists,* John Wiley & Sons, Inc., 2007.

Chapter 2: Method Development and Validation for the Simultaneous Quantitation

of Dimethicone and Cyclomethicone in Skin Protective Ointments by FTIR

2.1   Background/Objective

Dimethicone, which is Polydimethylsiloxane (PDMS), is the most widely used silicon-based organic polymer, and is particularly known for its unusual rheological (or flow) properties. It is optically clear, and is generally considered to be inert, non-toxic and non-flammable. The chemistry structure of dimethicone is shown in Figure 2-1.

Cyclomethicone is a cyclic dimethyl polysiloxane. It is a clear, odorless silicone. It leaves a silky-smooth feel when sprayed on the skin. Cyclomethicone stays completely blended and crystal clear without shaking. The molecular structure of cyclomethicone is shown in Figure 2-2.
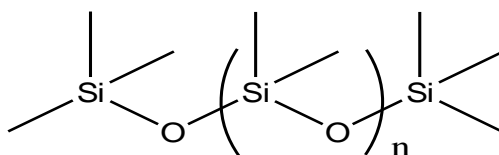
Figure 2-1   Chemical structure of dimethicone
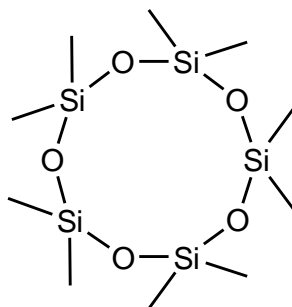
Figure 2-2   Chemical structure of cyclomethicone

Silicone compounds are versatile materials. They are very inert and have excellent biocompatibility. Dimethicone and cyclomethicone are two common types of silicones used in cosmetic products. Common applications include dry oil sprays, hair conditioners, and lotions. The use rates vary widely depending upon the application. Dimethicones has a wide variety of properties based upon the length of the chain. Relative chain length is often differentiated by viscosity. The ultra-light ones are often blended with cyclomethicones for very quick soak-in. The medium weight oils are commonly used to improve the feel of lotion products and can act as skin protectants.

As a very common monograph over the counter (OTC) active ingredient in skin protectant products, dimethicone often needs to be analyzed quantitiatively. One of the current methods for analyzing dimethicone is by FTIR[1]. The infrared spectrum of dimethicone has a characteristic band at ~1260 cm^{-1} which is due to the symmetrical deformation vibration of the methyl group attached to the silicon atom (CH_3-Si). This band is commonly used for quantitation. However, for the formulations also contain cyclomethicone, which exhibits very similar characteristic bands in the IR spectrum, the quantitation of dimethicone is very problematic. The FTIR spectra of dimethicone and cyclomethicone in o-xylene solvent are shown in the Figure 2-3 and Figure 2-4.
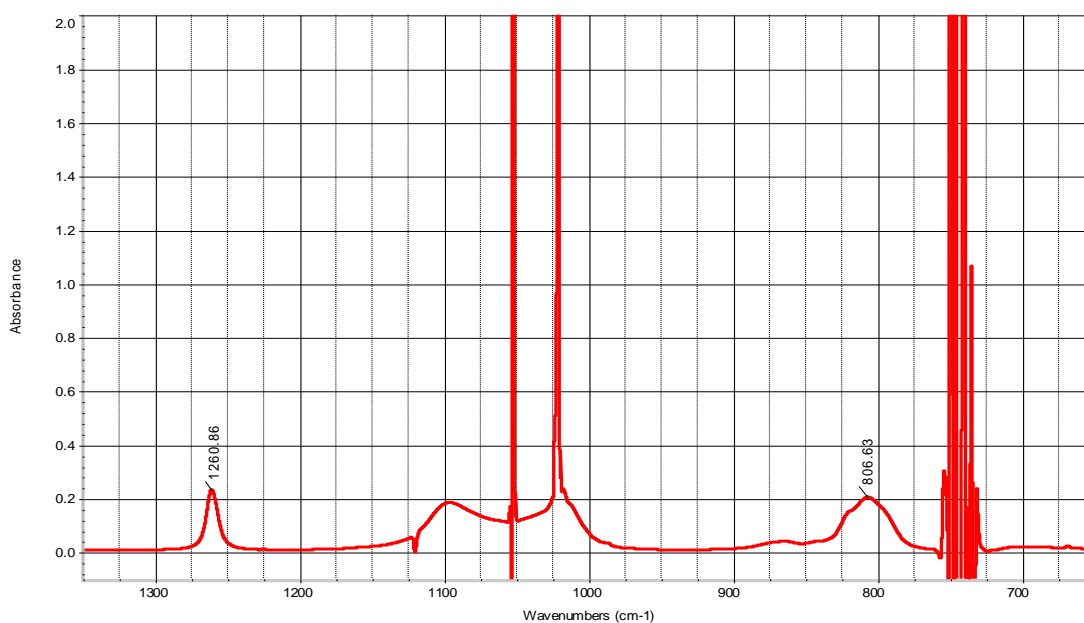
Figure 2-3   FTIR spectrum of dimethicone in o-xylene solvent
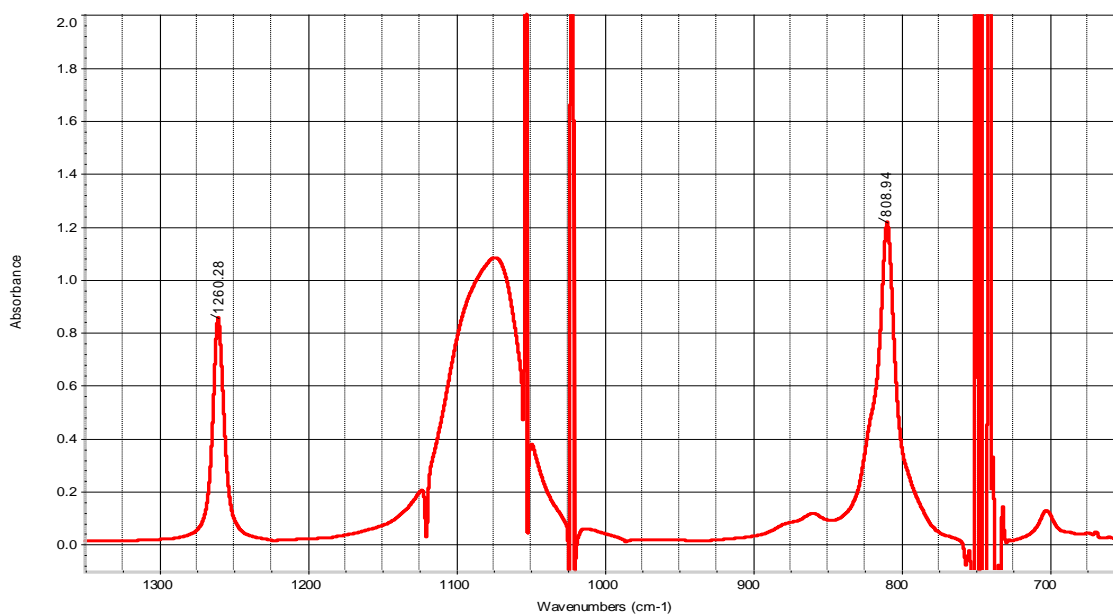
Figure 2-4   FTIR spectrum of cyclomethicone in o-xylene solvent

Dimethicone is an ingredient that is very difficult to analyze using typical chromatographic methods. It contains no UV chromophores and therefore UV detection is not possible. Since dimethicone is a mixture of different molecular weights of

polydimethylsiloxane oligomers, these oligomers can be separated in the High-performance liquid chromatography (HPLC) column with gradient mobile phase and Evaporative Light Scattering detector (ELSD) but show many peaks[2]. Some of the peaks are often interfered by the components from sample matrix and it is very difficult to separate them. Often samples containing dimethicone also have similar components such as cyclomethicone or dimethicone copolyol. The extraction and recovery of only dimethicone from a sample containing similar components can be very challenging. In addition, high molecular weight dimethicone is non-volatile organic polymers, to analyze it using a gas chromatographic method is virtually impossible.

Therefore, the goal of this research project is to first-time develop an analytical method that can determine the concentration of dimethicone in the presence of cyclomethicone in skin protective ointment product (Formula # 9286-018) and to further demonstrate that the developed method is accurate through a series of carefully designed validation experiments. To date, no methods were reported on this subject matter.

2.2   Method Development

In this research project, a unique FTIR method that utilizes two IR absorbance bands (Maximum ~1260 cm^{-1} and ~808 cm^{-1}) to determine the concentrations of dimethicone and cyclomethicone in skin protective ointment product (F# 9826-018, contains ~ 9% of dimethicone and ~ 33.8% of cyclomethicone) using two simultaneous equations has been developed. The theory and development are discussed below.

Quantitative IR spectrometry is based on the Beer's law, which is expressed as:

$$A = \varepsilon bc \qquad\qquad (2\text{-}1)$$

where:

A　　=　　absorbance of the sample at a specified wavenumber,

ε　　=　　absorptivity of the component at this wavenumber,

B　　=　　sample path length,

C　　=　　concentration of the component.

The absorbance of a component is proportional to its concentration when the cell path length are kept constant during the sample analysis in a certain concentration range, and this can be expressed as $A = KC$, in which K is a component specific constant (called response factor in this study), and C is the component concentration in the sample. Hence, for a mixture of two independently absorbing components at a single wavenumber, the total absorbance is:

$$A = K_1C_1 + K_2C_2 \qquad\qquad (2\text{-}2)$$

In order to solve for the two component concentrations C_1 and C_2, two independent equations containing 2 absorbances measured at 2 different wavenumbers are necessary. This can be expressed as follows:

$$A_1 = K_{11}C_1 + K_{12}C_2 \qquad\qquad (2\text{-}3)$$

$$A_2 = K_{21}C_1 + K_{22}C_2 \qquad\qquad (2\text{-}4)$$

where

A_1　　=　　total absorbance at wavenumber 1,

A_2　　=　　total absorbance at wavenumber 2,

K_{11}　　=　　response factor of component 1 at wavenumber 1,

K_{12}　　=　　response factor of component 2 at wavenumber 1,

K_{21}　　=　　response factor of component 1 at wavenumber 2,

K_{22} =   response factor of component 2 at wavenumber 2,

C_1 =   concentration of component 1 in the mixture,

C_2 =   concentration of component 2 in the mixture.

Absorbances are obtained from instrument measurements, and response factors are calculated from standard calibrations with known standard concentrations. Therefore, the component concentrations in an unknown samples can be calculated by solve the two simultaneous equations (2-3) and (2-4).

The theory summarized above can be used to determine the concentrations of dimethicone and cyclomethicone in skin protective ointment product (Formula # 9286-018). Both dimethicone and cyclomethicone exhibit very similar IR absorbance bands with characteristic absorption at maximum wavenumbers around ~1261 cm^{-1} and ~808 cm^{-1}, when o-xylene is used as the solvent (see Figures 2-3 and 2-4). Figure 2-5 shows a typical IR spectrum of the skin protective ointment sample and figure 2-6 shows the IR spectrum of a placebo sample (sample matrix without dimethicone and cyclomethicone) dissolved in o-xylene. There were no IR bands observed in the spectrum of the placebo at wavenumbers around ~1261 cm^{-1} and ~808 cm^{-1}, and this indicated that the two absorption bands at ~1261 cm^{-1} and ~808 cm^{-1} observed in sample spectrum were purely from dimethicone and cyclomethicone. Therefore, the concentrations of dimethicone and cyclomethicone can be determined using the two simultaneous equations approach.
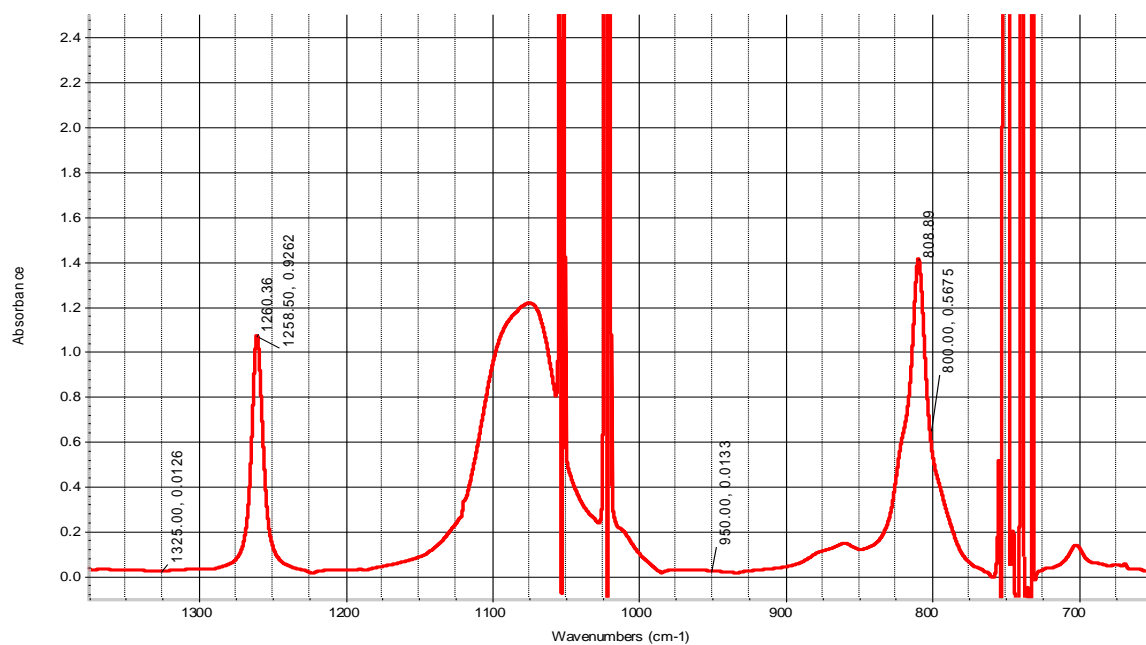
Figure 2-5   A typical IR spectrum of a skin protective ointment sample in o-xylene
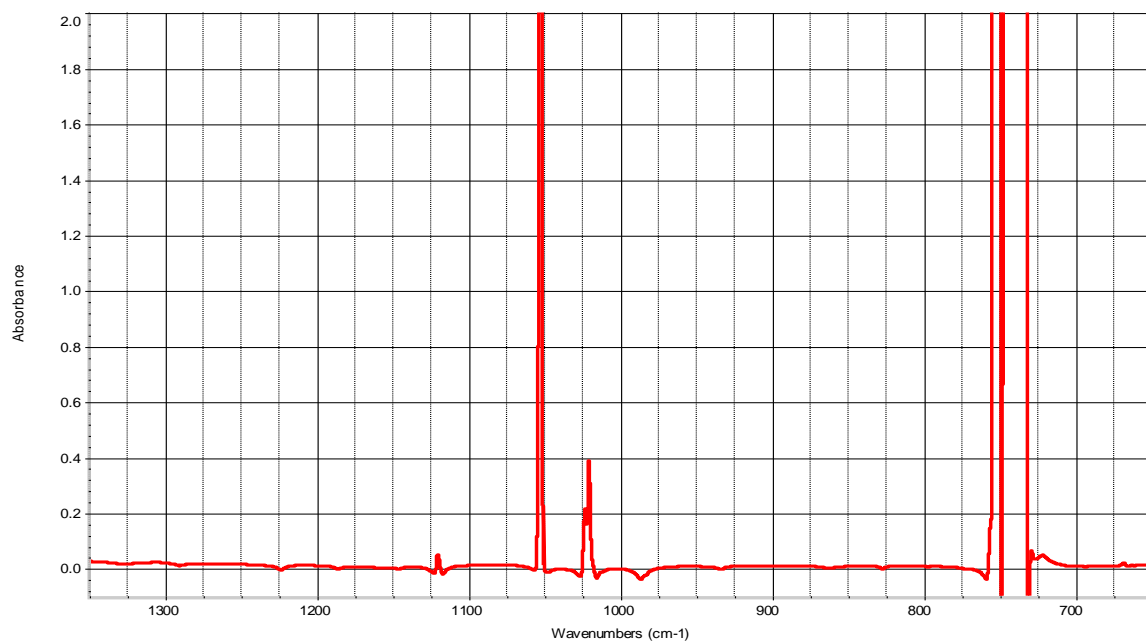
Figure 2-6   IR spectrum of a placebo sample in o-xylene

The next step of the method development is to choose the appropriate wavenumbers for the absorbance measurements and baseline corrections. The following factors were considered for vavenumber selections:

- In order to obtain solutions (calculate C_1 and C_2) from the two simultaneous linear equations (2-3) and (2-4), the slope of the two equations must not be the same, ie, $K_{11}/K_{12} \neq K_{21}/K_{22}$. So response factors of the two components at the selected wavenumbers should meet this condition.

- The maximum absorbance wavenumbers shift slightly from sample to sample depending on concentration, so fixed wavenumbers should be considered.

- The absorbance values at the selected wavenumbers should fall within the acceptable accurate range of the spectrometer used. In general, it is in the range of 0.2 – 0.8 absorbance units (AU) for quantitation purpose. However, the sensitivity of FTIR spectrometer is such that lower absorbance values can be used quite effectively, but the accuracy should be proved through validation. Absorbance greater than 1.5 AU should be avoided due to instrumental non-linear effect.

- The correction of raw absorbance data for baseline absorbance is necessary. Since the bands of interest are baseline resolved, one baseline point should be suitable for baseline correction. The guiding factor in the selection of the wavenumbers for baseline correction is the reproducibility of the results, and this can be proved through method validation.

Based on all the factors summarized above and a series of experimental runs of evaluating different wavenumbers, the method was finalized as follows:

Two bands at fixed wave numbers 1258.50 cm^{-1} and 800.00 cm^{-1}, with baseline correction at 1325.00 cm^{-1} and 950.00 cm^{-1} respectively, were used to determine the concentrations of dimethicone and cyclomethicone using two simultaneous linear equations:

$$A'_{1258.50} = K_{di\,(1258.50)}\,C\,\text{di-sp} + K_{cyclo\,(1258.50)}\,C_{cyclo}\text{-sp} \qquad (2\text{-}5)$$

$$A'_{800.00} = K_{di\,(800.00)}\,C\,\text{di-sp.} + K_{cyclo\,(800.00)}\,C_{cyclo}\text{-sp} \qquad (2\text{-}6)$$

where,

$A'_{1258.50}$ = sample absorbance at 1258.50 cm^{-1} with the baseline correction at 1325.00 cm^{-1},

$A'_{800.00}$ = sample absorbance at 800.00 cm^{-1} with the baseline correction at 950.00 cm^{-1},

$K_{di(1258.50)}$ = response factor of dimethicone at 1258.50 cm^{-1},

$K_{di(800.00)}$ = response factor of dimethicone at 800.00 cm^{-1},

$K_{cyclo(1258.50)}$ = response factor of cyclomethicone at 1258.50 cm^{-1},

$K_{cyclo(800.00)}$ = response factor of cyclomethicone at 800.00 cm^{-1},

$C_{di}\text{-sp}$ = concentration of dimethicone in sample solution,

$C_{cyclo}\text{-sp}$ = concentration of cyclomethicone in sample solution.

By solving the two simultaneous equations, the concentration of dimethicone and cyclomethicone in the sample solution can be calculated as follows:

$$C_{di-sp} = \frac{A'_{1258.50} \times K_{cyclo(800.00)} - A'_{800.00} \times K_{cyclo(1258.00)}}{K_{di(1258.50)} \times K_{cyclo(800.00)} - K_{di(800.00)} \times K_{cyclo(1258.00)}} \qquad (2\text{-}7)$$

$$C_{cyclo-sp} = \frac{A'_{1258.50} \times K_{di(800.00)} - A'_{800.00} \times K_{di(1258.00)}}{K_{di(800.00)} \times K_{cyclo(1258.00)} - K_{di(1258.50)} \times K_{cyclo(800.00)}} \qquad (2\text{-}8)$$

in which, $A'_{1258.50} = A_{1258.50} - A_{1325.00},$ $A'_{800.00} = A_{800.00} - A_{950.00}$

where,

$A'_{1258.50}$ =   Net absorbance of sample solution at 1258.50 cm^{-1},

$A_{1258.50}$ =   Absorbance of sample solution at 1258.50 cm^{-1},

$A_{1325.00}$ =   Absorbance of sample solution at 1325.00 cm^{-1} (baseline),

$A'_{800.00}$ =   Net absorbance of sample solution at 800.00 cm^{-1},

$A_{800.00}$ =   Absorbance of sample solution at 800.00 cm^{-1},

$A_{950.00}$ =   Absorbance of sample solution at 950.00 cm^{-1} (baseline).

$$K_{di(1258.50)} = \frac{\left(A_{di(1258.50)} - A_{di(1325.00)}\right)}{C_{di}}$$

$$K_{di(800.00)} = \frac{\left(A_{di(800.00)} - A_{di(950.00)}\right)}{C_{di}}$$

$$K_{cyclo(1258.50)} = \frac{\left(A_{cyclo(1258.50)} - A_{cyclo(1325.00)}\right)}{C_{cyclo}}$$

$$K_{cyclo(800.00)} = \frac{\left(A_{cyclo(800.00)} - A_{cyclo(950.00)}\right)}{C_{cyclo}}$$

where,

$K_{di\,(1258.50)}$ =   Response factor of dimethicone at 1258.50 cm^{-1},

$A_{di(1258.50)}$ =   Absorbance of dimethicone standard at 1258.50 cm^{-1},

$A_{di(1325.00)}$ =   Absorbance of dimethicone standard at 1325.00 cm^{-1} (baseline),

$K_{di\,(800.00)}$ =   Response factor of dimethicone at 800.00 cm^{-1},

$A_{di(800.00)}$ =   Absorbance of dimethicone standard at 800.00 cm^{-1},

$A_{di(950.00)}$ =   Absorbance of dimethicone standard at 950.00 cm^{-1} (baseline),

$K_{cyclo\,(1258.50)}$ =   Response factor of cyclomethicone at 1258.50 cm^{-1},

$A_{cyclo(1258.50)}$ =   Absorbance of cyclomethicone standard at 1258.50 cm^{-1},

$A_{cyclo(1325.00)}$ =   Absorbance of cyclomethicone standard at 1325.00 cm^{-1} (baseline),

$K_{cyclo\,(800.00)}$ =   Response factor of cyclomethicone at 800.00 cm^{-1},

$A_{cyclo(800.00)}$ =   Absorbance of cyclomethicone standard at 800.00 cm^{-1},

$A_{cyclo(950.00)}$ =   Absorbance of cyclomethicone standard at 950.00 cm^{-1} (baseline),

C_{di} =   concentration of dimethicone standard in mg/mL,

C_{cyclo} =   concentration of cyclomethicone standard in mg/mL.

2.3   Method Procedures

2.3.1   Materials

Dimethicone, NF, Dow Corning Q7-9170, 100 cst.

Cyclomethicone, Dow Corning 345 Fluid.

Sample solvent, o-Xylene, HPLC grade, CAS# 95-47-6, Sigma-Aldrich

Skin protective ointment product, Formula # 9286-018, Lab batch # 9884-106.

Placebo containing no added dimethicone and cyclomethicone, NB# 10217/070.

Placebo containing no added dimethicone, NB# 10217/071.

2.3.2   Instrumentation and Instrument Settings

Infrared spectrophotometer, single beam – Nicolet Magna IR 550.

Liquid cell (KBr), 0.2 mm path length -- Wilmad Cat. #l05A4W

Scans: 32 scans

Resolution: 2 cm^{-1}

Velocity: 0.6329

Aperture: 69

Range: 1375 to 650 cm^{-1}

Collect background every 60 minutes

2.3.3   Standard and Sample Preparation

Approximately 50 ± 5 mg of dimethicone reference standard were weighed into

25 mL volumetric flask, diluted to volume with o-xylene.

Approximately 187.5 ± 10 mg of cyclomethicone reference were weighed into a

25 mL volumetric flask, diluted to volume with o-xylene.

Approximately 550 ± 30 mg of Skin protective ointment sample were weighed

into a 25 mL volumetric flask and 15 mL of o-xylene were added to dissolve the sample. Then diluted to volume with o-xylene and mixed well.

2.3.4 Test Procedures

Using a glass syringe with a Luer-Lok fitting, carefully fill the liquid IR cell with o-xylene and stopper tightly. Record the background IR baseline from 1375 cm^{-1} to 650 cm^{-1}.

Remove the cell and carefully fill it with the first standard solution after flushing the cell with 1 mL of the solution.

Place the sample cell in the sample beam and record the absorbances at 1258.50, 1325.00, 800.00, and 950.00 cm^{-1}. The absorbance reading should be taken by moving the cursor to the exact wavenumber and reading the absorbance manually to four digits after the decimal (for example, 0.2017).

Repeat above Steps for the background, standards and samples solutions as necessary.

2.4 Method Validation

In order to demonstrate that the two linear simultaneous equations approach is applicable and prove that the sample system is free from intermolecular interaction which could cause nonlinear effects, and to demonstrate that the method meets the FDA requirements for the OTC active analysis, a comprehensive validation was designed and performed, and the method was found to be linear, accurate, precise, and specific. The detail validation procedures, results, and discussions are described in the sections below.

2.4.1   Additive Absorbance Responses for Dimethicone and Cyclomethicone

Both dimethicone and cyclomethicone exhibit very similar IR absorption bands with characteristic maximum absorptions around 1261 cm^{-1} and 808 cm^{-1}, when o-xylene is used as the solvent. The absorbances at two fixed wavenumbers 1258.50 cm^{-1} and 800.00 cm^{-1} (with baseline correction at 1325.00 cm^{-1} and 950.00 cm^{-1}, respectively) are used to determine the concentrations of dimethicone and cyclomethicone by solving two simultaneous equations (Ref. section 2.2). In order for the simultaneous equations to be valid, the absorbance responses of dimethicone and cyclomethicone must be additive.

Three individual dimethicone (Di) and three individual cyclomethicone (Cyclo) standard solutions were prepared at 75%, 100%, and 125% of the target standard concentration of 2.0 mg/mL of dimethicone and 7.5 mg/mL of cyclomethicone. Three standard mixtures (Di + Cyclo) of dimethicone and cyclomethicone solutions were also prepared containing exactly the same concentrations of dimethicone and cyclomethicone as that in the corresponding individual solutions. The absorbance response additive property was evaluated by comparing the absorbance of the standard mixture with the calculated total absorbance of the individual dimethicone and cyclomethicone solutions for the same concentration levels. The % differences between the absorbances were calculated and the results are presented in Table 2-1. The % differences of absorbances at both 1258.50 cm^{-1} and 800.00 cm^{-1} were within 1.0% for all the three concentration levels. This demonstrated that the absorbance responses are additive at the two absorbance wavenumbers.

The absorbance response additive property was further verified by preparing five standard mixtures of dimethicone and cyclomethicone solutions at 50%, 75%, 100%,

125%, and 156% of the target concentrations of 2.0 mg/mL of dimethicone and 7.5

mg/mL of cyclomethicone. The absorbances of the five mixtures were calculated from the

response factors and concentrations of dimethicone and cyclomethicone according to the

two equations. Then the % differences (%diff) between the calculated absorbance

(Cal.Abs) and the experimental absorbance (Exp. Abs) of the mixtures were evaluated.

The results are presented in Table 2-2.

<div align="center">Table 2-1   Absorbance Response Data Comparison</div>

Concentration Level – 75%	Absorbance at 1258.50 cm^{-1}	Absorbance at 800.00 cm^{-1}
Di (1.4970 mg/mL)	0.1352	0.1227
Cyclo (5.6251 mg/mL)	0.5486	0.2943
Di (1.4970 mg/mL) + Cyclo (5.6251mg/mL)	0.6828	0.4175
Calculated Total Absorbance*	0.6838	0.4170
% Difference**	0.15	0.12
Concentration Level – 100%	Absorbance at 1258.50 cm^{-1}	Absorbance at 800.00 cm^{-1}
Di (1.9959 mg/mL)	0.1805	0.1642
Cyclo (7.5001 mg/mL)	0.7275	0.3901
Di (1.9959 mg/mL) + Cyclo (7.5001mg/mL)	0.9000	0.5522
Calculated Total Absorbance	0.9080	0.5543
% Difference	0.88	0.38
Concentration Level – 125%	Absorbance at 1258.50 cm^{-1}	Absorbance at 800.00 cm^{-1}
Di (2.4949 mg/mL)	0.2256	0.2058
Cyclo (9.3751mg/mL)	0.9047	0.4869
Di (2.4949mg/mL) + Cyclo (9.3751mg/mL)	1.1236	0.6928
Calculated Total Absorbance	1.1303	0.6927
% Difference	0.59	0.01

* Calculated Total Absorbance:

The total absorbance of individual dimethicone and cyclomethicone solutions.

** % Difference:

The difference between the absorbance of the mixture and calculated total absorbance of the

individual solutions divided by the calculated total absorbance.

Table 2-2   Absorbance Response Data Comparison

Mixture	Cal. Abs 1258.50 cm^{-1}	Cal. Abs 800.00 cm^{-1}	Exp. Abs 1258.50 cm^{-1}	Exp. Abs 800.00 cm^{-1}	% diff. 1258.50 cm^{-1}	% diff. 800.00 cm^{-1}
50% Di + Cyclo	0.4540	0.2772	0.4577	0.2789	0.82	0.63
75% Di + Cyclo	0.6810	0.4157	0.6828	0.4175	0.26	0.43
100% Di + Cyclo	0.9080	0.5543	0.9000	0.5522	0.88	0.38
125% Di + Cyclo	1.1350	0.6929	1.1236	0.6928	1.00	0.01
156% Di + Cyclo	1.4187	0.8661	1.4080	0.8711	0.76	0.57

All the observed % differences were within 1.0%. This demonstrated that the

Absorbance response of the mixture is a linear combination of the individual responses of

Dimethecone and cyclomethicone. Therefore, the two simultaneous equations that are

used to calculate the concentrations of dimethicone and cyclomethicone were shown to be

valid.

2.4.2 Linearity

1. Varying concentration of dimethicone without added cyclomethicone:

Seven dimethicone standard solutions, ranging in concentration from 1.0323 mg/mL to

4.1291 mg/mL, were prepared and analyzed using the method conditions outlined in

section 2.3. This represents a range between 50% - 200% of the typical standard solution

with a target concentration of 2.0 mg/mL of dimethicone. The correlation coefficient was

found to be 0.99997 for the absorbance response at 1258.50 cm^{-1} and 0.99995 at 800.00 cm^{-1}. The linearity results are presented in Table 2-3 and Figures 2-7 and 2-8.

2. Varying concentration of cyclomethicone without added dimethicone: Six cyclomethicone standard solutions, ranging in concentration from 3.7505 mg/mL to 13.1274 mg/mL, were prepared and analyzed using the method conditions. This represents a range between 50% - 175% of the typical standard solution with a target concentration of 7.5 mg/mL of cyclomethicone. The correlation coefficient was found to be 0.99990 for the absorbance response at 1258.50 cm^{-1} and 0.99982 at 800.00 cm^{-1}. The linearity results are presented in Table 2-4 and Figures 2-9 and 2-10.

3. Varying the concentration of dimethicone while maintaining a constant cyclomethicone concentration: Five mixtures of dimethicone and cyclomethicone solutions were prepared with varying concentrations of dimethicone, ranging from 1.0070 mg/mL to 3.0210 mg/mL, while maintaining the concentration of cyclomethicone constant at 7.5016 mg/mL. The mixtures were analyzed using the conditions. This represents a range between 50% - 150% of the typical standard solution with a target concentration of 2.0 mg/mL of dimethicone. The correlation coefficient was found to be 0.99160 for the absorbance response at 1258.50 cm^{-1} and 0.99727 at 800.00 cm^{-1}. The linearity results are presented in Table 2-5 and Figures 2-11 and 2-12.

4. Varying the concentration of cyclomethicone while maintaining a constant dimethicone concentration: Five mixtures of dimethicone and cyclomethicone solutions were prepared with varying concentrations of cyclomethicone, ranging from 3.7508 mg/mL to 11.2524 mg/mL, while

maintaining the concentration of dimethicone constant at 2.0140 mg/mL. The mixtures were analyzed using the method conditions. This represents a range between 50% - 150% of the typical standard solution with a target concentration of 7.5 mg/mL of cyclomethicone. The correlation coefficient was found to be 0.99996 for the absorbance response at 1258.50 cm^{-1} and 0.99998 at 800.00 cm^{-1}. The linearity results are presented in Table 2-6 and Figures 2-13 and 2-14.

All the correlation coefficient results (> 0.99) in the above four sets of experiments demonstrated a linear absorbance response over a concentration range between 50% - 150% of the expected dimethicone and cyclomethicone concentrations in the samples.

Table 2-3   Linearity Data of Dimethicone without Cyclomethicone

Dimethiocne Concentration (mg/mL)	Absorbance at 1258.50 cm^{-1}	Absorbance at 800.00 cm^{-1}
1.0323	0.0932	0.0846
1.5484	0.1412	0.1283
2.0646	0.1859	0.1692
2.5807	0.2337	0.2124
3.0968	0.2799	0.2538
3.6130	0.3264	0.2973
4.1291	0.3729	0.3400
Slope	0.09019	0.08227
Intercept	0.00055	-0.00011
R^2	0.99997	0.99995

Table 2-4   Linearity Data of Cyclomethicone without Dimethicone

Cyclomethicone Concentration (mg/mL)	Absorbance at 1258.50 cm^{-1}	Absorbance at 800.00 cm^{-1}
3.7505	0.3694	0.1979
5.6259	0.5467	0.2926
7.5012	0.7210	0.3861
9.3765	0.9080	0.4887
11.2518	1.0891	0.5877
13.1274	1.2623	0.6838
Slope	0.09566	0.05206
Intercept	0.00883	0.00010
R^2	0.99990	0.99982

Table 2-5   Linearity Data of Dimethicone with Constant

Cyclomethicone Concentration

Dimethicone Concentration (mg/mL)	Cyclomethicone Concentration (mg/mL)	Absorbance at 1258.50 cm^{-1}	Absorbance at 800.00 cm^{-1}
1.0070	7.5016	0.8155	0.4732
1.5105	7.5016	0.8675	0.5182
2.0140	7.5016	0.9104	0.5587
2.5175	7.5016	0.9516	0.5994
3.0210	7.5016	0.9821	0.6324
Slope	-	0.08286	0.07936
Intercept	-	0.73853	0.39654
R^2	-	0.99160	0.99727

Table 2-6 Linearity Data of Cyclomethicone with Constant
Dimethicone Concentration

Dimethicone Concentration (mg/mL)	Cyclomethicone Concentration (mg/mL)	Absorbance at 1258.50 cm^{-1}	Absorbance at 800.00 cm^{-1}
2.0140	3.7508	0.5508	0.3641
2.0140	5.6262	0.7274	0.4600
2.0140	7.5016	0.9104	0.5587
2.0140	9.3770	1.0870	0.6561
2.0140	11.2524	1.2630	0.7536
-	Slope	0.095126	0.05199
-	Intercept	0.19412	0.16846
-	R^2	0.99996	0.99998

$$y=0.09019x+0.00055$$
$$R^2=0.99997$$
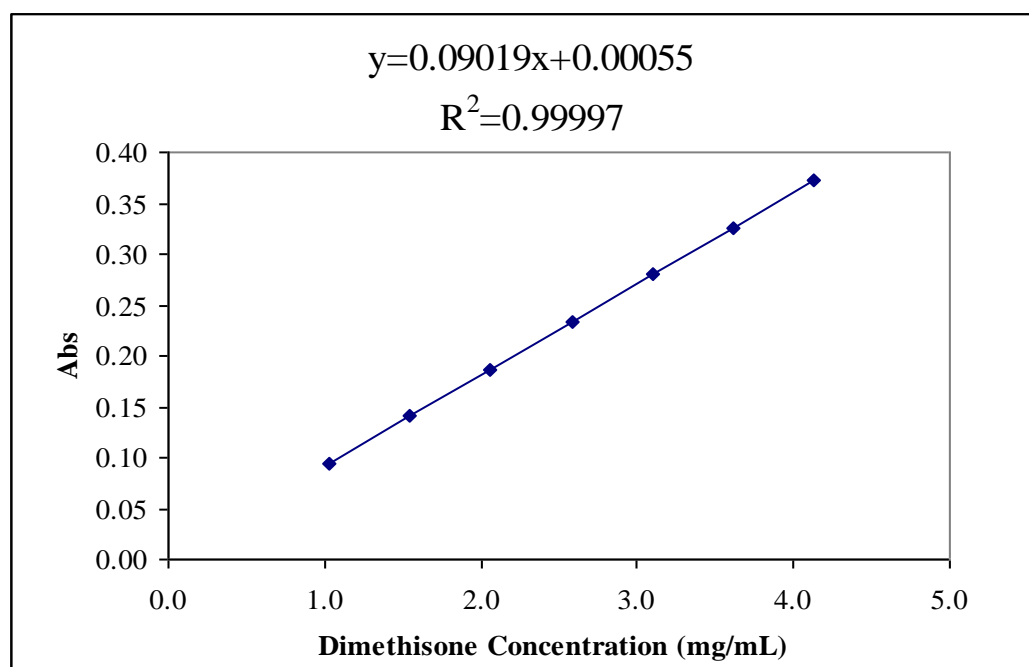
Figure 2-7   Linearity of dimethicone without cyclomethicone at 1258.50 cm^{-1}
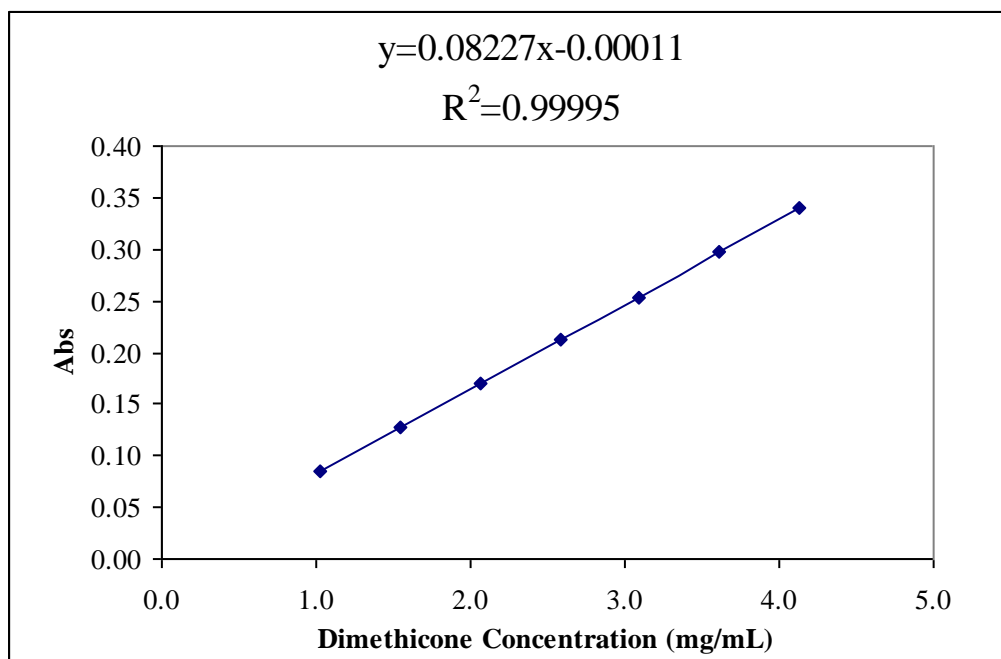
Figure 2-8   Linearity of dimethicone without cyclomethicone at 800.00 cm^{-1}
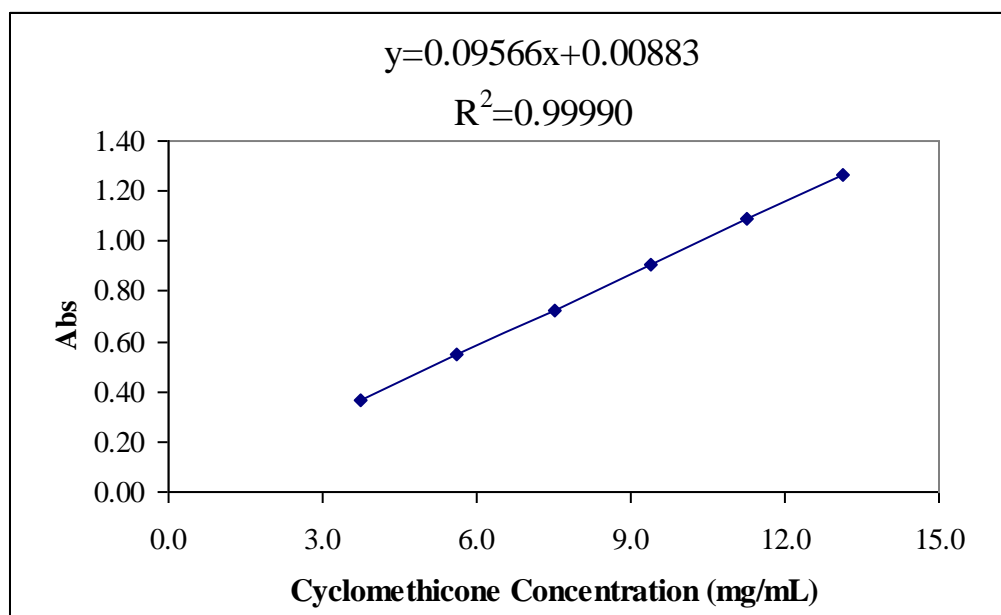
Figure 2-9   Linearity of cyclomethicone without dimethicone at 1258.50 cm^{-1}
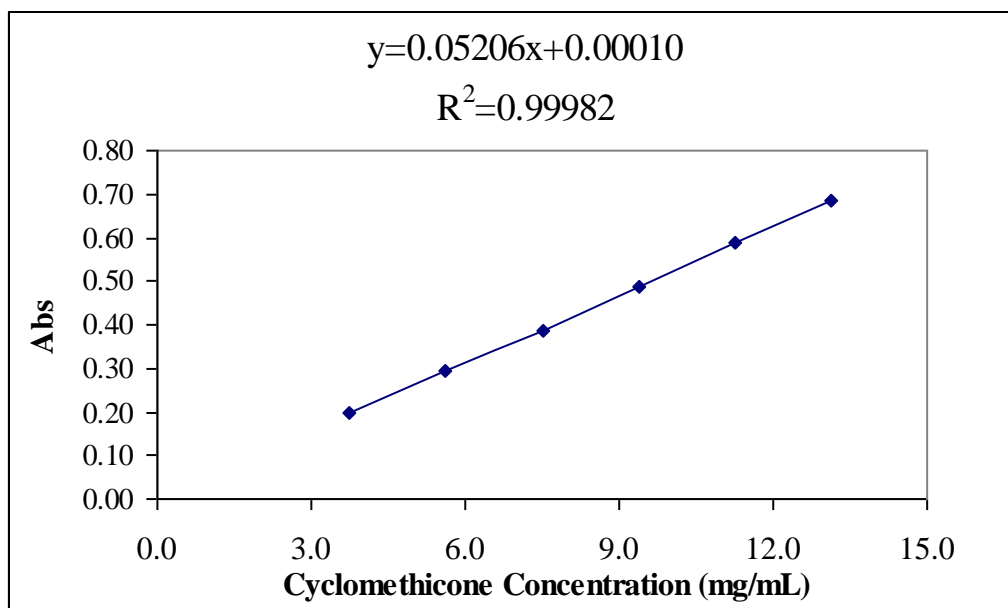
Figure 2-10　　Linearity of cyclomethicone without dimethicone at 800.00 cm^{-1}
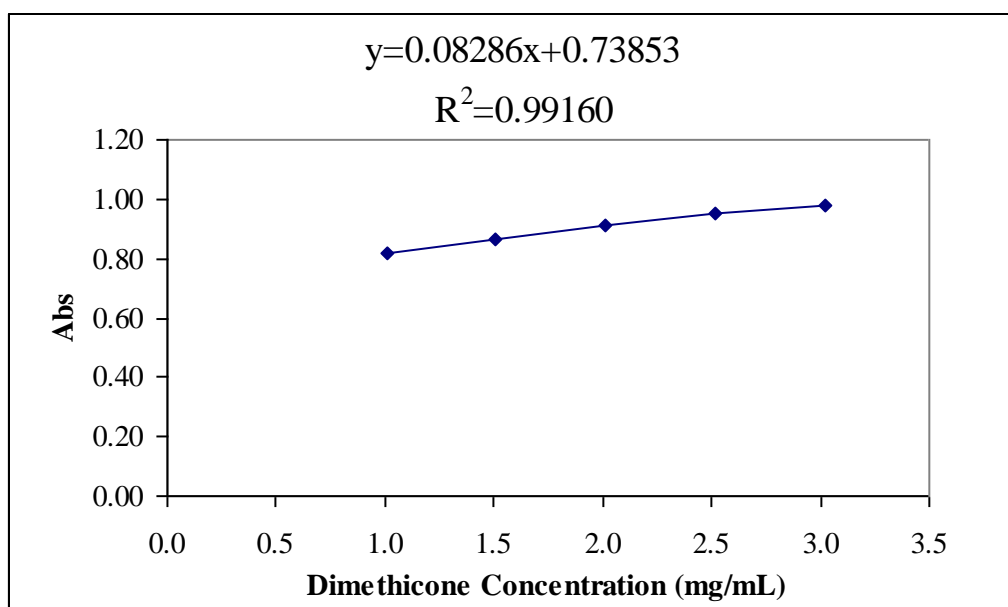
Figure 2-11　　Linearity of dimethicone with constant cyclomethicone concentration at 1258.50 cm^{-1}
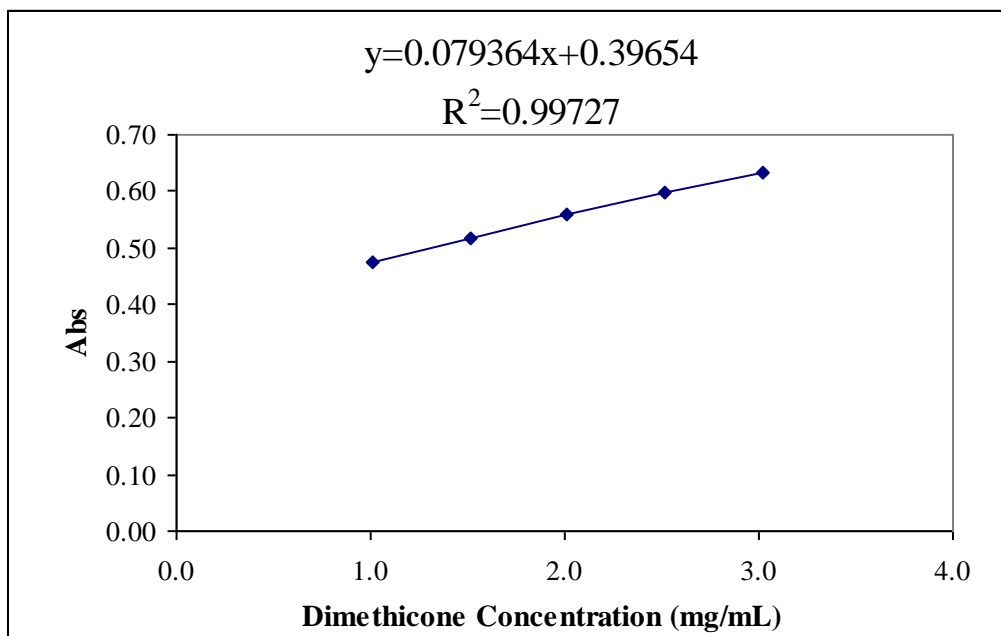
Figure 2-12   Linearity of dimethicone with constant cyclomethicone
                concentration at 800.00 cm^{-1}
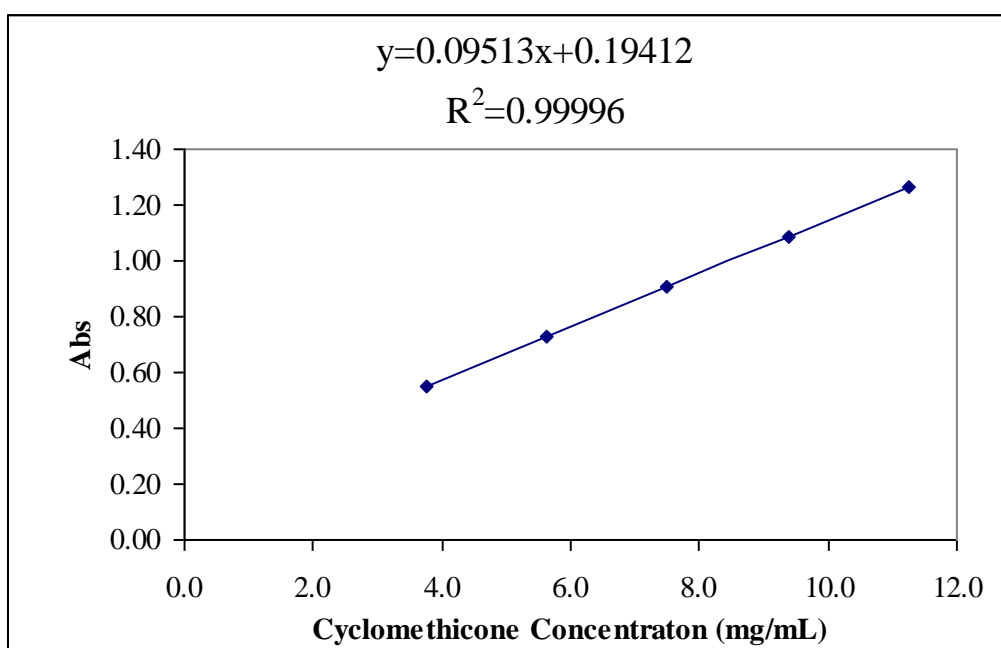
Figure 2-13   Linearity of cyclomethicone with constant dimethicone
                concentration at 1258.50 cm^{-1}

$$y=0.05199x+0.16846$$
$$R^2=0.99998$$
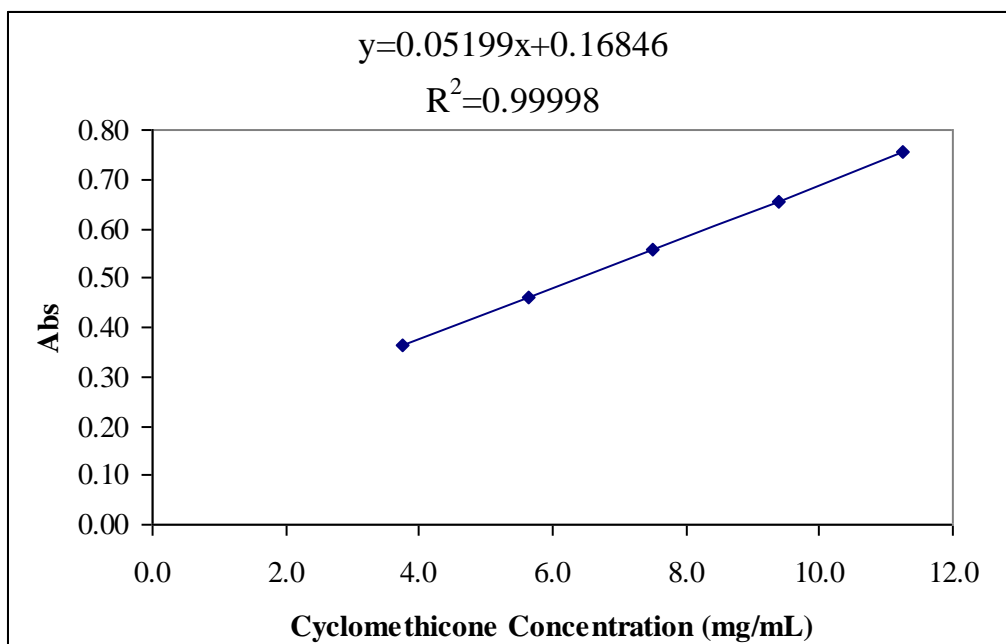
Figure 2-14   Linearity of cyclomethicone with constant dimethicone concentration at 800.00 cm^{-1}

2.4.3 *Accuracy*

A placebo sample of the Skin protactive ointment formulation, containing no added dimethicone (Di) and cyclomethicone (Cyclo), was spiked with five concentration combinations of 80% Di + 80% Cyclo, 80% Di + 120% Cyclo, 100% Di + 100% Cyclo, 120% Di + 80% Cyclo, and 120% Di + 120% Cyclo, of the expected dimethicone concentration of 2.0 mg/mL and cyclomethicone concentration of 7.5 mg/mL. The spiked placeboes were analyzed using the method conditions outlined in Section 2.3. The average recovery was found to be 102.12% (1.17 % RSD) for dimethicone and 99.93% (0.54% RSD) for cyclomethicone, and the individual recoveries were found to be between 99.48% - 105.47% for dimethicone and 98.62% - 101.18% for cyclomethicone. The recovery results are presented in Table 2-7.

Since dimethicone is the active that is required to be tested, the accuracy of

the method for the dimethicone analysis was further verified. This was done by spiking a

placebo, containing no added dimethicone, with 80%, 100%, and 120% of the expected

dimethicone concentration of 2.0 mg/mL. The spiked placebo samples were then

analyzed using the method conditions. The average recovery of dimethicone was found

to be 99.09% (1.34% RSD), and the individual recoveries were found to be between

96.00% - 100.60%. The results are summarized in Table 2-8.

All the average recovery results were between 98% - 102%. All the individual

recovery results were between 96% - 105%, which is acceptable for a typical FTIR

quantitation method. This demonstrated satisfactory accuracy over a range of

concentrations between 80% - 120% of the target dimethicone and cyclomethicone

concentrations for a typical sample solution.

Table 2-7   Summary of Accuracy Results

Concentration Combinations	% Recovery of Dimethicone	% Recovery of Cyclomethicone
1. 80% Di + 80% Cyclo, *n=2	101.91	100.57
	99.48	101.18
2. 120% Di + 80% Cyclo, n=2	101.56	100.17
	100.78	100.52
3. 100% Di + 100% Cyclo, n=2	101.97	99.47
	101.27	99.72
4. 80% Di + 120% Cyclo, n=2	103.42	99.70
	101.88	99.87
5. 120% Di + 120% Cyclo, n=2	103.46	99.49
	105.47	98.62
Global Average	102.12	99.93
Global RSD %	1.17	0.54

* n = number of preparations

Table 2-8   Summary of Accuracy Results

Concentrations		% Recovery of Dimethicone
1.	80% Di, * n=3	100.05 98.77 98.48
2.	100% Di, n=3	96.00 99.54 99.32
3.	120% Di, n=3	99.15 100.60 99.91
Global Average		99.09
Global RSD %		1.34

* n = number of preparations

2.4.4   Precision

- Repeatability:

The repeatability of the method with respect to the formulation under this study

was evaluated by analyzing six sample preparations of a sample (Batch# 9884-106). The

relative standard deviation of the dimethicone assay results was found to be 1.02% for the

six sample preparations. The results are summarized in Table 2-9. The results

demonstrated a satisfactory precision (≤2.0% RSD) for the sample analysis.

Table 2-9 Summary of Repeatability Results

Sample Replicate	Dimethicone (% w/w)
1	8.6539
2	8.8001
3	8.8611
4	8.8908
5	8.8944
6	8.8271
Average	8.8212
RSD %	1.02

- Reproducibility:

The reproducibility of the method was demonstrated by analyzing three

batches of the skin ointment (F# 9286018) in triplicate at two different laboratories

(CPC and LEK). The % differences were calculated by dividing the difference between

the average assay results obtained by the two laboratories by the average results of CPC.

All the results are summarized in Table 2-10. The % differences for dimethicone ranged

between 0.70% and 1.83% demonstrating satisfactory reproducibility (≤3.0% RSD).

Table 2-10   Summary of Repeatability Results

Sample ID	%w/w Dimethicone in Skin Ointment F# 9286018					
	Sample #1 B# 0014K		Sample #2 B# 9884-106		Sample #3 B# 3124	
	CPC	LEK	CPC	LEK	CPC	LEK
1	9.6074	9.8720	8.8142	8.9284	8.9343	9.2150
2	9.9439	9.6394	8.2867	8.5939	8.6948	8.8946
3	9.9588	9.7917	8.5130	8.5609	9.1167	8.9187
Mean	9.8367	9.7677	8.5380	8.6944	8.9153	9.0094
%Diff.	-	0.70	-	1.83	-	1.17

2.4.5   *Specificity*

A skin protective ointment placebo, containing no added dimethicone and

cyclomethicone, was analyzed under the test method conditions. No interferences were

observed within the 1258.50 cm^{-1} and 800.00 cm^{-1} absorbance band regions. The FTIR

spectra of the prepared standards, sample, and placebo on o-xylene are presented in

Figures 2-3, 2-4, 2-5, and 2-6.

A skin protective ointment placebo, containing no added dimethicone and cyclomethicone, was subjected to elevated temperature and photodegradation conditions for a period of 7 days. The stressed placebo samples were then prepared and analyzed under the test method conditions. No degradant/impurity bands were found within the 1258.50 cm^{-1} and 800.00 cm^{-1} absorbance band regions. The stress conditions and results are summarized in Table 2-11 and the FTIR spectra of the stressed placebo samples are presented in Figures 2-15 and 2-16.

The dimethicone (Di) and cyclomethicone (Cyclo) standard materials, and a sample (Batch# 9884-106) of skin protective ointment were also subjected to the elevated temperature and photodegradation stress conditions for a period of 7 days. The stressed standards and sample were then prepared and analyzed using the method conditions. The two wavenumbers (cm^{-1}) at the maximum absorbance were evaluated. In addition, the assay results of the stress standards and samples were calculated. All the results are summarized in Table 2-12. The FTIR spectra of the stressed standard and sample solutions are presented in Figures 2-17, 2-18, 2-19, 2-20, 2-21, and 2-22.

The results showed that the two wavenumbers at the maximum band absorption of the stressed standards and samples were very consistent with that of their corresponding controls. No band shifts, which would indicate dimethicone polymer chain degradation and/or degradation of cyclomethicone, were observed. This demonstrated that dimethicone and cyclomethicone were very stable both in the pure material and in the product formulation, and there were no evidence of degradants. The assay results of the stressed standards and samples further confirmed that both dimethicone and cyclomethicone are very stable.

The results for all conducted experiments demonstrated that there were no

degradants and /or impurities interfering with the analysis of dimethicone. The method

has been shown to be specific and selective for the analysis of dimethicone in the skin

protective ointment formulation under this study.

Table 2-11   Summary of Placebo Stress Conditions and Results

Conditions	Evidence of Interference
Control	No
Elevated Temperature 70°C / 7 days	No
Light Chamber / 25°C / 7 days	No

Table 2-12   Summary of Standard and Sample Stress Conditions and Results

Sample/Conditions	Di Assay %w/w	Cyclo Assay %w/w	Max. Abs. cm^{-1}	Max. Abs. cm^{-1}	Evidence of Degradation
Di Standard Control	-	-	1260.86	806.63	-
Di Standard 70°C / 7 days	99.4	-	1260.87	806.69	No
Di Standard light Chamber /7 days	99.8	-	1260.87	806.51	No
Cyclo Standard Control	-	-	1260.28	808.94	-
Cyclo Standard 70°C / 7 days	-	100.7	1260.28	808.94	No
Cyclo standard light Chamber /7 days	-	100.5	1260.27	808.96	No
Lab Batch Sample Control	8.821	33.85	1260.36	808.89	-
Lab Batch Sample 70°C / 7 days	8.987	33.67	1260.36	808.86	No
Lab Batch Sample light Chamber /7 days	8.978	33.89	1260.36	808.89	No
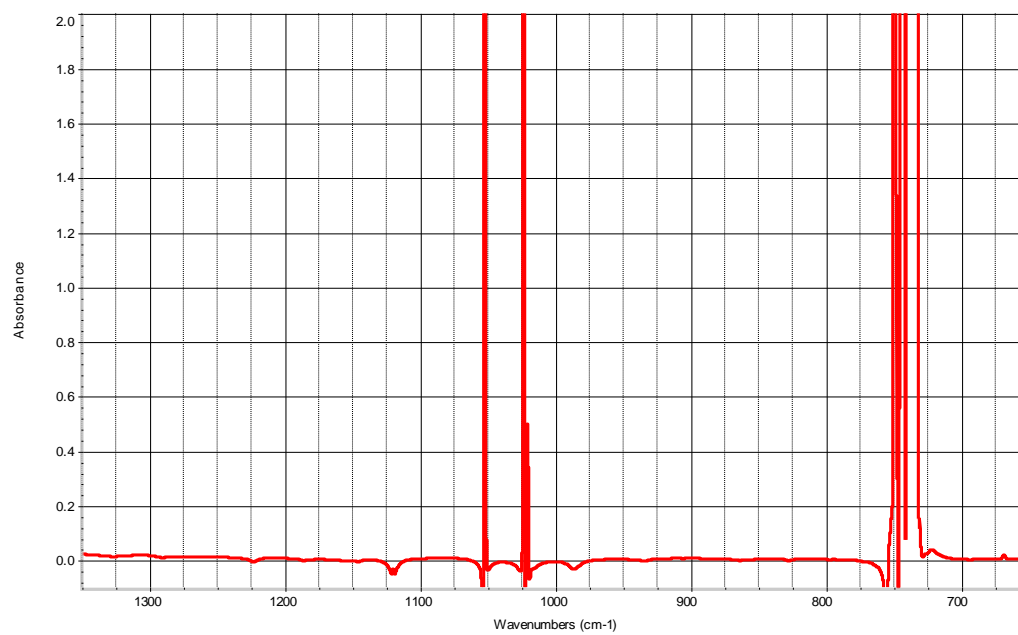
Figure 2-15   IR spectrum of placebo stored at 70ºC / 7 days
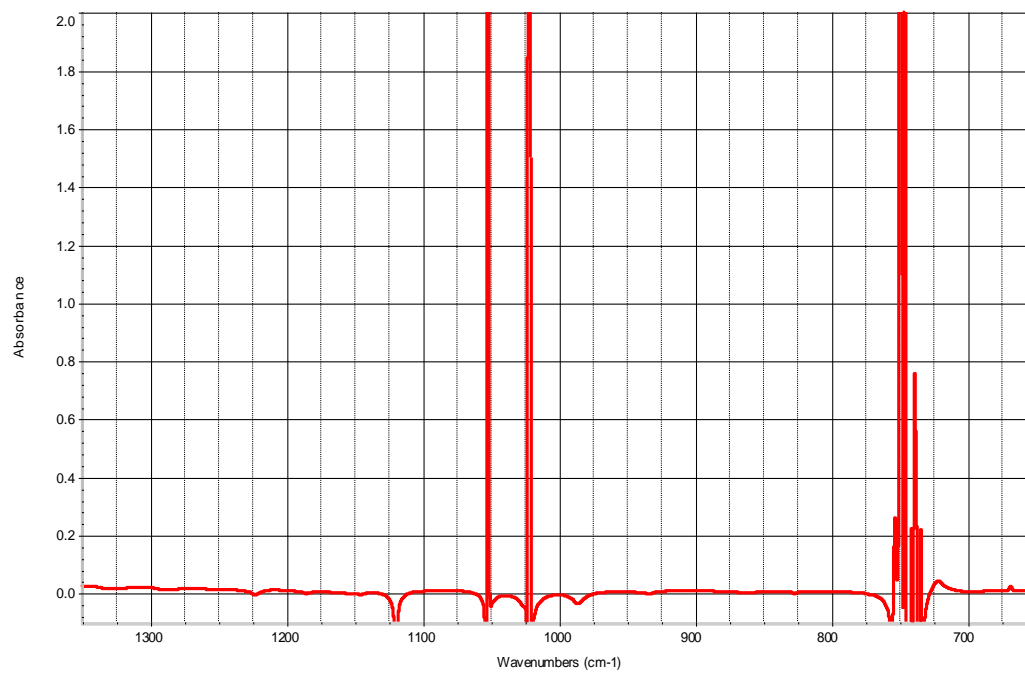
Figure 2-16   IR spectrum of placebo stored under light / 7 days
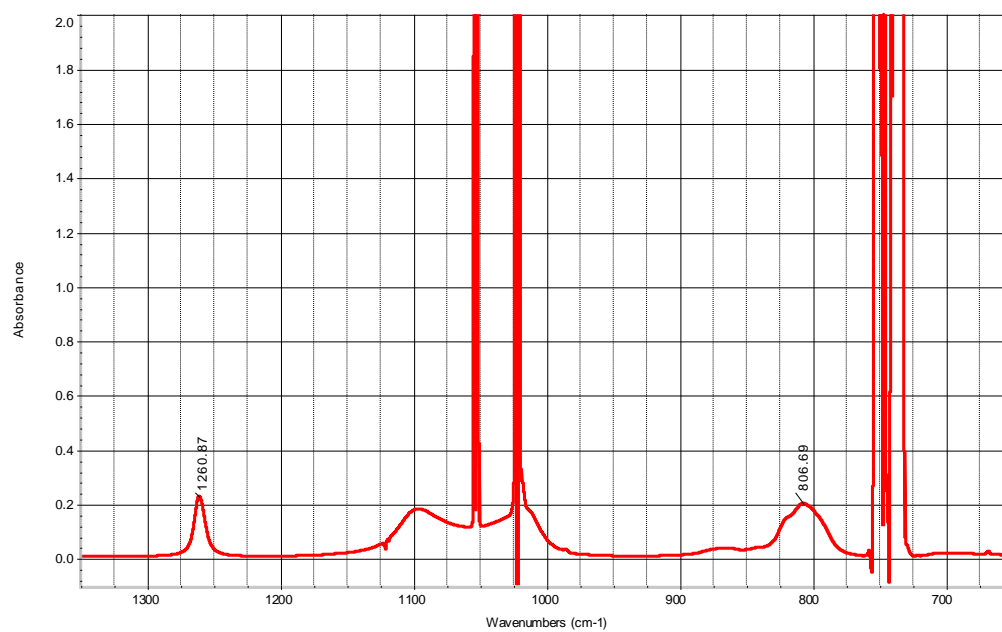
Figure 2-17   IR spectrum of dimethicone standard stored at 70℃ / 7 days
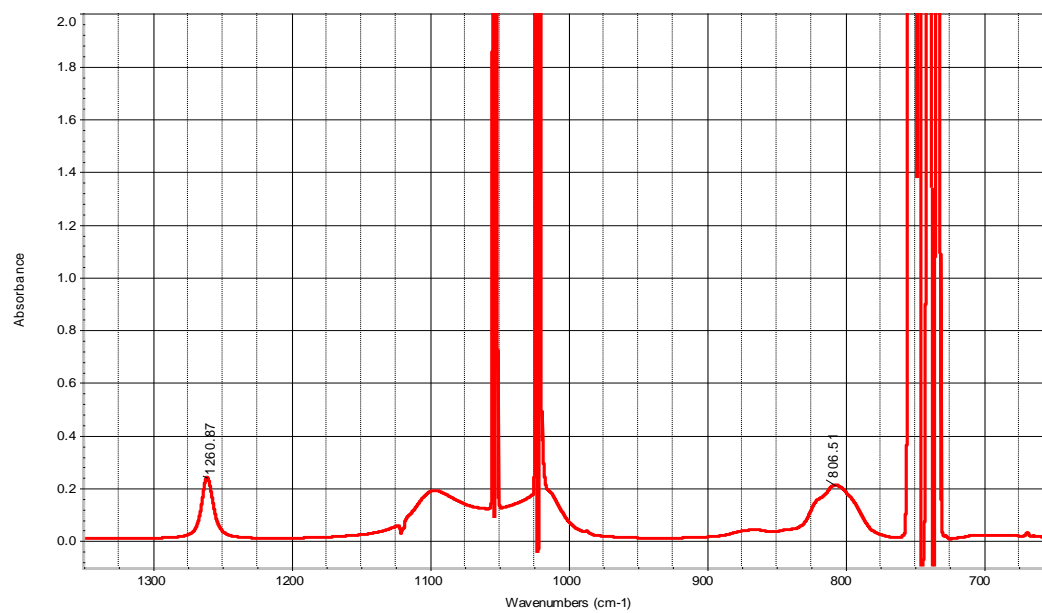
Figure 2-18   IR spectrum of dimethicone standard under light / 7 days
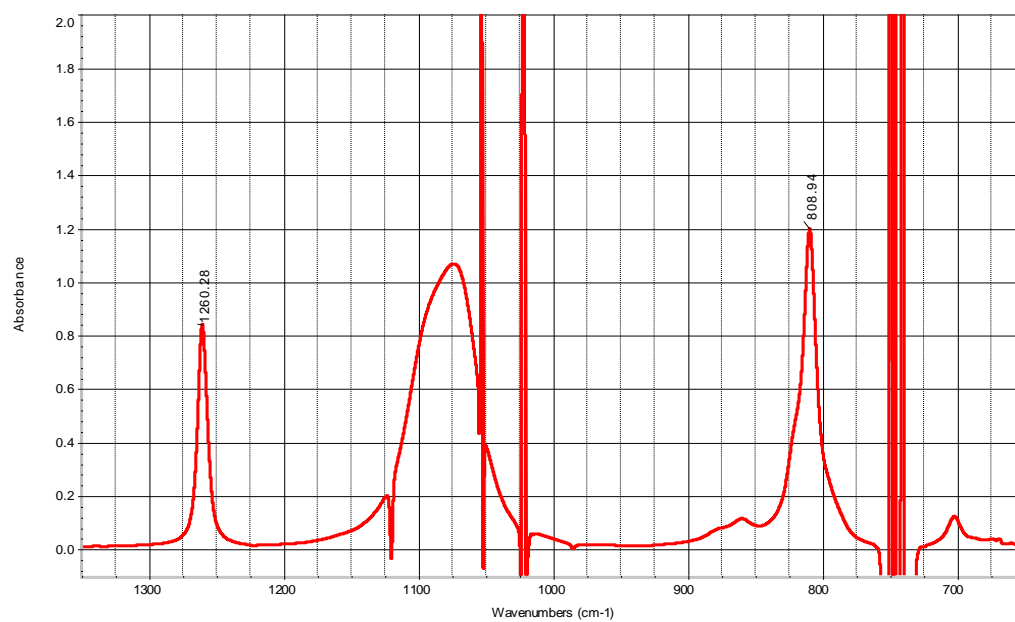
Figure 2-19   IR Spectrum of cyclomethicone standard at 70ºC / 7 days
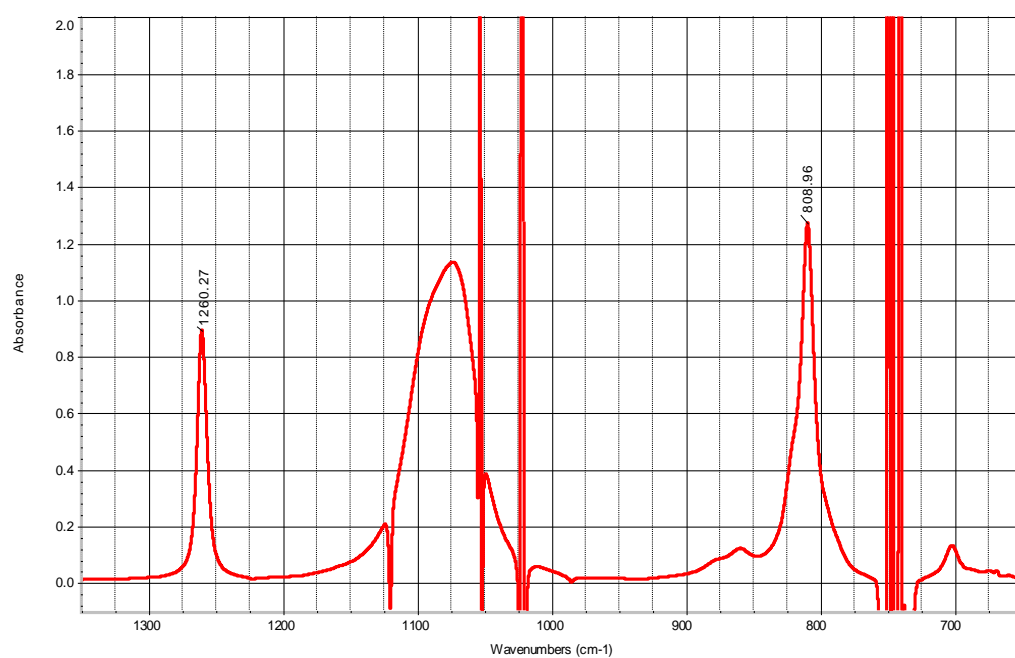
Figure 2-20   IR spectrum of cyclomethicone standard under light / 7 days
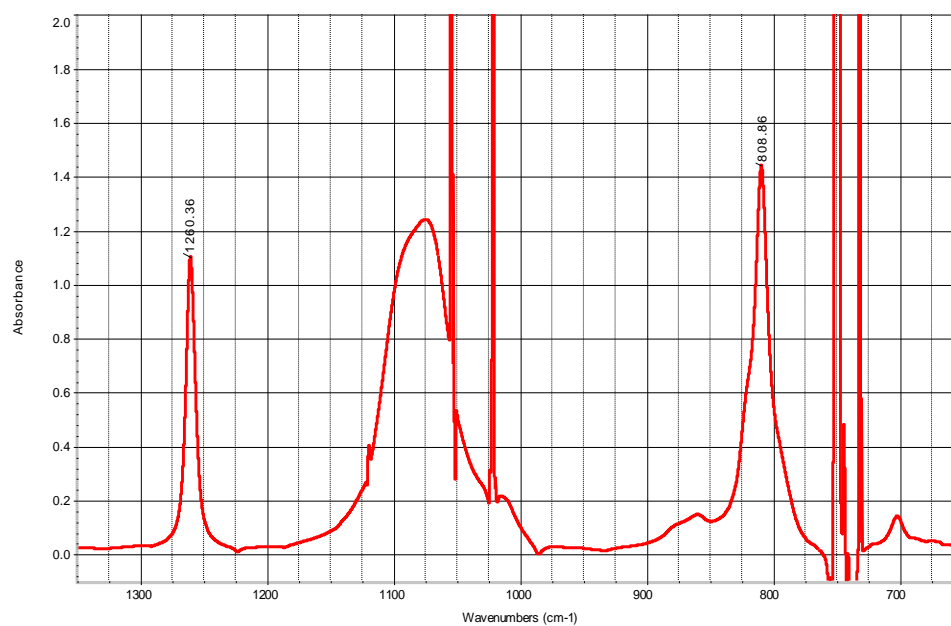
Figure 2-21   IR spectrum of sample stored at 70ºC / 7 days
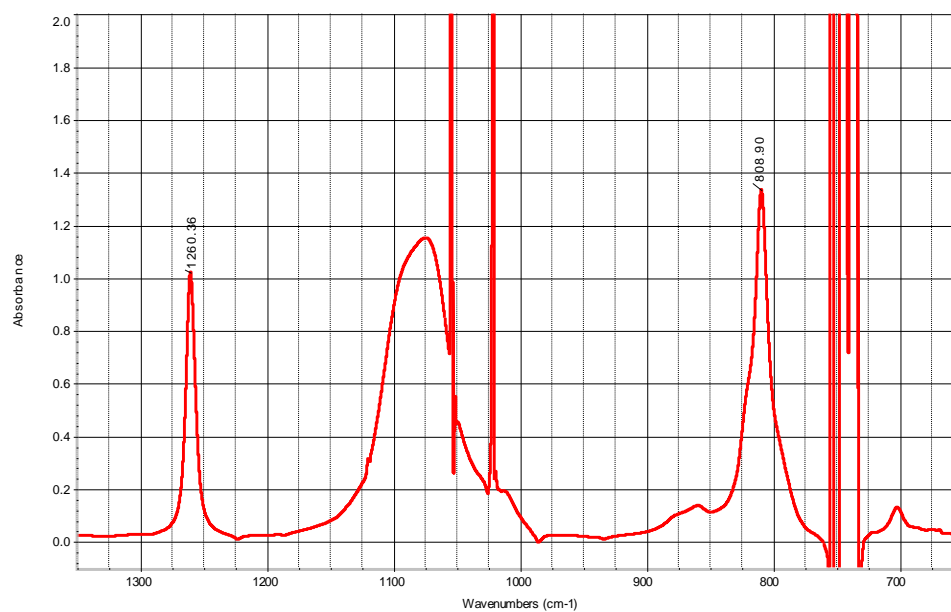
Figure 2-22   IR spectrum of sample stored under light / 7 days

2.4.6   Standard Material Lot to Lot Variation

Two different lots of dimethicone and cyclomethcone standard material of the same grade were used as standards for the assay of dimethicone on the same sample solutions (Batch # 0014K). All the standard and sample solutions were prepared at the same day and tested in the same sequence. The assay results are summarized in Table 2-13.

Significant difference (14.9%) between the average assay results using different lots of standard material were observed. This indicated that the quantitative results of dimethicone are sensitive to the lot of standard material that was used for the testing. This was especially true for cyclomethicone. Therefore, it was concluded that the same lot of the raw material that was used in the formulation should be used as the reference standard material for the testing of the products.

Table 2-13   Assay Results by Different Lots Standards

Dimethicone Standard	Cyclomethicone Standard	% w/w of Dimethicone
Lot # 0001349098	Lot# 0001693756	9.6074 9.9439 9.9588 Avg. 9.8367
LEK Lot# 89013	LEK Lot# 00358	8.2376 8.5779 8.5966 Avg. 8.4707
-	**-**	% difference **14.9**

2.4.7   Standard and Sample Solution Stability

The standard and sample solution stability was evaluated by analyzing a dimethicone standard solution, a cyclomethicone standard solution, and a sample solution

after they were made and stored at the ambient laboratory conditions up to 5 days relative to the freshly made standard solutions. The recovery results of 100.3% (dimethicone standard solution), 100.2% (cyclomethicone standard solution), and 99.2% (dimethicone in the sample solution) demonstrated that the standard and sample solutions were stable up to 5 days when they were stored at ambient laboratory conditions.

2.5   Conclusion

The results of the experiments outlined in this study indicated that the unique IR method developed for simultaneous quantitation of dimethicone and cyclomethicone using two simultaneous absorbance – concentration equations at two fixed wavenumbers of 1258.50 cm^{-1} and 800.00 cm^{-1} (with baseline correction at 1325.00 cm^{-1} and 950.00 cm^{-1}, respectively) is applicable. The method has been successfully validated for the analysis of dimethicone and cyclomethicone in consumer products such as skin protective ointment (Formula # 9286-018, contains ~ 9% of dimethicone and ~ 33.8% of cyclomethicone). The method was shown to be linear, accurate, precise, and specific.

Chapter 2 References

1. G.Torrado, A. Garcia-Arieta, F. de los Rios, J.C. *Menendez, Journal of Pharmaceutical and Biomedical Analysis*, 19, 285-292 (1999).

2. Alltech Application Note #0048E, Alltech Associates, Inc.

Chapter 3: Characterization of Fish Oil Supplements

3.1   Introduction of Fish Oil Supplements

3.1.1   Background

Fish oil is oil derived from the tissues of oily fish such as sardines and mackerel, etc. Fish oil is recommended for a healthy diet because it contains the omega-3 fatty acids. Omega-3 is the single most important essential nutrient that is almost entirely missing from our diets today. There is now overwhelming scientific evidence from thousands of clinical studies[1-12] that omega-3 can improve health and help prevent disease including lowering triglycerides, general heart benefits, improving brain functioning, as well as helping with diabetes, strokes, depression, arthritis, allergies, circulation problems, ADHD (Attention-deficit hyperactivity disorder), Alzheimer's, skin disorders, gout, and many others. In fact, the American Heart Association states "Healthy people, people at high risk of Cardiovascular Disease (CVD) and patients with preexisting CVD all benefit" and that "some people with high triglyceride (blood fats) and patients with CVD may benefit from more Omega-3 fatty acids than they can easily get from diet alone. These people should talk to their doctor about taking supplements to reduce heart disease risk." Because of the health benefits of the omega-3 fatty acids, there are loads of fish oil supplements under different brands on the market today.

Omega-3 fatty acids are a family of polyunsaturated fatty acids that have in common a final carbon–carbon double bond in the n-3 position, that is, the third bond from the methyl end of the fatty acid (See Figures 3-1 and 3-2). Important nutritionally essential n-3 fatty acids are: α-linolenic acid (ALA), eicosapentaenoic acid (EPA), and docosahexaenoic acid (DHA), all of which are polyunsaturated. These three

polyunsaturates have either 3, 5 or 6 double bonds in a carbon chain of 18, 20 or 22

carbon atoms, respectively. All double bonds are in the *cis*-configuration, i.e. the two

hydrogen atoms are on the same side of the double bond.

All the fish oil supplements claim active ingredients omega-3 fatty acids – EPA

and DHA. EPA and DHA play different roles in human body. DHA is important

component of cellular membranes and is highly concentrated in all nervous systems.

EPA is a precursor to a class of hormone-like chemicals called eicosanoids that reduce

inflammation throughout the body. The chemical structure of EPA is shown in Figure

3-1 and the chemical structure of DHA is shown in Figure 3-2.
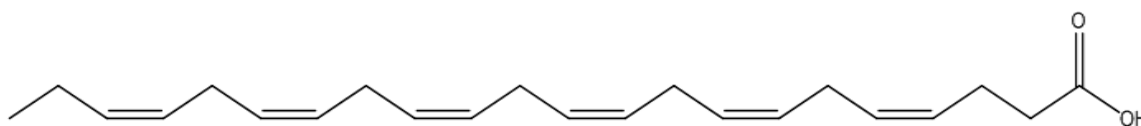
Figure 3-1   Chemical structure of EPA
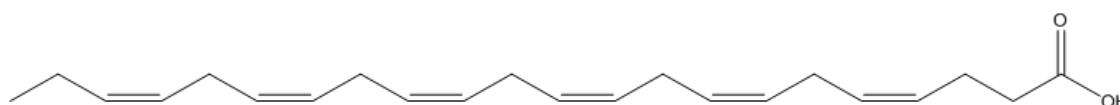
Figure 3-2   Chemical structure of DHA

Fatty fish like mackerel, lake trout, herring, sardines, albacore tuna and salmon

are high in omega-3 fatty acids, but these species are often predators, which can

accumulate toxic substances due to their position at the top of the food chain. For this

reason, many people have turned to fish oil supplements to get adequate omega-3 fatty

acids.

3.1.2   *Natural triglyceride and ethyl esters of EPA and DHA*

Natural triacylglycerol (TAG), it is also called triglyceride (TG), and ethyl ester concentrates are different chemical forms that supply the active ingredients of EPA and DHA in fish oil supplements that are currently available on the market. The chemical structures of triglyceride and ethyl ester of EPA are shown in Figures 3-3 and 3-4, respectively.
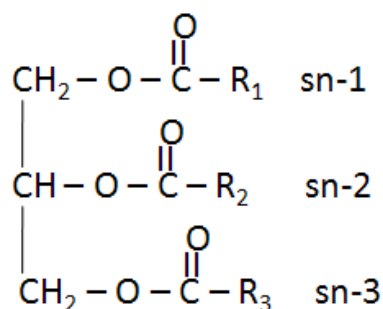
Figures 3-3   TAG where R's are EPA or DHA or combinations
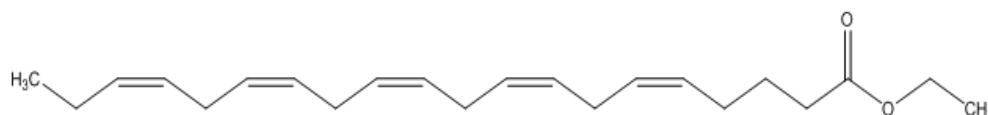
Figure 3-4   Ethyl ester of EPA

The term natural fish oil denotes that no synthetic chemicals are used/added during the processing and the omega-3 fatty acids remain in their natural state, the triglyceride form. Most natural fish oils have omega-3 content between 20-30%.

The ethyl ester concentrates are produced in a purification process where crude fish oil is reacted with ethanol to form a synthetic substrate called an omega-3 ethyl ester. Under vacuum, the solution is heat distilled ("molecular distillation") to separate the volatile component, the omega-3 ethyl ester. The resulting condensate is a concentrated omega-3 ethyl ester solution. The concentration of the omega-3 fatty acids depends on

the variables of the distillation process but normally results in a 50-70% omega-3 solution.

3.1.3   Fish Oil Production

Not all fish oil is created equal and it's important to understand the basics of fish oil production in order to understand which fish oil dietary supplement is the best. In fish oil production, fish oil is taken from the tissues of fatty fish and is then processed into the supplements that consumers take. If the fish oil product process includes a refining process, the label is likely to say that the fish oil supplement is "pharmaceutical grade" or that it is "molecularly distilled". An example process[13] of fish oil production is shown in the following steps:

1. Harvesting – Choose fish that provides fish oil with high EPA and DHA.

2. Washing – Wash out free fatty acids and other water soluble proteins.

3. Freezing – Get rid of excess saturated fats.

4. Filtration – Remove proteins and other volatiles that can make the oil smell bad. Also, any heavy metals or toxins are removed at this stage.

5. Steam-washing – Final clean and deodorization.

6. Natural Oil – Makes natural fish oil. No synthetic elements or chemicals have been added, and any environmental pollutants have been cleaned out. It is oil in nature form that is as a triglyceride.

7. Concentration – Triglyceride is difficult to concentrate, it also degrades easily. So to concentrate, a process of deconstruction and reconstruction need to be done.

8. Esterification – Break off the glycerol, and marries some ethanol to free fatty acid to form ethyl ester, a synthenic oil form that is easy to concentrate.

9. Molecular Distillation – This is vital stage of concentration. The ethyl esters are distilled at specific temperature that will evaporate unwanted fatty acids. So a certain heat will be good for long chain EPA and DHA, and the resulting distilled EPA and DHA is concentrated.

10. Reconstruction – Some manufacturers sell ethyl esters, but this synthetic format is not very bioavailable. So a further step is needed to reconstituting the synthetic ethyl esters back into natural form triglycerides. This can be done by mixing the ethyl esters with natural glycerol, and at a certain temperature the elements marry.

11. Super Refining –Further clean any remaining volatiles or impurities including any ethanol alcohol from the previous process. The result is super-refined concentrated omega-3 oil on a natural triglyceride form.

Fish oil supplements manufacturers could sell the products generated from above step 6 (EPA and DHA in triglyceride form but low concentration such as 20-30%, the natural fish oil), step 9 (EPA and DHA in ethyl ester form, high concentration such as 50 -70%, molecular distilled), and step 11 (EPA and DHA in triglyceride form, super-refined, high concentration such as 50%).

3.1.4   Fish Oil Absorption – Bioavailability

Fish oil absorption, i.e. the bioavailability of the natural triglycerides vs. synthetic ethyl esters is currently being debated in the medical arena. Recently, much emphasis has been placed on fish oil quality and purity but another important factor to be considered for fish oils is bioavailability. There were studies[14-15] that have addressed this issue and have presented evidence that fish oil in its natural triglyceride form is substantially better absorbed than the synthetic ethyl ester form. One of the apparent

reasons for the poor bioavailability of the ethyl ester form is due to its greater resistance to digestive enzymes. During the digestive process, pancreatic lipase enzymes hydrolyse (cleave) the oils to liberate the fatty acids. This stage of digestion prepares the fatty acids for subsequent absorption. The ethyl ester form has been demonstrated to be 10-50 times more resistant to this enzymatic process than the natural triglyceride form. Since our bodies can only use nutrients that get absorbed, consuming omega-3 fatty acids in their natural triglycerides form offers substantially better absorption over the ethyl ester form. These statements were part of a marketing campaign by NutraSea.

However, two of the studies[16-17] did not find a significant difference between the bioavailability of the triglyceride form of fish oil vs. the ethyl ester form. But no studies have shown the ethyl ester form to be superior. Minami Nutrition's marketing campaign states that several scientific studies revealed that post-24 hour absorption rates are identical and that ethyl esters may be the preferred form in the prevention of heart failure[18]. Because of the increasing controversy about absorption, it is very important then to characterize the fish oil supplements.

3.2   Objective of Fish Oil Supplement Characterization

As more health claims appear in the scientific literature, the market of fish oil supplements has rapidly expanded, and there are many different brands of the products sold in the local stores and online. Most of the products on the market claim the active ingredient EPA and DHA on the labels, but the chemical form of EPA and DHA are not indicated. This is misleading since most of consumers who are not familiar with the products may think that fish oil supplements contain EPA and DHA free acids.

Therefore, the consumer has no idea what form of DHA or EPA they are ingesting. Figure 3-5 shows a typical label of fish oil products without indication of the chemical form. Only a few products indicate the chemical form on the labels, for example Figure 3-6 shows a label that states the chemical form, "containing omega-3 fatty acids (as natural triglycerides) supplying EPA and DHA …".

Supplement Facts		
Serving Size:		2 Softgels
Servings Per Container:		50
Amount per Serving		
Calories Total	25	
from Fat	20	
		% Daily Value$^+$
Total Fat	2.5 g	4%
Saturated Fat	1 g	5%
Polyunsaturated fat	1 g	
Monounsaturated fat	0.5 g	
Cholesterol	25 mg	8%
Protein	2 g	
Fish Oil Concentrate	2400 mg*	
Omega-3 (EPA) Eicosapentaenoic Acid	360 mg*	
Omega-3 (DHA) Docosahexaenoic Acid	288 mg*	

* Daily Value not established.
+ Percent Daily Values are based on a 2,000 calorie diet. Your daily values may be higher or lower depending on your calorie needs.

Supplement Information:

1 bottle: 60 softgels
Serving size: 2 softgels

Servings per container: 30 (1 month supply)

3cm 2cm 1cm 0cm

Supplement	Amount per serving	% Daily value
Calories	13	
Calories from fat	13	
Total Fat	1.4 g	2%
Cholesterol	0 mg	
Fish oil	1400 mg	*
Vitamin E (as d-alpha tocopherol)	33.3 IU	111%
containting omega-3 fatty acids (as natural triglycerides) supplying	840 mg	*
EPA (eicosapentaenoic acid)	420 mg	*
DHA (docosahexaenoic acid)	280 mg	*
Other Omega-3 fatty acids	140 mg	*
Total tocopherols, natural	200 mg	*
Total tocotrienols, natural	28 mg	*
Coenzyme Q10	20 mg	*

*Daily Value not established

Figure 3-5 A typical fish oil product label   Figure 3-6 An example of correct label

Since bioavailability of fish oil supplements is related to the chemical form of DHA and EPA, it is necessary to develop a quick qualitative screening method to identify the chemical form of the active ingredients EPA and DHA in fish oil products.

Also, there are only a few fish oil manufacturers but many distributors and hundreds of products on the market with vastly different prices. It would be interesting to find out the fish oil supplements that possibly made by the same manufacturers with equal quality but sold under different brands and prices.

With rapid increasing of the market for health foods enriched with omega-3 fatty acids including DHA and EPA, the quality of these important nutrients in marine products should be strictly controlled. For this purpose polyunsaturated fatty acids in fish and fish oils are routinely analyzed by gas chromatography (GC)[19-22]. However, GC methods are time-consuming, involve considerable manipulation steps that may cause oxidation of lipids, may give variable results depending on the columns used, and pose difficulty in correctly identifying each fatty acid in the chromatograms[23]. The GC method does not provide any information on whether the supplements contain triglyceride or ethyl ester forms of the essential omega-3 fatty acids.

FTIR has been widely used for the analysis of edible oils and fats[24-29], such as analysis of free fatty acids, the content of trans-double bonds, oxidation of fatty acids, characterization, authentication of vegetable oils, etc. There were also few studies[30-31] on the determination of polyunsaturated fatty acids in pork fat and vegetable oils using ATR-FTIR supported by multivariate statistical methods. Raman spectroscopy has also been used for the analysis of cis/trans-isomer ratio of oils and fats[32], the level of conjugated fatty acids in milk fat[33], oil and fat classification[34], predictions of various single fatty acids[35], and characterization of the degree of fatty acid unsaturation of salmon[36]. ^{1}H nuclear magnetic resonance (^{1}H NMR) in the study of oils and fats has already been reviewed[37]. It has been recently shown that polyunsaturated fatty acids in fish and fish oils could be determined ^{1}H and ^{13}C NMR (carbon nuclear magnetic resonance) spectroscopy[38-39].

Even though there are many publications about the analysis of fatty acids and esters in dietary oils and fats using various techniques as listed above, currently there

were no reports on the characterization of fish oil supplements using FTIR and Raman. Therefore, the goal of this research project was to utilize ATR-FTIR and Micro-Raman, which are non-destructive and require no sample preparation, to develop a quick qualitative screening method to identify the chemical form of the active ingredients EPA and DHA in fish oil products, to classify the fish oil supplements on the markets by means of principle component analysis, to develop a method for quantitative analysis of EPA and DHA using standard addition approach, and to study the temperature dependent spectral properties of polyunsaturated fatty acids such as EPA esters using 2D IR correlation analysis.

3.3 Qualitative Characterization of Fish Oil Supplements by ATR-FTIR

3.3.1 Fish Oil Samples and Reference Material

About 75 different brands of fish oil supplement samples were purchased from local grocery and drug stores, and online. Most of the samples were in the form of softgels with others being liquid. An example list of products together with the chemical forms, manufacturers, distributors, and label claims, etc. are summarized in Table 3-1.

The reference standards of triglyceride of EPA and DHA, ethyl ester of EPA and DHA, were purchased in > 99% purity from Nu-Chek Prep. Inc. (Elysian, MN).

3.6.2 ATR-FTIR Instrumentation and Spectral Acquisition

A Bruker Equinox 55 FTIR spectrometer (Bruker Optics, Billerica, MA) fitted with a DuroScope (Smith's Detection System, Danbury, CT) diamond ATR and equipped with a DTGS (Deuterated Triglycine Sulfate) detector was used to measure the IR spectra of fish oil samples. The reference standard material or fish oil supplement liquids (~ 40 uL) were placed on the single bounced diamond ATR crystal with a micro

pipette. One hundred (100) co-added scans were taken and averaged and measurements were taken at a resolution of 4 cm^{-1} between 4000 - 400 cm^{-1}. The background was collected before every sample was measured. After each sample analysis, the diamond ATR crystal was cleaned with acetone.

3.3.3   Software Assistance

The software BioRad's KnowItAll version 7.0 (BioRad, Philadelphia, PA) was used for spectra evaluation and reports. Advanced Chemical Development (ACD) Curve Manager version 9.0 (Toronto, Ontario, Canada) was used for band assignments and database building. Thermo Galactic's Spectral ID software version 3.02 (Thermo-Fisher Scientific, Waltham, MA) was used for building the IR spectra library of fish oil supplements to determine sample similarities and/or differences. Camo Unscrambler Version 9.7 (Edison, NJ) was used for chemometrics - principle components analysis.

3.3.4   ATR-FTIR Spectra Analysis and Discussion

Total about 50 fish oil samples were analyzed with ATR-FTIR. Figure 3-7 shows one of the typical FTIR Spectra of fish oil supplement samples (MaxEPA Fish Oil Concentration). The corresponding band assignments are tabulated in Table 3-2. The assignments of the major bands referenced some of the early studies of the IR spectra of fatty acids and esters in edible oils and fats by Guillen and Cabo[40] and book *Spectral Properties of Lipids* by Richard J. Hamilton (page 241-242). Although fish oil sample spectra seem to be similar, they show differences in the intensity of their bands as well as in the exact frequency at which the maximum absorbance is produced in each case, due to the different nature and composition of fish oils under study.

Table 3-1   Fish Oil Supplement Sample List

Fish Oil Supplement Name	Form of EPA and DHA	Manufacturer	Distributor
Barleans Fresh Catch Fish Oil Omega-3 EPA/DHA	x*	Barlean's Organic Oils	x
California Health Omega 3-6-9 Essential Oils	x	x	California Health
Carlson Super-DHA 500 mg of DHA	x	x	J.R. Carlson Lab
Carlson Fish Oil liquid from Norway	x	x	J.R. Carlson Lab
Eskim -3 Fish Oil Ultra-pure Omega-3	x	x	Enzymatic Therapy
GNC Fish Body Oils 1000	x	x	GNC
Health from the Sea PFO Pure Fish Oil	x	x	Arkopharma
Health from the Sun Total EFA Omega 3-6-9	x	x	Arkopharma
Iceland Health Max strength Omega-3	x	x	Iceland Health, Inc.
Jean Carper's Omega T Formular	tryglyceride	x	Stop Aging now
Jarrow Formulas Max DHA liquid	tryglyceride	x	Jarrow Formulars
KAL MaxEPA 180 EPA 120 DHA	x	Nutracetical Corp	x
The Original MaxEPA 1000 mg Omega-3 Fish Oils	x	x	Mason Vitamins
Minami MorEPA 581 EPA 70 DHA	ethyl ester	x	Minami Nutrition Inc.
Mind 1st PuraEPA 300 EPA Borage Oil	x	x	www.mindist.co.uk
EFAs Natrol Omega-3 Fish Oil 1000 mg	x	x	Natrol, Inc.
Natrure's plus EPA and DHA Omega 3 Complete	x	x	Natures's Plus
Natrures Weigh Essential Fatty Acids	x	x	x
Natrures Weigh MaxEPA Omega-3 1000 mg	x	x	x
Nature Answer EPA Fish Oil EPA/DHA Blend 1000 mg	x	Nature's Answer	x
Nature Made Omega-3 Fish Oil 1200 mg	x	x	Nature Made Nutri. Prod.
Natures Bounty Norwedgian Cod Liver Oil	x	Nature's Bounty, Inc	x
Natures Bounty Omega 3-6-9 Fish Flax Borage, 1200 mg	x	Nature's Bounty, Inc	x
Natures Bounty Omega-3/Omega-6 Fish Oil 1200 mg	x	Nature's Bounty, Inc	x
Natures Bounty Organic Flax Oil, 1200 mg	x	Nature's Bounty, Inc	x
Natures Bounty Vitamin E pure d-alpha	x	Nature's Bounty, Inc	x
Nordic Naturals Ultimate Omega	triglyceride	Nordic Naturlas	x
Now High Potency DHA 250 EPA 100 mg	x	Now Foods	x

Table 3-1 Continued

Now Omega-3 Fish Oil Liquid	x	Now Foods	x
Olympian Labs Superior Glyceride Omega-3 Fish Oils Liquid	triglyceride	x	Olympian Labs
OmacorOmega-3-acid Ethyl Esters	ethyl ester	Cardinal Health	Reliant Pharmacetical
Pathmark Natural Omega-3 180 EPA 120 DHA	triglyceride	x	Pathmark
PharmAssure Fish Body Oil EPA 240 mg DHA 200 mg	x	x	PharmAssure Inc.
PharmAssure Flax Seed Oil	x	x	PharmAssure Inc.
PharmAssure Megasol (concentrated EPA DHA)	x	x	PharmAssure Inc.
PharmAssure Omega 3-6-9 1200 mg Borage Flax Fish Oils	x	x	PharmAssure Inc.
Rite Aid Borage-Fish-Flax Oil Omega 3-6-9	x	x	Rite Aid Corporation
Rite Aid Fish oil 1000 mg	x	x	Rite Aid Corporation
RxOmega-3 Factors Pharm Grade EPA 400 mg/DHA 200mg	x	Natural Factors	Natural Factors
RxOmega-3 Factors Pharm Grade Liquid 1500 epa 750 dha	x	Natural Factors	Natural Factors
Shop Rite Norwegian Cod Liver Oil	x	x	Wakefern Food Corp.
Solaray Samon Oil	x	Nutrcetical Corp.	Solaray
Solgar Natural MaxEPA Fish Oil Concentrate	x	x	Solgar Vitamin and Herb
Source Naturals ArticPure DHA cap	x	Source Naturals, Inc	x
SourceNaturals Neuromins DHA 200 mg	x	Source Naturals, Inc	x
Spectrum Norwegian fish oil EPA 180 / DHA120	x	x	Spectrum Essentials
Sundown Fish oil 1000 mg	x	x	Rexall Sundown. Inc
Sundown Salmon oil 1000 mg	x	Sundown, Inc.	x
Vitamin Shoppe Mega Fish Oil EPA-DHA	x	x	The Vitamin Shoppe
VSB Basics EPA/DHA 180/120	x	x	The Vitamin Shoppe
Walgreens Finest Naturals Extra Strength Fish Oil Concentrate	x	x	Walgreen Co.
WINOmeg3 Complex EPA-DHA 60/15	ethyl ester	x	Wellness Internatinal Network.
xtendlife Omega 3 DHA Esters	ethyl ester	Xtend-Life Nature Product	x
* x means unknown			
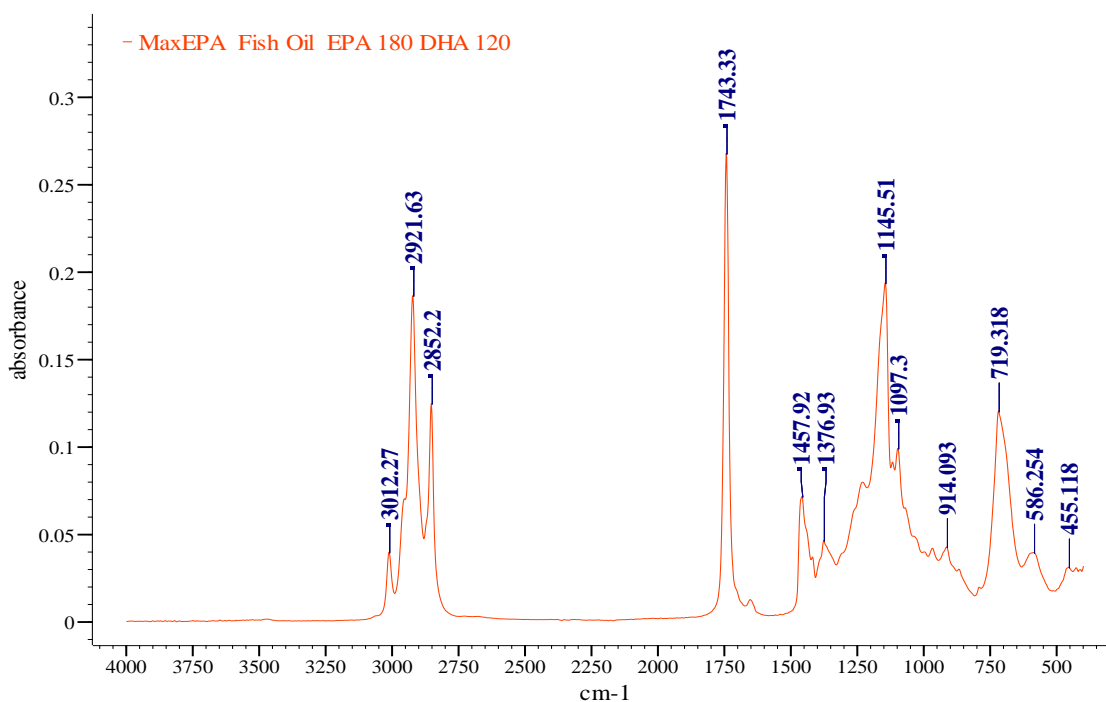
Figure 3-7   A typical FTIR spectrum of fish oil supplements

Table 3-2   Major characteristic IR absorption bands of fish oils

Approx. Band Positions (cm^{-1})	Assignments
3012	=C-H (cis, stretching)
2954	-C-H (CH$_3$ groups, asym stretching)
2921	-C-H (CH$_2$ groups, asym stretching)
2852	-C-H (CH$_2$ and CH$_3$ groups, sym stretching)
1743	-C=O (ester stretching)
1653	-C=C- (cis double bond stretching)
1457	-C-H (CH$_2$ scissoring bending)
1376	-C-H (CH$_3$ sym bending)
1230	-C-O, CH$_2$ (stretching , bending)
1145	-C-O (stretching)
1097	-C-O (stretching)
968	=C-H (trans, bending out of plane)
914	=C-H (cis, bending out of plane)
719	-(CH$_2$)$_n$, =C-H cis (rocking, bending out)

In general, the position of the band due to the C-H stretching vibration of *cis*

double bonds (=C-H) depends on the number of double bonds in the fatty acid chain,

shifting from 3005 cm^{-1} for one double bond (such as C18:1) to 3012 cm^{-1} for multiple

double bonds (such as C20:5 and C22:6). Study[31] has showed that the band at 3012 cm^{-1}

is caused mainly by the increase of polyunsaturated fatty acids such as EPA and DHA,

and therefore this band can be used as a marker for the analysis of total EPA and DHA

esters in fish oil samples. It can be expected that the ratios between the bands due to

=CH– cis group (3012 cm^{-1}) and the bands due to –CH$_2$– groups (2921 cm^{-1} or 2852

cm[-1]) may be used to compare the EPA and DHA contents in the fish oil supplements.

Higher ratios (typically of band height) indicate higher total EPA and DHA concentration

(in ester forms). For example, Figure 3-8 shows the FTIR spectra of two samples

MaxEPA Fish Oil Concentration and Jean Carpers Omega T formula, it is obvious that

the ratio of the band heights at 3012 cm^{-1} and 2923 cm^{-1} is higher for Jean Carpers Omega

T formula. This indicates that Jean Carpers Omega T formula contains higher

concentration of total EPA and DHA triglycerides.
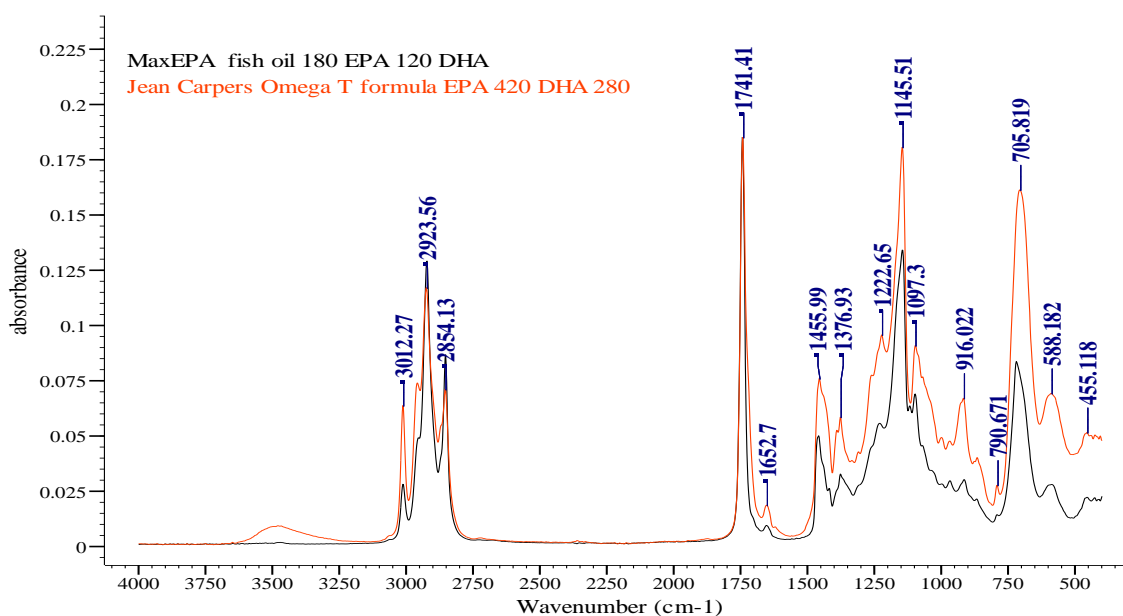
Figure 3-8   FTIR spectra of samples MaxEPA Fish Oil Concentration and Jean
              Carpers Omega T formula

Four reference standards, triglycerides of EPA and DHA, ethyl esters of EPA and DHA, were analyzed with ATR-FTIR, and the spectra of the four compounds are shown in Figures 3-9 and 3-10.
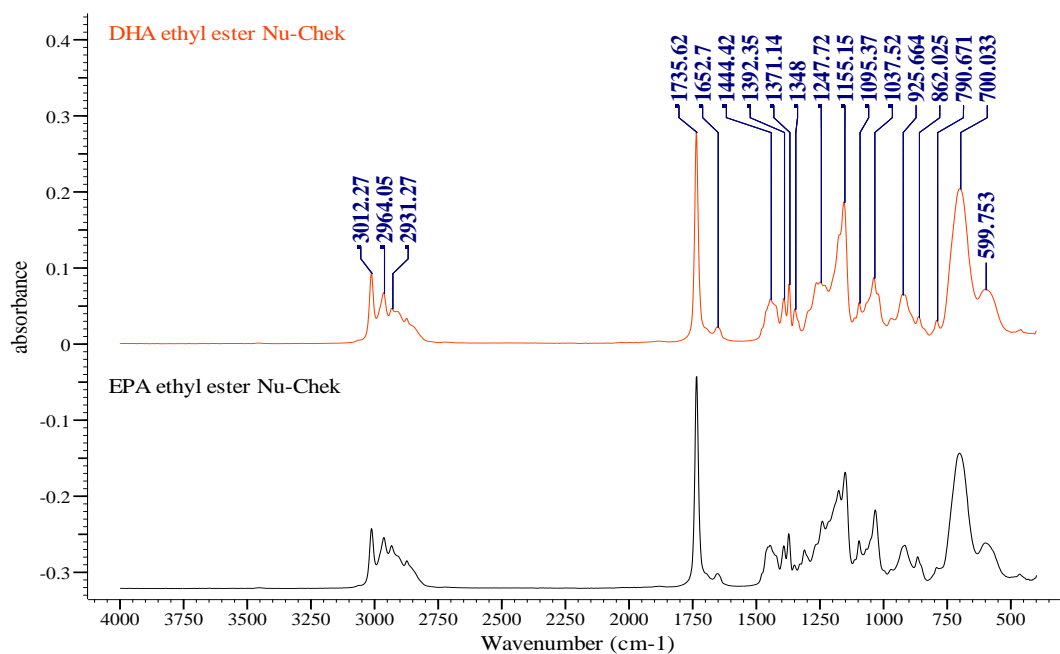
Figure 3-9   FTIR spectra of ethyl esters of EPA and DHA
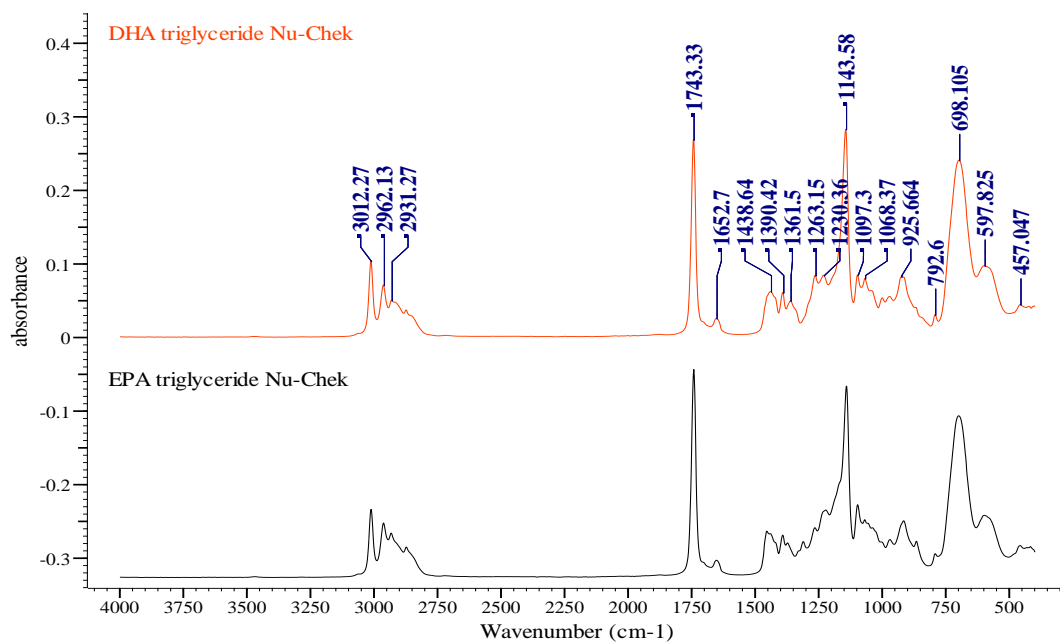
Figure 3-10   FTIR spectra of triglycerides of EPA and DHA

The FTIR spectra showed that the maximum absorption of the carbonyl functional group in ethyl esters is at ~ 1735 cm^{-1}, and in triglycerides is at ~ 1742 cm^{-1}. This can be easily used to differentiate these compounds and identify the chemical forms of the active ingredients EPA and DHA in fish oil supplements. Figure 3-11 shows the carbonyl IR band of the four compounds.
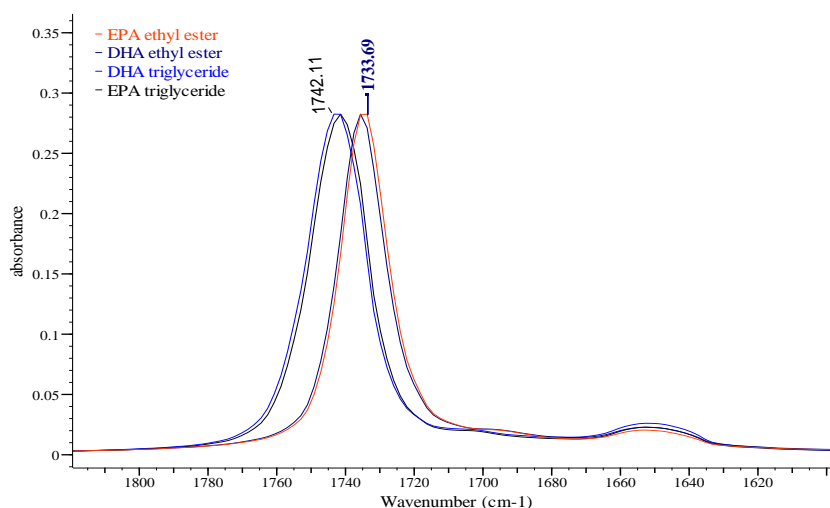
Figure 3-11   The carbonyl bands of the four reference standards

Figure 3-12 shows the carbonyl (ester) band position comparison of some representative fish oil supplements such as MaxEPA, Natures Weigh, Barleans, Minami MorEPA, Jean Carpers together with DHA ethyl ester standard. The carbonyl band maximum absorption is at ~ 1743 cm^{-1} for MaxEPA, Natures Weigh, Barleans, and Jean Carpers, and this indicates that these samples contain EPA, DHA and other fatty acids in triglyceride form. The carbonyl band maximum absorption is at ~ 1736 cm^{-1} for Minami MorEPA and DHA ethyl ester standard, and this indicates that these samples contain EPA, DHA and other fatty acids in ethyl ester form.
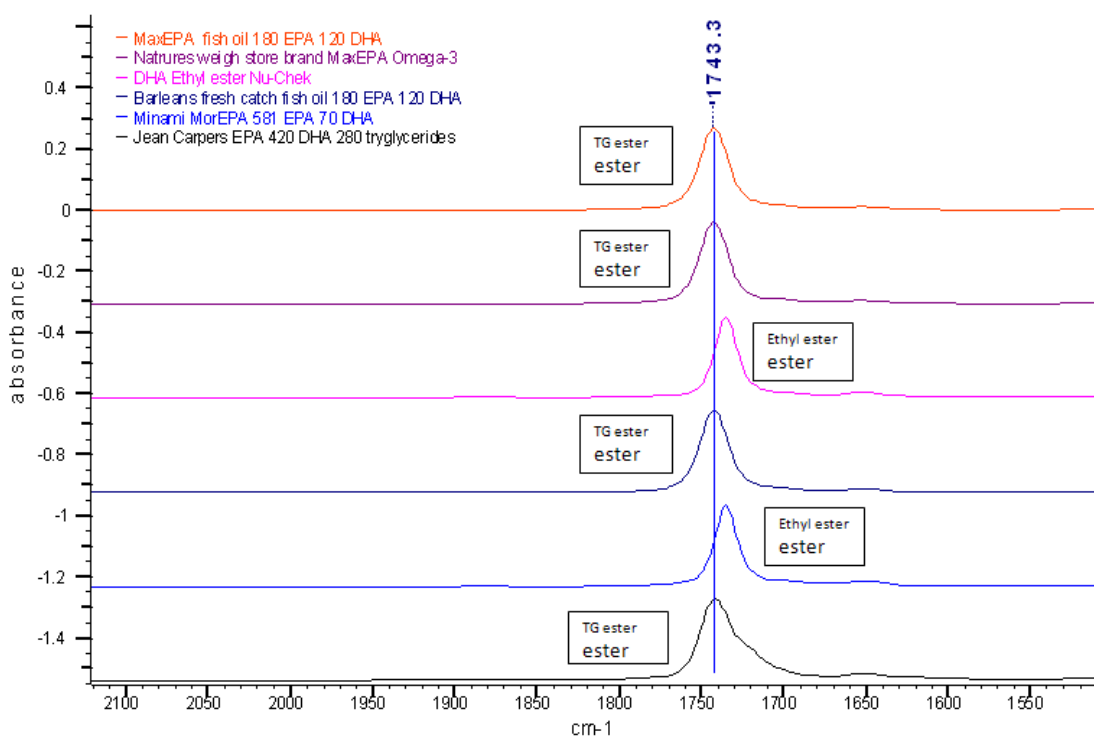
Figure 3-12   Differentiate fish oil supplements with –C=O (ester) bands

In addition, the FTIR spectra showed a strong C-O stretching band at ~ 1153 cm^{-1} for ethyl esters of EPA and DHA, and at ~ 1143 cm^{-1} for triglycerides of EPA and DHA This may also be used to differentiate the chemical forms of EPA and DHA in fish oil supplements depending on the composition of samples.

3.3.5   *Principle Components Analysis (PCA) of FTIR Spectra*

PCA was applied in this study to identify the similarities and differences between sample spectra and therefore to view the interrelationships among the commercial fish oil supplements and to detect and interpret sample patterns and groupings (classification).

Software Camo Unscrambler, Version 9.7, was used for the PCA analysis. The analysis parameters are as follows:

Sample Sets: 47;   Variable Sets: 510 – 1940 cm^{-1}, 2700 – 3210 cm^{-1}

Center data;   Number of PCs: 6;   Model Size: Full.

Since the spectra showed very good repeatability for the same sample analyzed multiple times on the same and different days, there was no spectra pre-treatment performed before PCA analysis. Figure 3-13 shows the overlay spectra of sample MaxEPA Fish Oil Concentration which was analyzed at different time (on 03/19/07 and 04/14/07). The three spectra superimpose very well. In order to further demonstrate the spectra differences of the three samples, Figure 3-14 shows the subtracted spectra of MaxEPA fish oil r2_04-14-17 and MaxEPA fish oil_03-19-07 from the reference spectrum of MaxEPA fish oil r1_04-14-17. The subtracted spectra appear to be virtually straight line. This indicated that the FTIR spectra of fish oil samples collected at different days and different runs (r1 and r2 during the same day) are very close to each other, and therefore, no further spectrum treatments are required for PCA analysis.
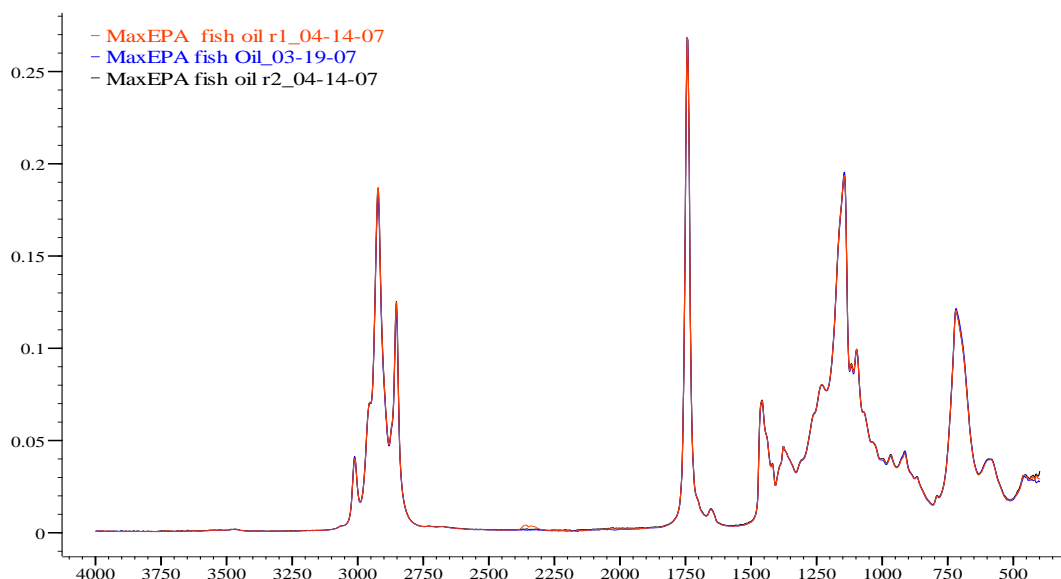
Figure 3-13   Overlay spectra of the MaxEPA Fish Oil Concentrate
analyzed at different time
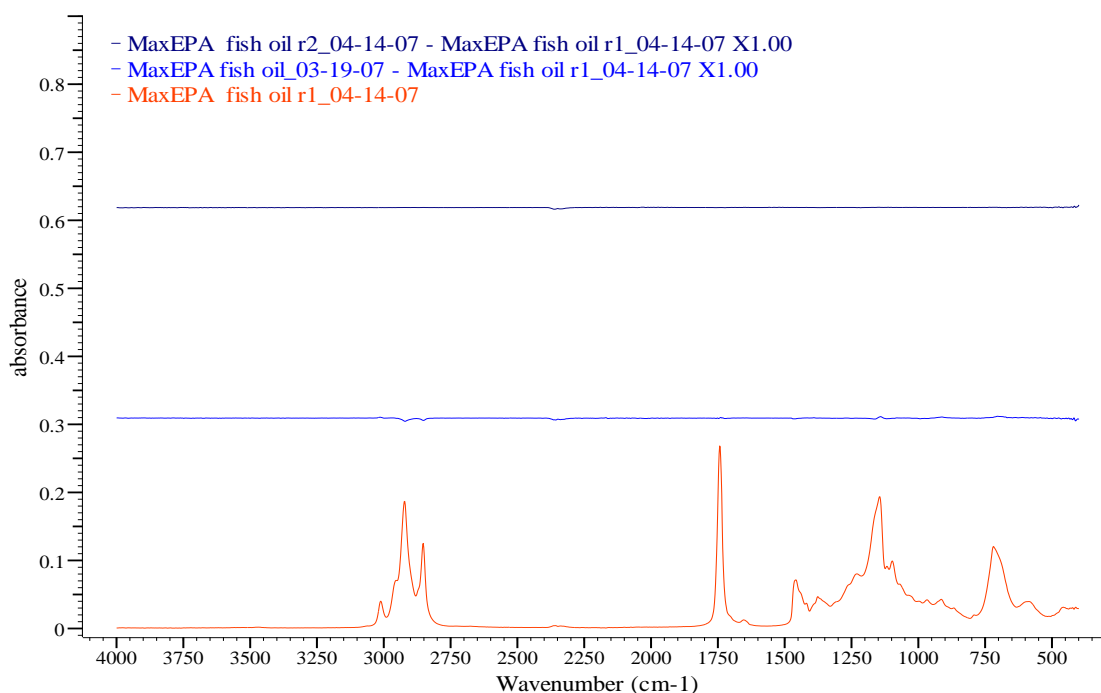
Figure 3-14   Subtracted spectra of MaxEPA fish oil r2_04-14-17and MaxEPA fish
oil_03-19-07 against reference spectrum of MaxEPA fish oil r1_04-14-17

The most commonly used plot in PCA is the score plot for PC1 versus PC2 since

these are the two directions along which the data swarm exhibits the largest and the

second largest variances. The PCA scores plot (PC1 vs. PC2) of the FTIR spectra of 47

fish oil supplements is shown in Figure 3-15. The first two principle components (PC1

and PC2) made up 94% of the variance. The corresponding PCA loadings plot (PC1 vs.

PC2) is shown in Figure 3-16. Each number in the PCA scores plot stands for a

particular fish oil supplement sample. Four groups (I, II, III, and IV) of spectra were

clearly separated from negative to positive values of the first score PC1. The loading plot

indicated the corresponding possible variables that differentiated each group. The PC1

was mainly related to the band position of ester carbonyl group in the samples. The fish

oil supplements containing fatty acids in ethyl ester form, which showed a C=O

absorption band at ~ 1735 cm^{-1}, were clustered into group I. The fish oil supplements containing fatty acids in triglyceride form, which showed a C=O absorption band at ~ 1742 cm^{-1}, were clustered into group IV.
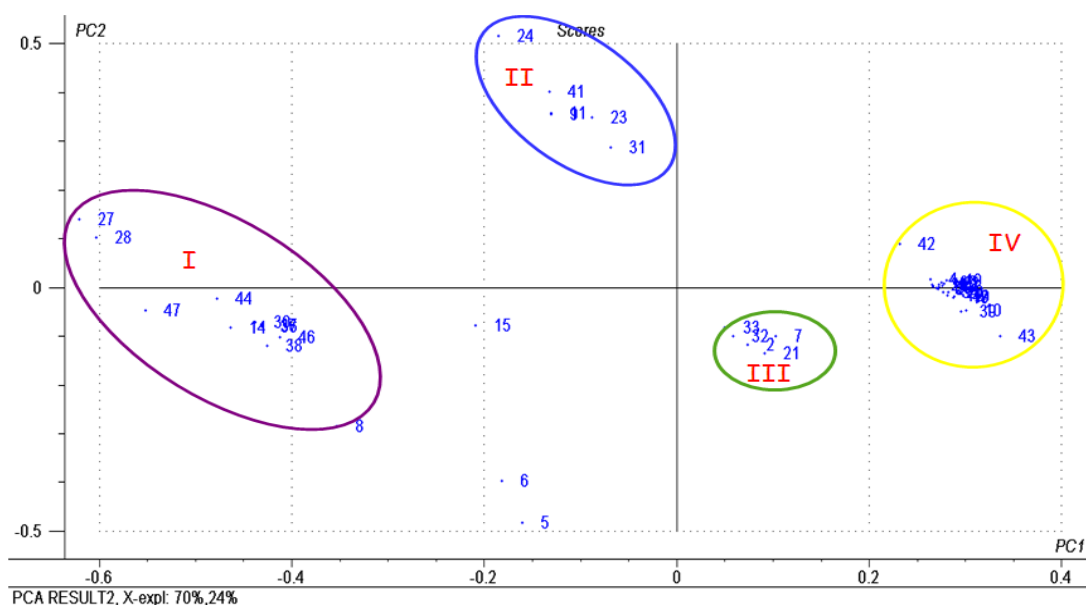
Figure 3-15   PCA scores plot (PC1 vs. PC2) of FTIR spectra of fish oil supplements
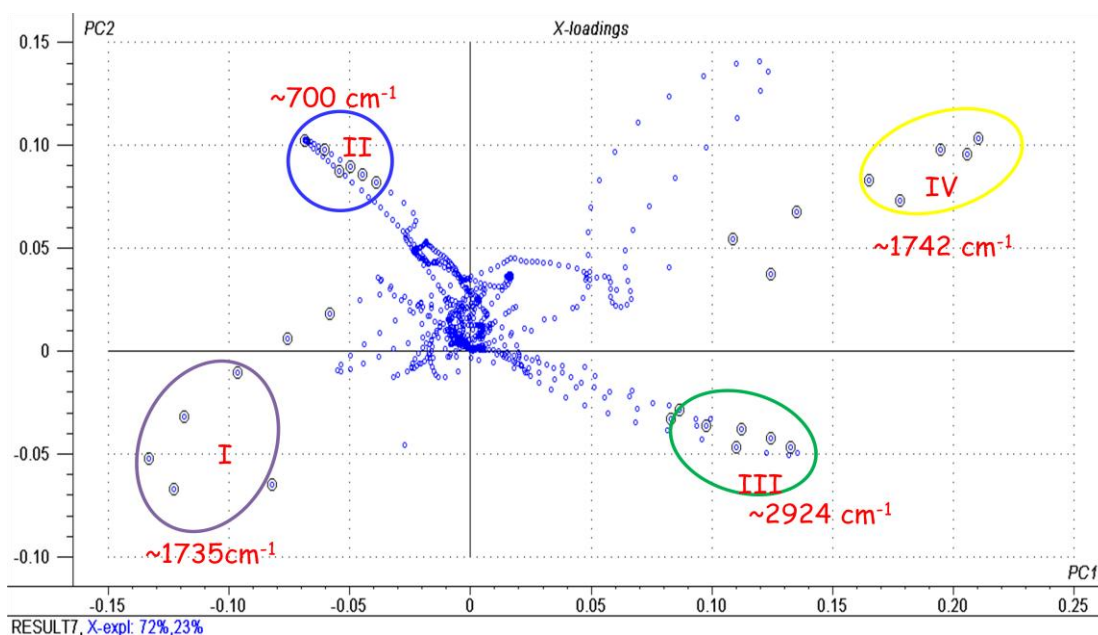
Figure 3-16   PCA loading plot (PC1 vs. PC2)

It seems that the PC2 was related to the concentration of polyunsaturated fatty acids such as EPA and DHA esters in the samples. The supplements with relative high IR intensity at ~ 2923 cm^{-1}, which was due to –C-H- (CH$_2$ groups) asymmetric stretching and also indicated low concentration of total EPA and DHA esters, were clustered into group III. Fish oil samples with relative high intensity at ~ 700 cm^{-1}, which was mainly due to =C-H (*cis*) bending and therefore showed higher EPA and DHA ester contents, are clustered into group II.

The fish oil supplements in group I are summarized in the Table 3-3, and the corresponding spectra of six representative samples are showed in Figure 3-17. As discussed above, fish oil supplements containing fatty acids including EPA and DHA in ethyl ester form were clustered in group I. There are total 8 samples (out of 47) in this group, only 3 samples indicated ethyl ester form on the product labels. Hence, the rest 5 samples should also contain EPA and DHA in ethyl ester form. The manufacturers of most of these products were unknown (x means unknown in table 3-3), but they were distributed by different drug stores and companies. Omacor (sample # 27) is the only prescription fish oil product on the market currently. The fish oil concentrates in this group are molecularly distilled as an ethyl ester. The prices of these products are various. The most common total EPA and DHA ethyl ester concentration is about 50% to 70%.

Table 3-3   Fish Oil Supplements in Group I by PCA Analysis

Sample #	Group #	Fish Oil Supplement	Form of EPA and DHA	Manufacturers	Distributors	Total mg per Softgel	EPA mg per Softgel	DHA mg per Softgel	Price $ per 1000 mg
14	I	Minami MorEPA 581 EPA 70 DHA	ethy lester	x*	Minami Nutrition Inc.	x	581	70	0.41
30	I	PharmAssure Fish Body Oil EPA 240 mg DHA 200 mg	x	x	PharmAssure Inc.	870	240	200	0.10
37	I	RxOmega-3 Factors Pharm Grade 400 EPA 200 DHA	x	Natural Factors	Natural Factors	1065	400	200	0.10
38	I	RxOmega-3 Factors Pharm Grade Liquid 1500 EPA 750 DHA	x	Natural Factors	Natural Factors	4400/5mL	1500/5mL	750/5mL	0.85
44	I	Vitamin Shoppe Mega Fish Oil EPA-DHA	x	x	The Vitamin Shoppe	x	300	120	0.28
46	I	Walgreens Finest Naturals Extra Strength Fish Oil Concentrate	x	x	Walgreen Co.	880	260	175	0.11
47	I	WINOmeg3 Complex EPA-DHA 60/15	ethyl ester	x	Wellness Internatinal Net.	x	540	160	0.97
27	I	Omacor 465 EPA 375 DHA Ethyl Esters	ethyl ester	Cardinal Health	Reliant Pharmacetical	1000	465	375	x
* x means unknown									
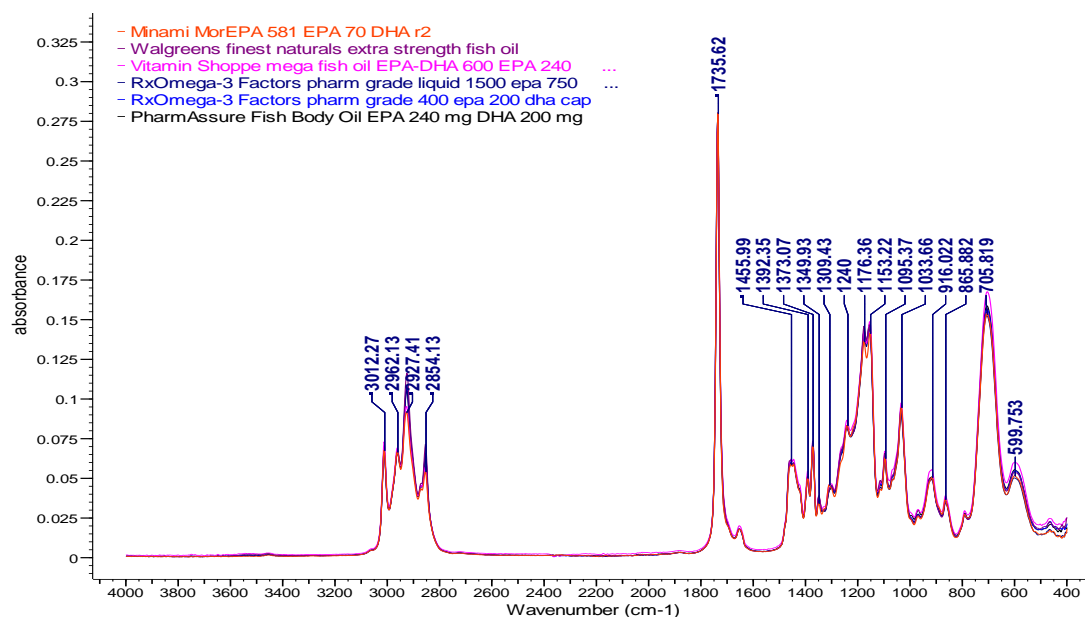
Figure 3-17   FTIR spectra of six fish oil samples in group I

The spectra are very similar including the band positions and intensities for the six samples in Figure 3-18. This indicated that the fish oil compositions (total concentration of EPA and DHA ethyl esters and others) of the samples are very similar even though their prices are quite different range from $ 0.10 to $ 0.41 per ~ 1000 mg fish oil (generally one capsule).

The fish oil supplements in group II are summarized in the Table 3-4, and the corresponding spectra of the samples are showed in Figure 3-18. Fish oil supplements containing fatty acids in triglyceride form but high total concentration of EPA and DHA triglycerides (more than 50%) are clustered in group II. There are total 6 samples (out of 47) in this group, two samples indicated triglyceride form on the product labels. None of the concentrated fish oils are "*Natural*" even though in triglyceride form. The concentrated triglyceride fish oils are also molecularly distilled before chemically, or enzymatically, forcing the fatty acids back onto the glycerol backbone, turning it into an

altered triglyceride, not a "*Natural"* triglyceride. The enriched triglycerides may have abnormal fatty acid distributions on the glycerol backbone, and this information is rarely provided. Therefore no bioavailability information specifically on the altered triglyceride is available. The concentrated triglyceride form of fish oil is selling for about the similar prices as the ethyl ester form, and in some cases, considerably more.

Table 3-4   Fish Oil Supplements in Group II by PCA Analysis

Sample #	Group #	Fish Oil Supplement	Form of EPA and DHA	Manufacturer	Distributor	Total mg per Softgel	EPA mg per Softgel	DHA mg per Softgel	Price $ per 1000 mg
9	II	Jean Carper's Omega T formular	triglyceride	x*	Stop Aging Now	700	240	140	0.43
23	II	Nordic Naturals Ultimate Omega 325 EPA 225 EPA	triglyceride	Nordic Naturlas	x	500	160	115	0.56
24	II	Now High Potency DHA 250 EPA 100 mg	x	Now Foods	x	625	100	250	0.15
31	II	PharmAssure Megasol (concentrated EPA DHA)	x	x	PharmAssure Inc.	~500	160	110	0.66
41	II	Source Naturals ArticPure DHA	x	x	Source Naturals, Inc.	600	275	40	0.16
* x means unknown									
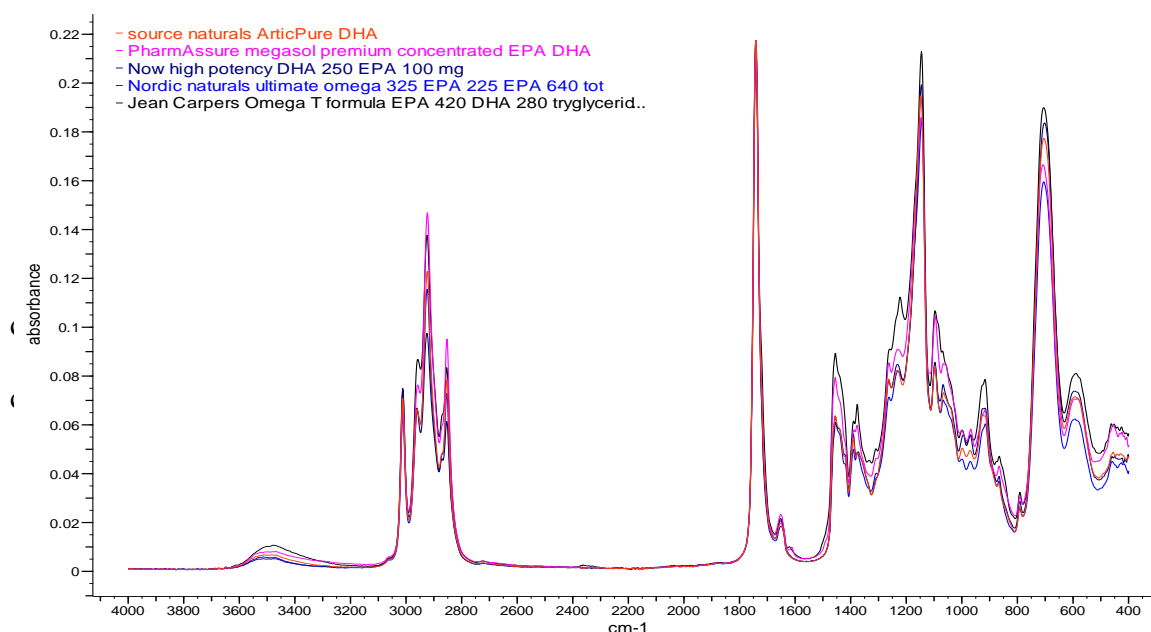
Figure 3-18   FTIR spectra of fish oil samples in group II

The fish oil supplements in group III are summarized in the Table 3-5, and the corresponding spectra of the samples are showed in Figure 3-19. Fish oil supplements containing omega 3, 6, and 9 fatty acids in triglyceride form were clustered in group III. There are total 5 samples (out of 47) in this group, and none of the samples indicated the chemical form on the product labels. The omega 3, 6 and 9 groups of fatty acids contain all essential fatty acids (EFA) necessary for good health. The difference between them lies in the position of the first double bond from the omega end of the carbon chain. As its name implies, the omega-3 fatty acids have their first double bond at the 3rd position from the end of the chain, and likewise with the other two. Omega-6 has its first double bond at the 6th position from the end and omega-9 has it at the 9th position from the end of the chain. Less research has been done on omega-6 than on Omega-3 EFA's. Most omega-6 fatty acids produce an inflammatory response that may be necessary for healthy immune system function. Omega-9 oils are monounsaturated, and are found in olive oil, and may be necessary for healthy immune system functioning. The fish oil supplements in group III contain high concentration of omega-6 and 9 fatty acid triglyceride, and low concentration of total EPA and DHA triglyceride (less than 20%). Only one product indicates the manufacturer (The Nature's Bounty, Inc) on the label. The FTIR spectra of the five samples were very similar to each other, and this indicated that there are no much differences among these products in terms of chemical form and compositions. The selling prices of the products are also comparable.

Table 3-5   Fish Oil Supplements in Group III by PCA Analysis

Sample #	Group #	Fish Oil Supplements	Form of EPA and DHA	Manufacturer	Distributor	Total mg per Softgel	EPA mg per Softgel	DHA mg per Softgel	Price $ per 1000 mg
2	III	California Health Omega 3-6-9 Essential Oils	x*	x	California Health	1200	120	80	0.23
7	III	Health from the Sun Total EFA Omega 3-6-9	x	x	Arkopharma	x	112	77	0.22
21	III	Natures Bounty Omega 3-6-9 Fish Flax Borage, 1200 mg	x	Nature's Bounty, Inc	x	1200	120	80	0.18
32	III	PharmAssure Omega 3-6-9 1200 mg Borage Flax Fish Oils	x	x	PharmAssure Inc.	1200	132	88	x
33	III	Rite Aid Borage-Fish-Flax Oil Omega 3-6-9	x	x	Rite Aid Corporation	x	132	88	x
* x means unknown									
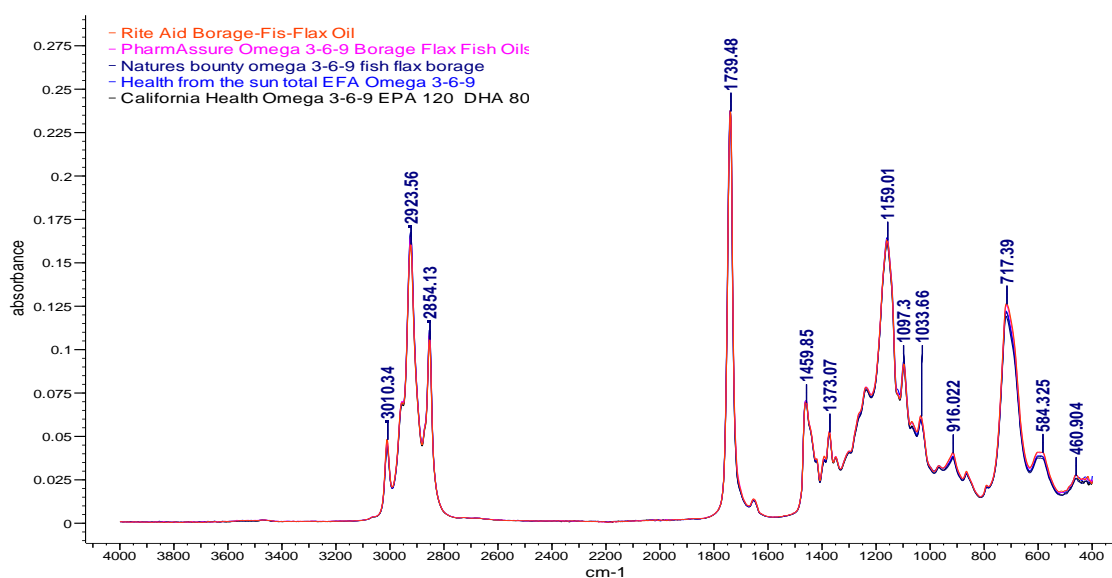
Figure 3-19   IR spectra of fish oil samples in group III

The fish oil supplements in the group IV are summarized in the Table 3-6, and the example spectra of six of the samples are shown in Figure 3-20. Fish oil supplements containing fatty acids in triglyceride form but lower concentration of total EPA and DHA (compare to group II) were clustered in group IV. Most of the fish oil supplements (total 21 out of 47 samples) are in this group, and only 2 of the samples indicated the chemical form on the product labels. The products in group IV contain natural fish oil that is about 30% EPA and DHA along with other fatty acid triglyceride. The most common EPA and

DHA ratio in natural fish oil is 18:12, meaning that the average 1,000 mg fish

oil capsule contains 180 mg of EPA and 120 mg of DHA triglyceride. Although natural

fish oils offer half the EPA and DHA concentration of ethyl ester fish oil (group I), it is

generally claimed that they are 2-3 times better absorbed by the body. Considering the

higher cost of ethyl ester concentrates, it could be that natural fish oils represent a much

better value for omega-3 supplementation. The spectra of the six samples in Figure 3-20

are almost identical and this may indicate that these products were made by the same

manufactures but sold by different distributors with wide range of prices from 6 to 20

cents per capsule.

Table 3-6   Fish Oil Supplements in the Group IV by PCA Analysis

Sample #	Group #	Fish Oil Supplement	Form of EPA and DHA	Manufacturer	Distributor	Total mg per Softgel	EPA mg per Softgel	DHA mg per Softgel	Price $ per 1000 mg
1	IV	Barleans Fresh Catch Fish Oil Omega-3 EPA/DHA	x*	Barlean's Organic Oils	x	1000	180	120	0.10
3	IV	Carlson Fish Oil Liquid from Norway	x	x	J.R. Carlson Lab	5ml	800/5ml	500/5ml	0.11
4	IV	Eskim -3 Fish Oil Ultra-pure Omega-3	x	x	Enzymatic Therapy	x	70	45	0.20
10	IV	Jarrow Formulas Max DHA Liquid	triglyceride	x	Jarrow Formulars	5mL	425-600	740-850	0.06
12	IV	KAL MaxEPA 180 EPA 120 DHA	x	Nutracetical Corp	x	1000	180	120	0.16
13	IV	The Original MaxEPA 1000 mg Omega-3 Fish Oils	x	x	Mason Vitamins	1000	180	120	0.11
16	IV	EFAs Natrol Omega-3 Fish Oil 1000 mg	x	x	Natrol, Inc.	1000	180	120	0.06
17	IV	Natrure's Weigh Essential Fatty Acids	x	x	Natures's Weigh	1200	69	46	0.11
18	IV	Natrures Weigh MaxEPA Omega-3	x	x	Natures's Weigh	1000	180	120	0.16
19	IV	Nature Answer Fish Oil EPA/DHA Blend 1000 mg	x	x	Nature's Answer	1000	180	120	0.07
20	IV	Nature Made Omega-3 Fish Oil 1200 mg	x	x	Nature Made Nutri. Prod.	1200	216	144	0.12
22	IV	Natures Bounty Omega-3/Omega-6 Fish Oil 1200 mg	x	Nature's Bounty, Inc	x	1200	216	144	0.10
25	IV	Now Omega-3 Fish Oil Liquid Molecular Distilled	x	Now Foods	x	5 ml	740/5ml	475/5ml	0.06
26	IV	Olympian Labs Superior Glyceride Omega-3 Fish Oils Liquid	x	Olympian Labs	x	x	740	460	0.10
29	IV	Pathmark Natural Omega-3 180 EPA 120 DHA	triglyceride	x	Pathmark	1000	180	120	x
34	IV	Rite Aid Fish Oil 1000 mg	x	x	Rite Aid Corporation	x	180	120	0.03
39	IV	Solaray Samon Oil	x	Nutrcetical Corp.	Solaray	1000	130	70	0.11
40	IV	Solgar Natural MaxEPA Fish oil Concentrate	x	x	Solgar Vitamin and Herb	1000	180	120	0.11
42	IV	Source Naturals Neuromins DHA 200 mg	x	x	Source Naturals, Inc	x	no	200	0.34
43	IV	Sundown Salmon Oil 1000 mg	x	Sundown, Inc.	x	1000	180	120	0.64
45	IV	VSB Basics EPA/DHA 180/120	x	x	The Vitamin Shoppe	x	180	120	0.06

* x means unknown
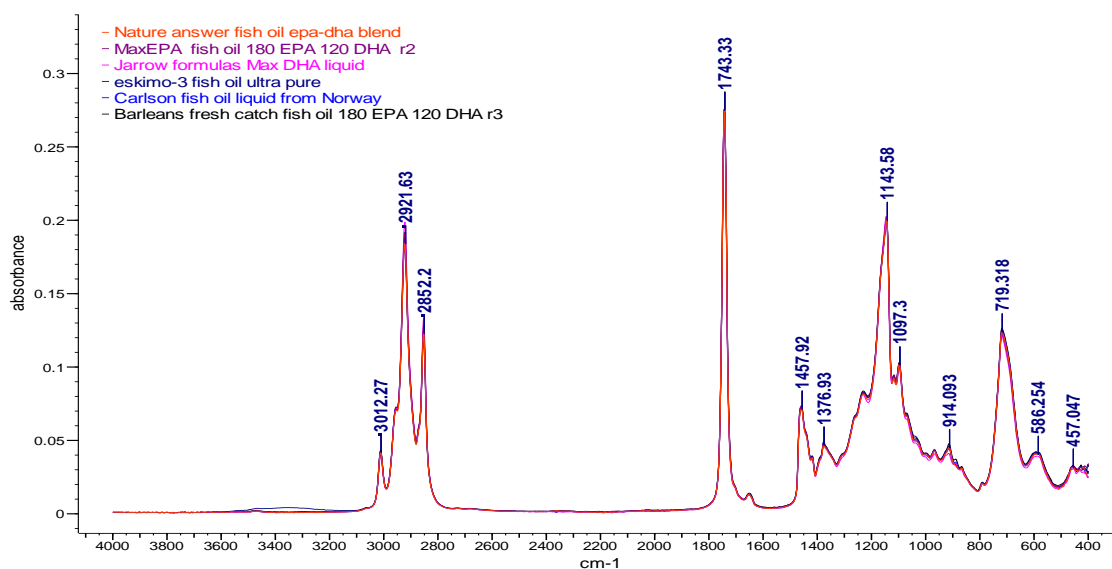
Figure 3-20   FTIR spectra of 6 fish oil samples in group IV

In summary, principal component analysis of ATR-FTIR spectra successfully classified the fish oil supplements under this study. The fish oil supplements are clearly clustered into the following four groups:

I.   Fish oil supplements containing fatty acids in ethyl ester form, the total EPA and DHA concentration is about $50 - 70\%$.

II.   Fish oil supplements containing fatty acids in triglyceride form, the total EPA and DHA concentration is more than 50%.

III.   Fish oil supplements containing omega 3, 6, and 9 fatty acids in triglyceride form, the total EPA and DHA concentration is less than 20%.

IV.   Fish oil supplements containing fatty acids in triglyceride form, the total EPA and DHA concentration is about 30%.

Most fish oil supplements (21 out of 47 samples) belong to group IV, which are nature fish oils and are believed to be better absorbed by body. Considering the relatively low price of this group, it would be a better option for omega-3 supplementation.

Based on the studies summarized in sections 3.3.4 and 3.3.5, the chemical forms of the studied fish oil supplements are identified and summarized in Table 3-7.

Table 3-7   Identified Chemical Forms of Fish Oil Supplements

Fish Oil Supplements	Labeled Form of EPA and DHA	Identified Form of EPA and DHA	Price $ per 1000 mg	Group #
Barleans Fresh Catch Fish Oil Omega-3 EPA/DHA	x*	triglyceride	0.10	IV
California Health Omega 3-6-9 Essential Oils	x	triglyceride	0.23	III
Carlson Fish Oil Liquid from Norway	x	triglyceride	0.11	IV
EFAs Natrol Omega-3 Fish Oil 1000 mg	x	triglyceride	0.06	IV
Eskim -3 Fish Oil Ultra-pure Omega-3	x	triglyceride	0.20	IV
Health from the Sun Total EFA Omega 3-6-9	x	triglyceride	0.22	III
Jarrow Formulas Max DHA Liquid	triglyceride	triglyceride	0.06	IV
Jean Carper's Omega T formular	triglyceride	triglyceride	0.43	II
KAL MaxEPA 180 EPA 120 DHA	x	triglyceride	0.16	IV
Minami MorEPA 581 EPA 70 DHA	ethyl ester	ethyl ester	0.41	I
Natrure's Weigh Essential Fatty Acids	x	triglyceride	0.11	IV
Natrures Weigh MaxEPA Omega-3	x	triglyceride	0.16	IV
Nature Answer Fish Oil EPA/DHA Blend 1000 mg	x	triglyceride	0.07	IV
Nature Made Omega-3 Fish Oil 1200 mg	x	triglyceride	0.12	IV
Natures Bounty Omega 3-6-9 Fish Flax Borage, 1200 mg	x	triglyceride	0.18	III
Natures Bounty Omega-3/Omega-6 Fish Oil 1200 mg	x	triglyceride	0.10	IV
Nordic Naturals Ultimate Omega 325 EPA 225 EPA	triglyceride	triglyceride	0.56	II
Now High Potency DHA 250 EPA 100 mg	x	triglyceride	0.15	II
Now Omega-3 Fish Oil Liquid Molecular Distilled	x	triglyceride	0.06	IV
Olympian Labs Superior Glyceride Omega-3 Fish Oils Liquid	x	triglyceride	0.10	IV
Omacor 465 EPA 375 DHA Ethyl Esters	ethyl ester	ethyl ester	x	I
Pathmark Natural Omega-3 180 EPA 120 DHA	triglyceride	triglyceride	x	IV
PharmAssure Fish Body Oil EPA 240 mg DHA 200 mg	x	ethyl ester	0.10	I
PharmAssure Megasol (concentrated EPA DHA)	x	triglyceride	0.66	II
PharmAssure Omega 3-6-9 1200 mg Borage Flax Fish Oils	x	triglyceride	x	III
Rite Aid Borage-Fish-Flax Oil Omega 3-6-9	x	triglyceride	x	III
Rite Aid Fish Oil 1000 mg	x	triglyceride	0.03	IV
RxOmega-3 Factors Pharm Grade 400 EPA 200 DHA	x	ethyl ester	0.10	I
RxOmega-3 Factors Pharm Grade Liquid 1500 EPA 750 DHA	x	ethyl ester	0.85	I
Solaray Samon Oil	x	triglyceride	0.11	IV
Solgar Natural MaxEPA Fish oil Concentrate	x	triglyceride	0.11	IV
Source Naturals ArticPure DHA	x	triglyceride	0.16	II
Source Naturals Neuromins DHA 200 mg	x	triglyceride	0.34	IV
Sundown Salmon Oil 1000 mg	x	triglyceride	0.64	IV
The Original MaxEPA 1000 mg Omega-3 Fish Oils	x	triglyceride	0.11	IV
Vitamin Shoppe Mega Fish Oil EPA-DHA	x	ethyl ester	0.28	I
VSB Basics EPA/DHA 180/120	x	triglyceride	0.06	IV
Walgreens Finest Naturals Extra Strength Fish Oil Concentrate	x	ethyl ester	0.11	I
WINOmeg3 Complex EPA-DHA 60/15	ethyl ester	ethyl ester	0.97	I

* x means unknown

3.3.6   IR Spectra Library of Fish Oil Supplements

Thermo Galactic Spectral ID version 3.02 was used to create a FTIR spectral library of fish oil supplements. A library file including the spectra of all the fish oil supplements was created in Spectral ID as a database to determine similarity and/or differences among the samples. The library can be used for rapid searching and product comparison every time a new fish oil supplement is analyzed.

Spectral ID optical spectral data searching of an unknown versus library spectra uses seven search algorithms. These seven algorithms were compared to determine the best search method based on Hit Quality Index (HQI) for the spectra of fish oil supplements. The 7 algorithms are: Euclidian Distance, Absolute Value, First Derivative, Least Squares, First Derivative Least Squares, Correlation, and First Derivative Correlation.

The First Derivative Correlation Algorithm method was chosen in this study. This algorithm is the same as the correlation algorithm except that the first derivative of both the unknown and library spectra are taken before calculating the HQI. In Correlation Algorithm, both the unknown and the library data are centered about their respective means before the vector dot products are calculated based on the equation 3-1:

$$HQI = 1 - (Lib_m \cdot Unk_m)^2/(Lib_m \cdot Lib_m)(Unkn_m \cdot Unkn_m) \qquad (3\text{-}1)$$

where the vectors are defined as the follows:

$$Lib_m = Lib - (\textstyle\sum_{i=1}^{n} Lib_i)/n \qquad\qquad Unkn_m = Unkn - (\textstyle\sum_{i=1}^{n} Unkn_i)/n$$

The mean centering step has one very important effect: the HQI is independent of the normalization of the spectra. In the other algorithms such as Euclidian Distance, the spectra must be normalized first before the calculation for library search. Even though the Correlation algorithm can compensate for signal-to-noise fluctuations and negative drop, it cannot correct for bad baselines. First derivative-based search algorithm attempts to remove the non-linear effects of the baseline. Therefore, the First Derivative Correlation Algorithm method was used for this study.

The interpretation of the HQI was based on the values from searching the library that contained the identical sample analyzed at a different time. This HQI established the appropriate value that was acceptable as being a "perfect match" between an unknown fish oil supplement and those in the library.   For example, for the FTIR spectrum from MaxEPA fish oil supplement was analyzed three times. Run 1 and Run 2 were added to the fish oil supplement library. Then Run 3 was searched against the library and a HQI value was determined to be 0.0007 (~0.001). This established that if a fish oil supplement was identical to MaxEPA, its HQI should be ~ 0.001. Further visual inspection of the spectra can reveal differences or similarities between the searches and assist the analyst in making the final decision about association between the two samples. It should be noted that the spectra should be in absorbance units for the search.

Figure 3-21 shows an application of the spectral ID library search. The spectrum of MaxEPA fish oil was searched against the library for fish oil supplements, and the HQI of 0.0009 - 0.0015 together with visual inspection showed that the spectrum of MaxEPA matched the spectra of five other fish oil products. This quickly demonstrated that all these products are very similar and may be made by the same manufacturer.
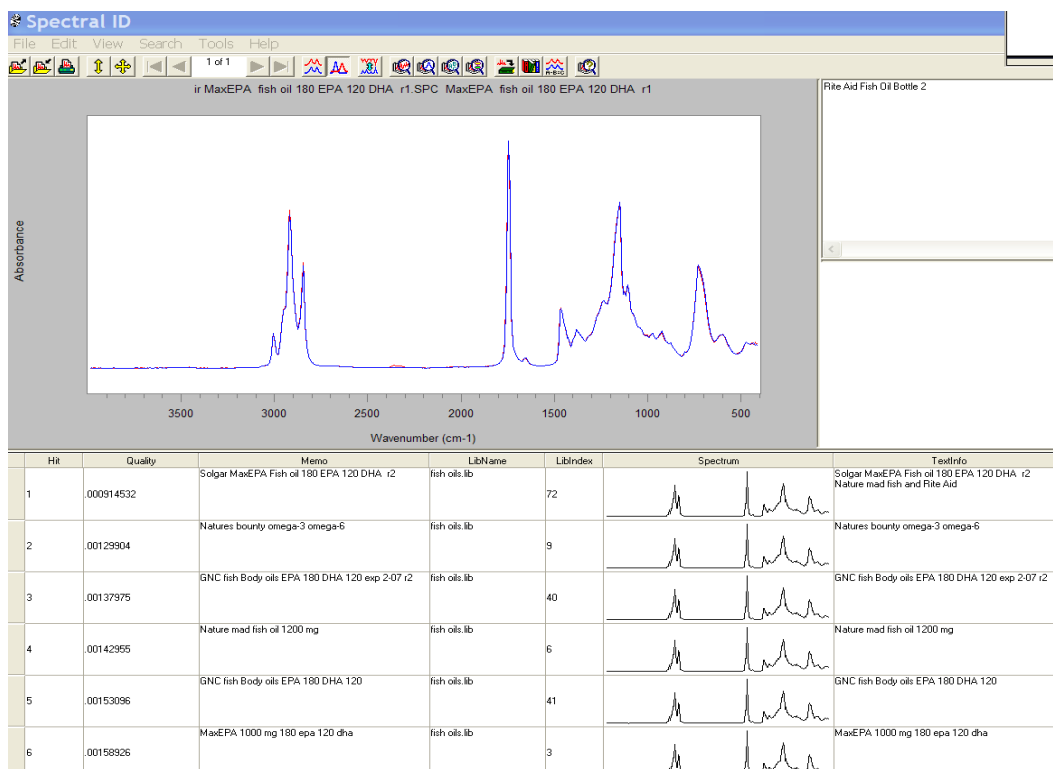
Figure 3-21   An example of spectral ID library search

3.4   Qualitative Characterization of Fish Oil Supplements by Micro-Raman

3.4.1   *Fish Oil Samples and Reference Material*

Reference Section 3.3.1.

3.4.2   *Micro-Raman Instrumentation and Spectral Acquisition*

A Renishaw 1000 Raman micro-spectrometer equipped with a highly sensitive

charged-coupled detector (CCD, which has a high quantum efficiency allowing detection

of ultra-low levels of light) and a long-wavelength 750 nm excitation lasers was used to

measure the spectra of fish oil supplements. The instrument was calibrated using pure

silicon daily before sample measurement. The reference standard material or fish oil

supplement liquids (~ 10 uL) were placed on aluminum foil substrate. The measurements

were taken in the Raman shift range of 1800 - 500 cm^{-1}. The background was collected

before every sample was measured. The other spectral acquisition parameters are as

follows:

- 50 mm slit width   - 50x objective

- 2 mm spot size   - 25 mW power

- 20s exposure time   - 5 accumulations

3.4.3   *Software Assistance*

The software BioRad's KnowItAll version 7.0 (BioRad, Philadelphia, PA) was

used for spectra evaluation and reports. Advanced Chemical Development (ACD) Curve

Manager version 9.0 (Toronto, Ontario, Canada) was used for band assignments and

database building. Camo Unscrambler Version 9.7 (Edison, NJ) was used for

Chemometrics - Principle Components Analysis.

3.4.4   *Micro-Raman Spectra Analysis and Discussion*

The reference standard ethyl ester of EPA was first applied on glass substrate for

Raman analysis and the signal was totally covered by fluorescence background. The

Raman signal was enhanced when the samples were analyzed on aluminum (Al) substrate.

This may be due to surface enhanced Raman scattering (SERS) affect. In the rest of the

studies, the samples were deposited on Al foil for spectra measurement. Figure 3-22

compares the Raman spectra of ethyl ester of EPA collected on glass and Al slides.

The Raman spectra of four reference standards, triglycerides of EPA and DHA

and ethyl esters of EPA and DHA, are shown in Figure 3-23. The major band assignments

are listed in Table 3-8 (referenced a critical evaluation of Raman spectroscopy for the

analysis of lipid by J. Renwick Besttie, etc. [41]). Figure 3-24 shows some example Raman spectra of fish oil supplements.
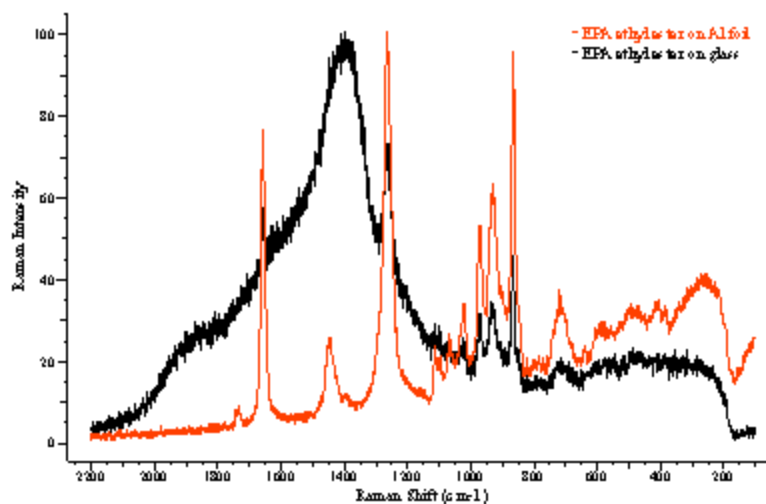
Figure 3-22   Raman spectra of ethyl ester of EPA collected on glass and Al slides
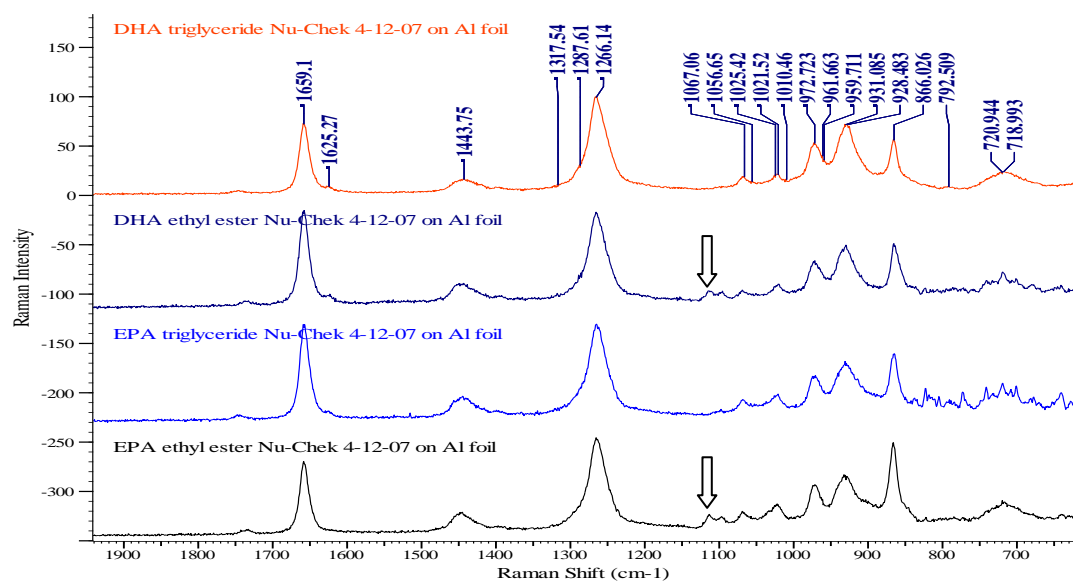
Figure 3-23   Raman spectra of 4 reference standards
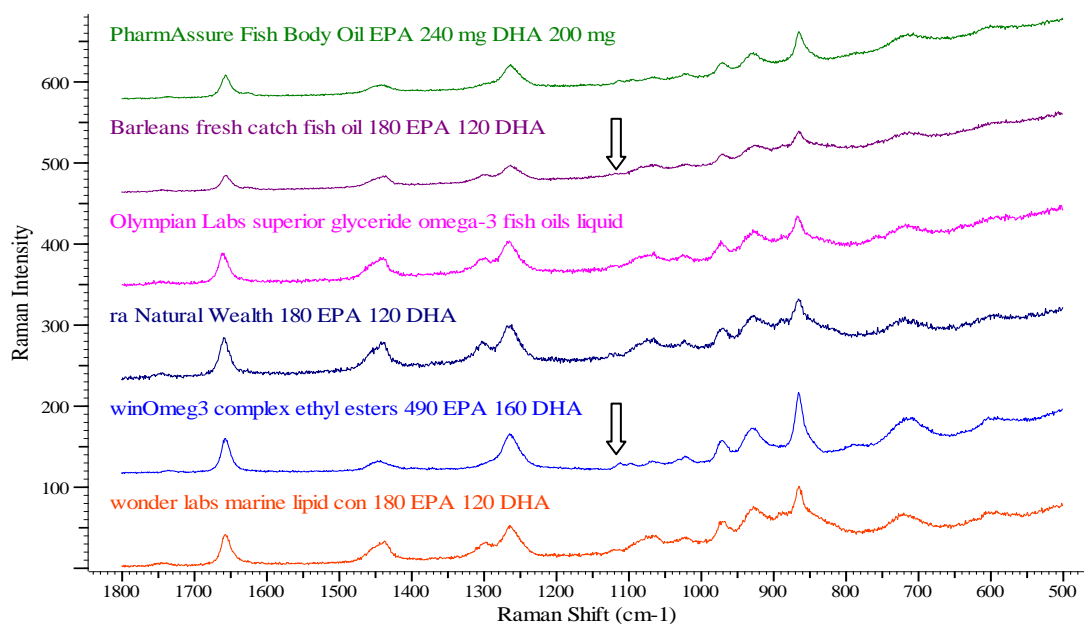
Figure 3-24   Examples of Raman spectra of fish oil supplements

Table 3-8   Major Raman Band Assignments of Fish Oils

Approx. Band Positions (cm^{-1})	Assignments
1730 - 1750	-C=O (carbonyl stretching)
1640 - 1665	-C=C- (cis double bond stretching)
1400 - 1500	-C-H (CH$_2$ scissoring bending)
1295 - 1305	-C-H (CH$_2$ twisting bending)
1250 - 1280	=C-H (In-plane CH bending)
1100 - 1135	-C-C (in-phase stretching, all-*trans*)
1080 - 1110	-C-C (liquid: stretching *in gauche*)
1060 - 1065	-C-C (out-of-phase stretching, all-*trans*)
~ 972	=C-H out-of-plane bending
~ 931/866	-C-C/C-O (mixture of stretches)

The Raman spectra of the four reference standards are very similar as shown in Figure 3-24. The major band positions at Raman shifts 1659 cm^{-1}, 1444 cm^{-1}, 1266 cm^{-1}, 972 cm^{-1}, 930 cm^{-1}, and 866 cm^{-1} are the same for both triglycerides of EPA and DHA and ethyl esters of EPA and DHA. A small band at ~1110 cm^{-1} was observed in the spectra of ethyl esters of EPA and DHA, but not observed in the spectra of triglycerides

of EPA and DHA, and hence, this band may be used as a marker to differentiate the two chemical forms. However, this band (arrow pointed at ~ 1110 cm^{-1}) is almost invisible in the spectra of fish oil samples as shown in Figure 3-24. Even though the reference standards which are colorless and exhibit good Raman signals, all the fish oil samples (with yellowish color) exhibit weak Raman signals due to florescence background (yellow color usually is an indication of florescence absorption). Therefore, there is no specific Raman band can be easily used to identify the chemical form of the fatty acids in the fish oil supplements under this study.

Raman is a complementary technique to FTIR. For example, in Raman, the bands (1658 cm^{-1} and 1266 cm^{-1}) related to non-polar functional group C=C are intense whereas in the FTIR they are weak. The band at ~ 1732 cm^{-1} related to polar functional group C=O is very weak in Raman but intense in FTIR. Figure 3-25 shows the comparison of IR and Raman spectra of ethyl ester of EPA.
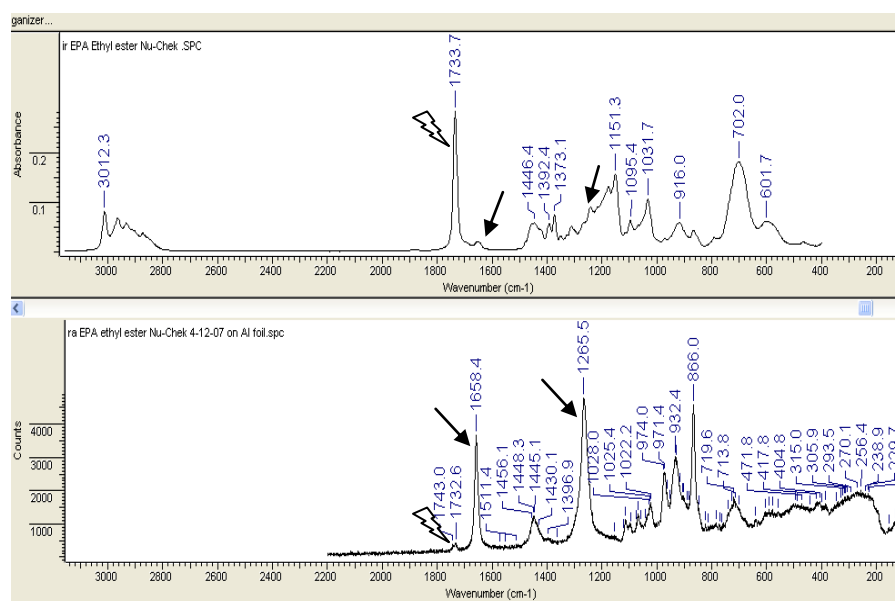
Figure 3-25   Comparison of IR and Raman spectra of ethyl ester of EPA

3.4.5   Principle Components Analysis of Raman Spectra

Total about 55 samples were analyzed by Micro-Raman. PCA was applied on the

spectra and to detect and interpret sample patterns and groupings for classification of fish

oil supplements. Software Camo Unscrambler, Version 9.7, was used for the PCA

analysis. The analysis parameters are as follows:

- Sample Sets: 54   - Center data;

- Number of PCs: 6   - Model Size: Full

- Variable Sets: 510 – 1800 cm^{-1}, full spectra range

Since the spectra baseline shifts between each sample analysis and the Raman

signals are weak with noisy baseline, all the spectra were first smoothed and then 1st

derivative (Savitsky-Golay, polynomial – 1 and smooth points - 25) was performed

before PCA analysis.

Figure 3-26 shows the PCA scores plot (PC1 vs. PC2) of the Raman spectra of

fish oil supplements. Figure 3-27 shows the corresponding loading plot (PC1 vs.

variables).   Each number in the PCA scores plot stands for a particular fish oil

supplement sample. Roughly four groups (I, II, III, and IV) of spectra were separated

from negative to positive values of the first score PC1. The corresponding loading plot

was also evaluated and it seemed that the band at Raman shift ~ 866 cm^{-1} (-C-C/C-O

stretching) was the major variable for PC1. There was essentially no sample distribution

along PC2 and this means that the contribution of PC2 to spectra grouping was minimal.

The first two principle components (PC1 and PC2) made up 71% of the variances.

Figures 3-28 to 3-31 show the PCA scores plots of PC1 vs. PC3, PC1 vs. PC4, PC1 vs.

PC4, and PC1 vs. PC6. Similar to the scores plot of PC1 vs. PC2, the samples were

meanly grouped along PC1. The contributions from other PCs for the sample grouping were not obvious.
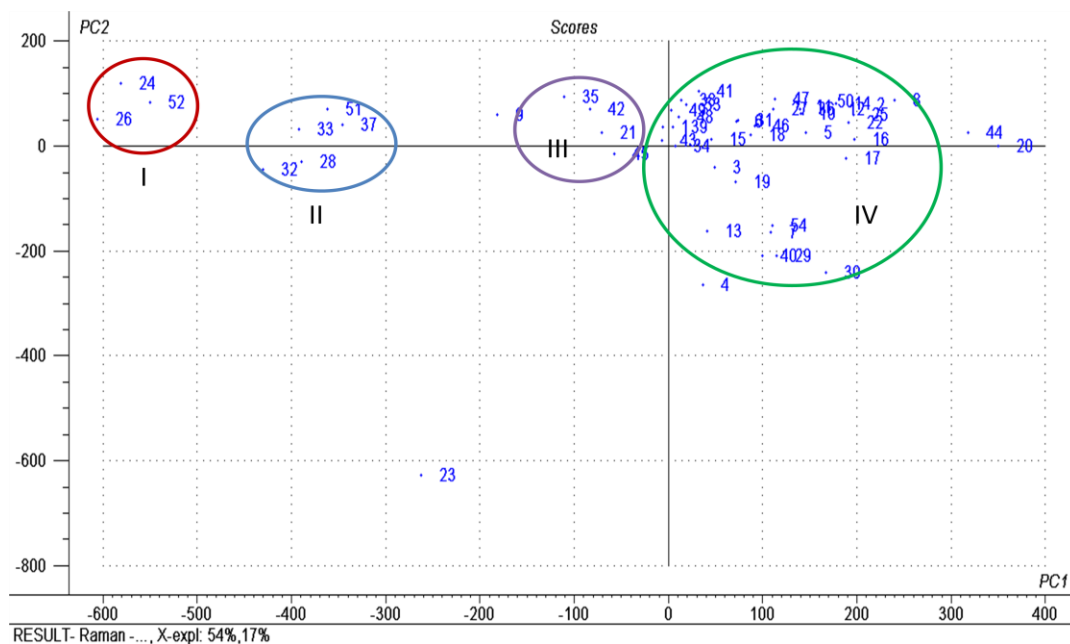
Figure 3-26   PCA scores plot (PC1 vs. PC2) of Raman spectra
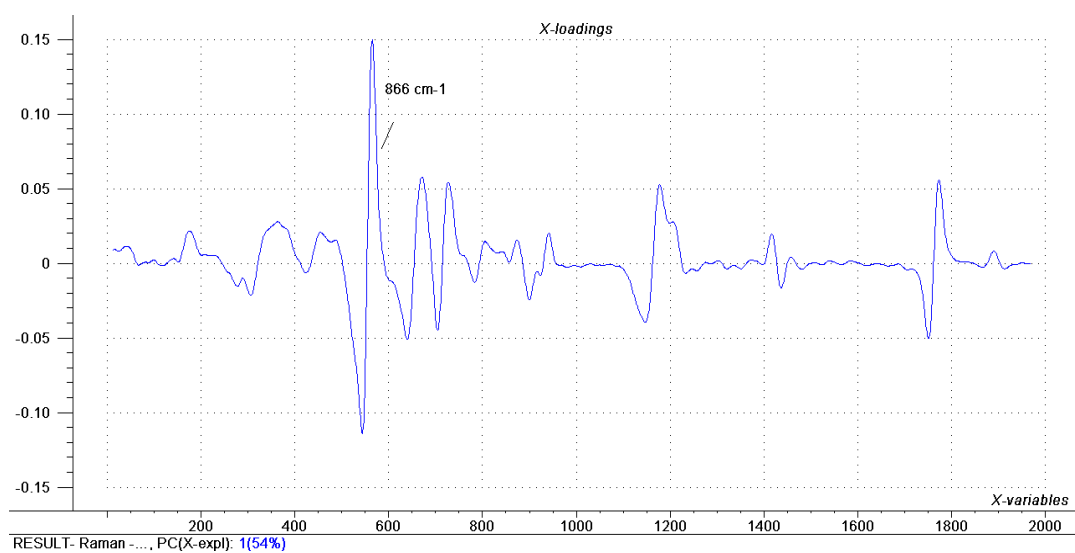
Figure 3-27   PCA loading plot (PC1 vs. variables)
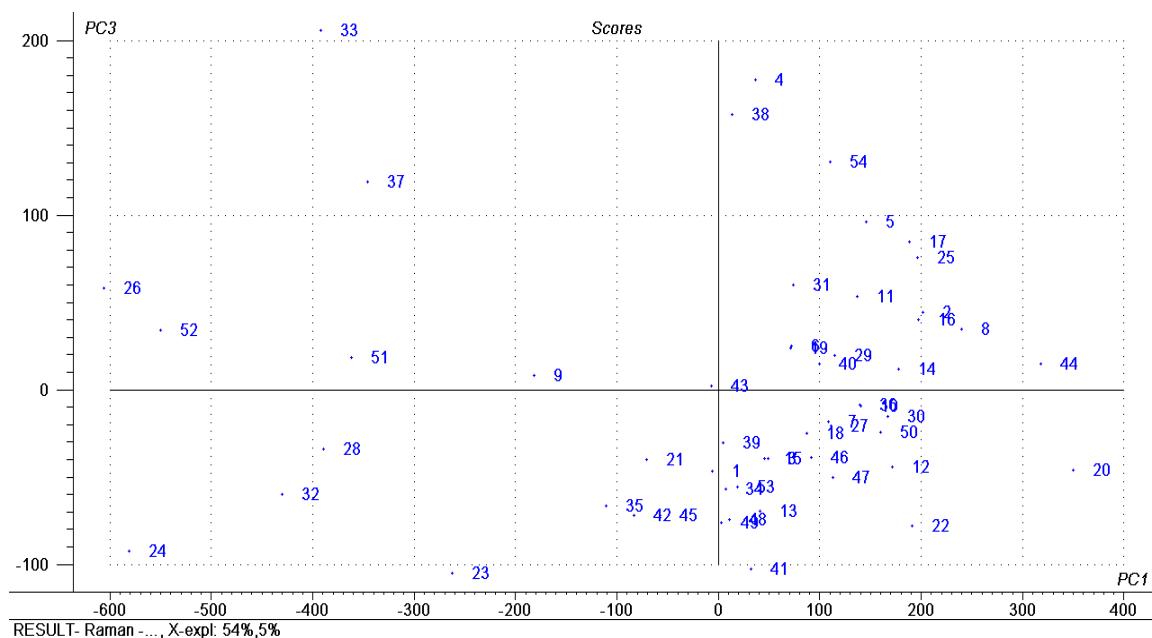
Figure 3-28   PCA scores plot (PC1 vs. PC3)
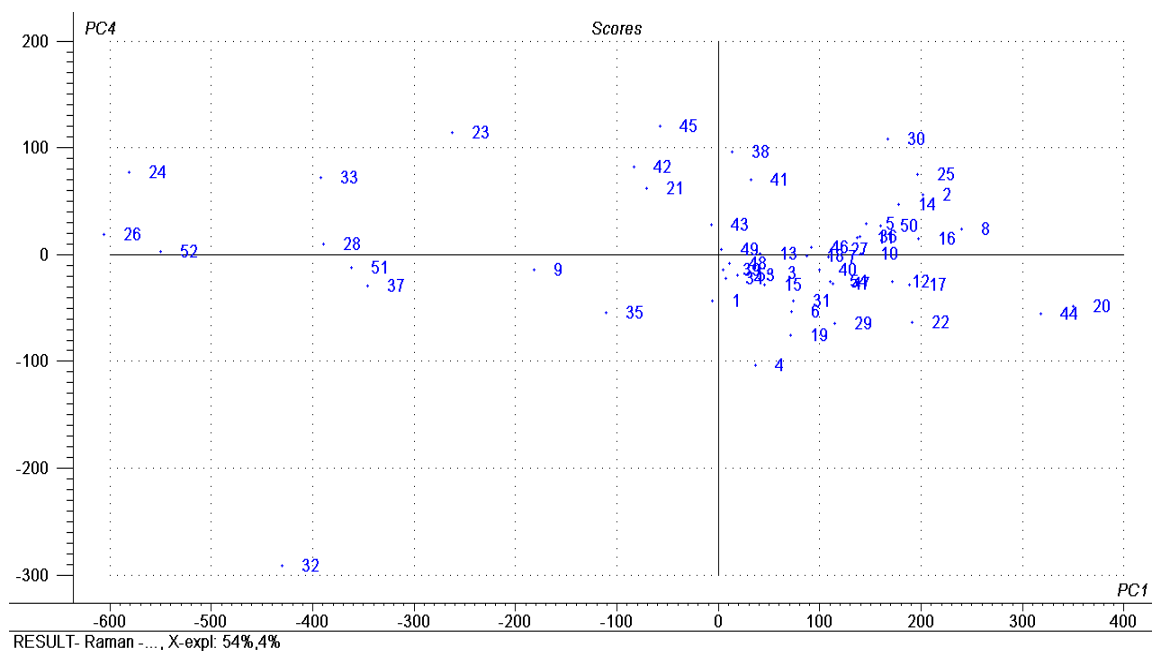
Figure 3-29   PCA scores plot (PC1 vs. PC4)
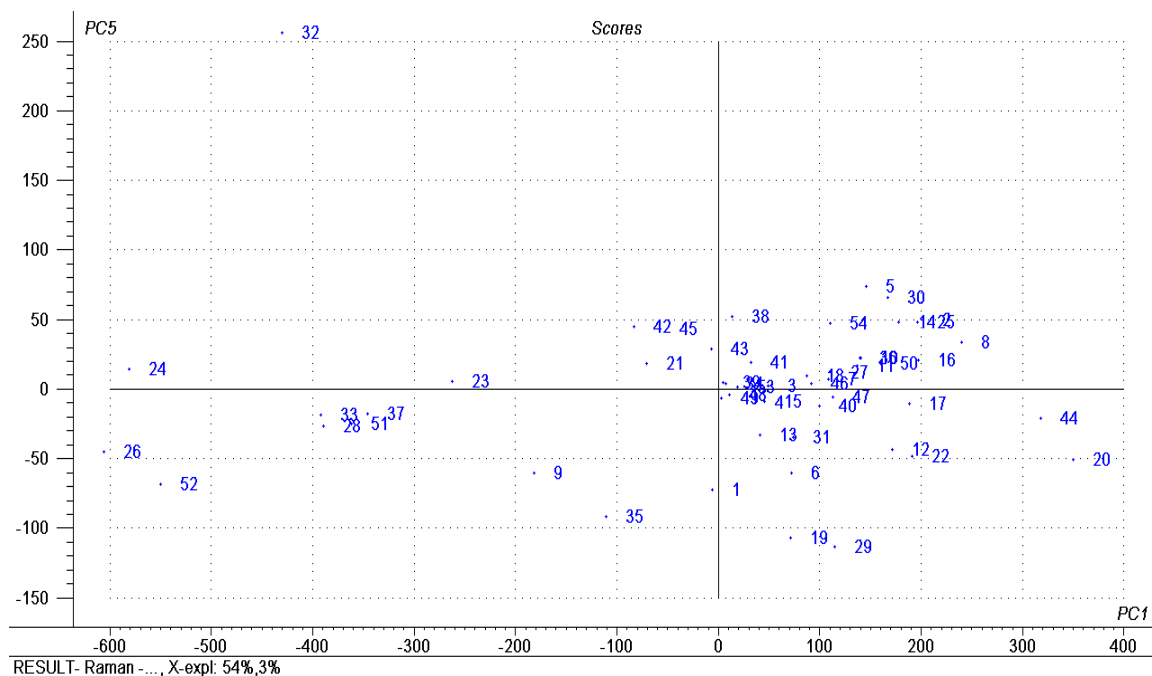
Figure 3-30   PCA scores plot (PC1 vs. PC5)
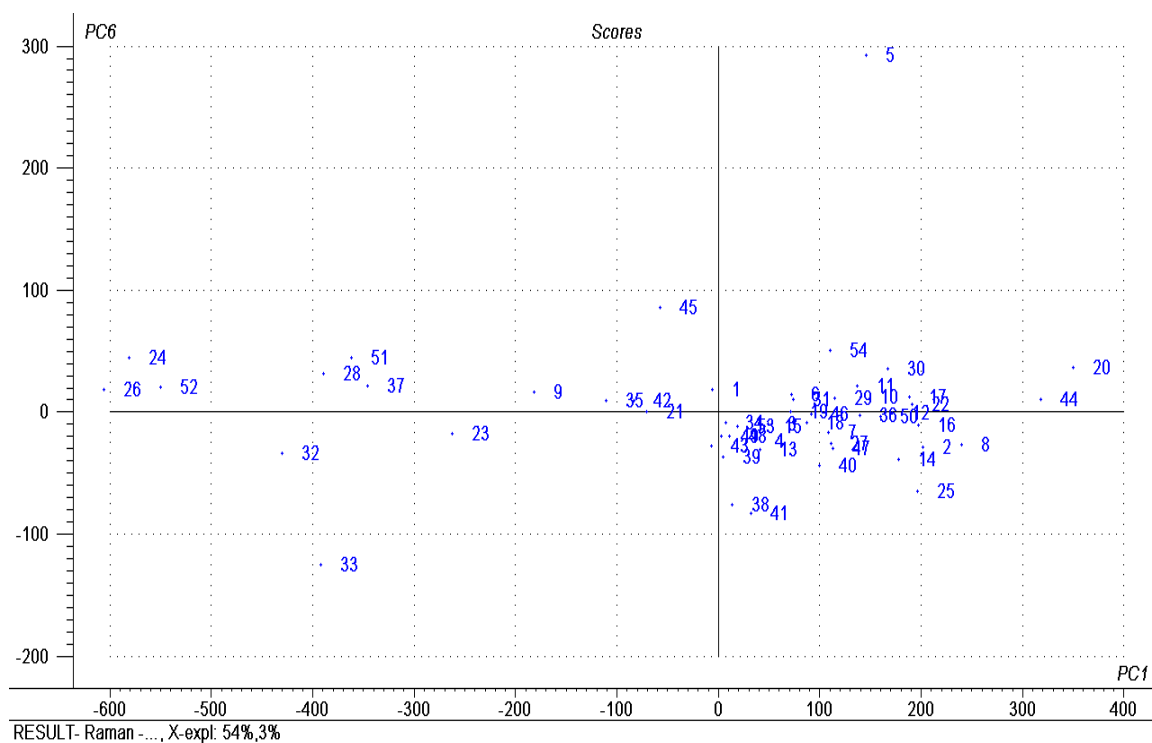
Figure 3-31   PCA scores plot (PC1 vs. PC6)

The fish oil supplements clustered in the groups I, II, and III are summarized in Table 3-9. Basically fish oil supplements containing high concentration of EPA and DHA in ethyl ester form were in group I, the supplements containing medium to high concentration of EPA and DHA also in ethyl ester form were in group II, and those containing high concentration of EPA and DHA in triglyceride form were clustered in group III.

Majority of the samples were clustered in group IV. Ever though the samples are quite mixed, generally the products contain natural fish oil that is about 30% of total EPA and DHA and omega 3, 6, and 9 fatty acids in triglyceride form were clustered in this group. Fish oil supplements in the group IV are summarized in Table 3-10.

Table 3-9   Fish Oil Supplements in the Group I, II, and III by Raman PCA

Sample #	Sample Name	Group
24	Nsi Nutracetical Sciences Superior DHA essencial fatty acids from fish oil	I ethyl esters, high EPA and DHA Concentration
26	Omax 562 EPA 137 DHA	
52	WinOmeg3 Complex Ethyl Esters 490 EPA 160 DHA	
32	PureGels Omega-3 300-200	II ethyl esters, medium to high EPA and DHA Concentration
28	PharmAssure Fish Body Oil EPA 240 mg DHA 200 mg	
33	Purity Products Ultra Pure Omega-3 325 EPA 250 DHA	
37	RxOmega-3 Factors Pharm Grade 400 epa 200 dha cap	
51	Walgreens Finest Naturals Extra Strength Fish Oil	
42	Source Naturals ArticPure DHA cap	III Tryglycerides, high EPA and DHA Concentration
21	Nordic Naturals Ultimate Omega 325	
35	Rite Aid Borage-Fish-Flax Oil	
45	Stop Aging Now Omega T Formular	

Table 3-10   Fish Oil Supplements in the Group IV by Raman PCA

Sample #	Sample Name	Group
1	California Health Omega 3-6-9 EPA 120 DHA 80	IV Tryglycerides, low EPA/DHA Concentration (about 20 -30%)
4	Eskimo-3 Fish Oil Ultra Pure	
7	Kal MaxEPA 1000 mg 180 EPA 120 DHA	
10	Natrol Omega-3 Fish Oil 180 epa	
11	Natrures plus Omega 3 Complete	
13	Natrures Weigh MaxEPA Omega-3	
15	Nature Answer Fish Oil EPA-DHA Blend	
19	Natures Bounty Organic Flax Oil	
31	PharmAssure Omega 3-6-9 Borage Flax Fish Oils	
38	RxOmega-3 Factors Pharm Grade Liquid	
40	Solga MaxEPA EPA 180 DHA 120 - 0	
41	Sound Body Fish Oil Concentrate 180 EPA 120 DHA	
46	Sundown Fish Oil 80 EPA 120 DHA	
47	Sundown Salmon Oil 80 EPA 120 DHA	
53	Wonder Labs Marine Lipid 180 EPA 120 DHA	
3	Barleans Fresh Catch Fish Oil 180 EPA 120 DHA	
6	Health from the Sun Total EFA Omega 3-6-9	
18	Natures Bounty Omega-3 Omega-6	
27	Optimum Nutrition Fish Oil 180 EPA 120 DHA	
29	PharmAssure Flax Seed Oil	
34	Res-Q Omega-3 1250 390-430 EPA 300-325 DHA	
39	SaveWorldHealth Fish Oil 180 EPA 120 DHA	
49	Ultimate Nutrition Fish Oil 180 EPA 120 DHA	
8	Major Fish Oil from Salmon Oil 45 EPA 55 DHA	
12	Natrures Weigh Essential Fatty Acids	
14	Natural Wealth 180 EPA 120 DHA	
16	Nature Made Fish Oil 1200 mg	
17	Natures Bounty Omega 3-6-9 Fish Flax Borage	
22	Norwegian Cod Liver Oil	
25	Olympian Labs Superior Glyceride Omega-3 Fish Oils Liquid	
30	PharmAssure Megasol Premium Concentrated EPA and DHA	
36	Rite Aid Fish Oil 1000 mg	
50	VSB Basics EPA-DHA 180-120 Fish Oil	
54	Xtendlife Omega 3 DHA Esters	

Although PCA of Raman spectra grouped the fish oil supplements quite well, the

PCA of IR spectra (discussed in section 3.3.5) provided better sample patterns and

grouping information. This may be because that IR bands were strong and detail spectra

differences were detected by means of PCA, but Raman bands were weak and spectra differences were not significant enough to generate clearer sample patterns.

3.5 Quantitative Characterization of Fish Oil Supplements by ATR-FTIR Standard Addition

3.5.1 Principle

Quantitative analysis with any analytical method or instrument requires calibration to ensure the accuracy of the results. Depending on the analysis being made, there are various calibration techniques that may be used such as external calibration, standard addition calibration, and internal standard calibration. External calibration is most commonly used to compare the response of the unknown to the standard calibration curve to determine concentration. When matrix effects appear or are to be expected, standard addition method can be the calibration method of choice.   In the study of environmental and biochemical systems and generally in ultra trace analysis, the standard addition method is frequently used. Standard addition is performed using the same amount of unknown make a series of solutions with increasing known amounts of added analyte into the mixture and associating it with the response. The x-intercept in a plot of response versus concentration of added analyte gives the concentration of unknown analyte. To find the x-intercept in equation 3-2, set y to zero:

$$y = mx + b \qquad\qquad (3\text{-}2)$$

set y to zero $0 = mx + b$, then $x = -b/m$

Therefore concentration of unknown can be calculated from:

$$\frac{y\ intercept}{slope} \qquad\qquad (3\text{-}3)$$

One of the goals for my studies was to develop a quantitative analysis method to determine the total contents of EPA and DHA in fish oil supplements using a rapid non-destructive technique such as FTIR. As discussed in section 3.3.4, the IR spectra of all different fatty acid esters found in fish oil supplements are very similar. The C-H stretching vibrational mode of the *cis*-alkene H-C=C-H form shows IR absorption at around 3010 cm^{-1}, and its peak position and intensity depends on the amount of double bonds in the fatty acid esters and the position or species (n-3, n-6, or monoene). An early study[31] showed that the alkene band can shift to over 12 cm^{-1} (from 3000 cm^{-1}), which is shifted to 3012 cm^{-1}. The shift is caused mainly by the concentration increase of EPA and DHA esters. Therefore, this band can potentially be used as a marker for the quantitative analysis of EPA and DHA ethyl esters and triglycerides. However, other bands, for example ~ 3005 cm^{-1} band from one of the common fish oil components oleic acid (C18:1), partially overlap with the 3012 cm^{-1} band of EPA and DHA as shown in Figure 3-32. This means that it would not be accurate to quantitatively analyze total EPA and DHA using 3012 cm^{-1} band with the external standard calibration due to band interferences. Therefore, the standard addition method should be a superior choice to analyze the total EPA and DHA using the characteristic IR 3012 cm^{-1} band.

The quantitative analysis of the fish oil supplements by standard addition was carried out by weighing known amounts of EPA and DHA ester standards and spiking the selected weighed samples with increasing concentration of the active ingredients. Then the IR of the spiked fish oil sample was recorded. The IR absorbance at 3012 cm^{-1} was measured manually (with baseline correction at 3040 cm^{-1}) using BioRad's KnowItAll software. After plotting the added concentration (spike) vs absorbance (standard addition

curve), the total concentration of EPA and DHA can be obtained where the line crosses the x axis.
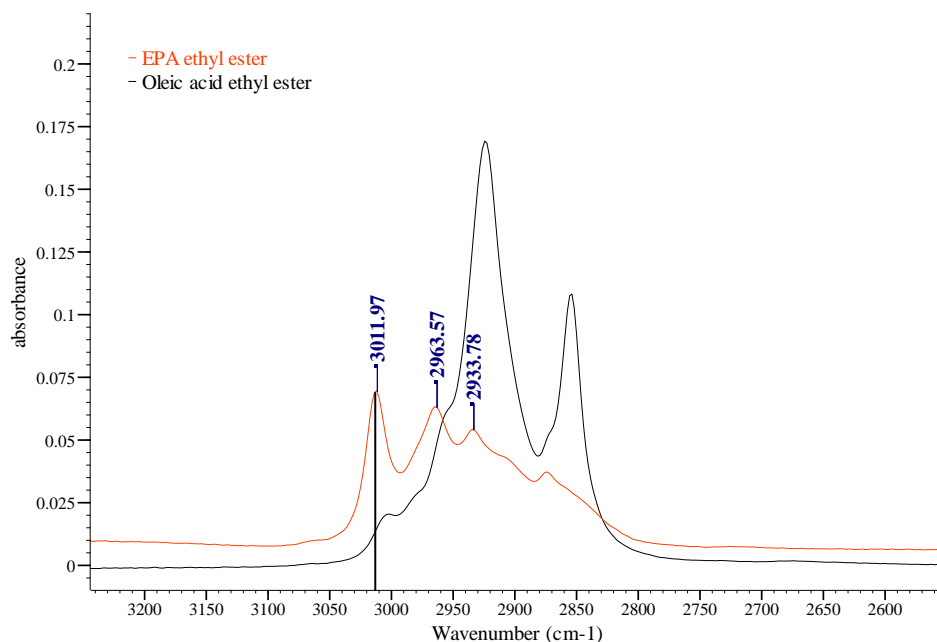
Figure 3-32   Overlay of IR Spectra of ethyl esters of EPA and oleic acid

3.5.2   *ATR-FTIR Instrumentation and Spectral Acquisition*

A Bruker Equinox 55 FTIR spectrometer fitted with a MIRacle[TM] single reflection horizontal ATR (Pike Technologies, Madison, WI) and equipped with a DTGS detector was used to acquire the spectra. Twenty micro liters (20 μL) of the sample were deposited on diamond ATR crystal. One hundred (100) co-added scans were taken at a resolution of 4 cm^{-1} between 4000 - 400 cm^{-1}. The background was collected before every sample was measured. After each sample analysis, the diamond ATR crystal was cleaned with acetone. The absorbance was obtained by manually reading using KnowItAll software.

3.5.3   Materials

Fatty acid esters were purchased from Nu-Chek-Prep. Inc. (Elysian, MN):

Ethyl Myristate, Lot # N-14E-J10-M, Purity >99%

Ethyl Palmitate, Lot # N-16E-S17-R, Purity >99%

Ethyl Oleate, Lot # U-46E-N5-R, Purity >99%

Ethyl EPA, Lot # U-99E-A29-S, Purity >99%

Ethyl DHA, Lot # U-99E-D11-S, Purity >99%

Tri EPA, Lot # T-325-N18-P, Purity >99%

Tri DHA, Lot # T-310-M5-S, Purity >99%

Sample Diluent: Mineral Oil, Lot # PY 02611LY, Aldrich Chemical Company

3.5.4   Fish Oil Samples

Fish oils are characterized by the wide range of fatty acid esters present and particularly by the highly unsaturated members. Any of the following saturated (C14:0 and C16:0), monoenoic (C16:1, C18:1, C20:1, and C22:1), and polyunsatuared (C20:5 and C22:6) can be major components. Fish oil compositions were studies by GC and ^{1}H NMR methods and were reported in literature[44]. Generally, major fatty acid esters in fish oils are the esters of myristic acid (C14:0, about 3 – 6 %), Palmitic acid (C16:0, about 15 – 20%), Palmitoleric acid (C16:1, about 5 – 8%), Stearic acid (C18:0, about 3 – 5%), Oleic acid (C18:1, 18 – 25%), EPA (C20:5, about 5 – 9%), and DHA (C22:6, about 10 – 25%).

According to information above, a simple fish oil dietary supplement sample was made by blending these constituents in a centrifuge tube listed in the Table 3-11, and this

sample was used to test the method accuracy using the proposed standard addition
calibration.

A dietary supplement Natural MaxEPA and FDA approved prescription fish oil
capsule from Omarcor (contains ethyl EPA 465 mg and ethyl DHA 375 mg in 1 gram
capsule, Lot# THE0056, distributed by Reliance Pharmaceutical) were also used for the
analysis of the total EPA and DHA ethyl esters concentrations using the proposed
standard addition method.

Table 3-11   Composition of in-house blended fish oil sample

Components	Fatty Acids	Weight (g)	%wt/wt
Ethyl Myristate	C14:0	0.03390	7.6
Ethyl Palmitate	C16:0	0.10644	24.0
Ethyl Oleate	C18:1	0.14076	31.7
Ethyl EPA	C20:5	0.09351	21.0
Ethyl DHA	C22:6	0.06968	15.7
Total Weight		0.44429	100.0
Total EPA and DHA		-	36.7

3.5.5   Procedures and Results

1.   In-house blended Fish Oil Sample Analysis:

Pipetted 50 µL (accurately weighted, average weight 45.12 mg) of the lab made
fish oil sample into 5 of 1-mL polypropylene centrifuge plastic tubes (Fisher Scientific),
respectively. Standards (mixture of ethyl EPA and DHA, EPA/DHA ratio is about 1.2)
were added in the amounts of 0 µL, 50 µL, 100 µL, 150 µL, 200 µL (all accurately
weighted) into the 5 tubes and accurately weighed to the nearest 0.00001 g on a
electronic balance (manufacturer, town, state). Then, the samples were diluted with
mineral oil to have the same final volume of 250 µL and weighed (final average weight is
about 220.77 mg). Mineral oil was selected as diluent because it is miscible with fatty
acid esters and has no IR absorbance at 3012 cm^{-1} (Figure 3-33 shows the overlay of IR

spectra of ethyl EPA and mineral oil at ~ 3000 cm^{-1} region). The mixtures were then

vortex mixed. The detail sample preparations are listed in Table 3-12.

Table 3-12   Details of Standard Addition Sample Preparations

Sample Preparation #	In-house made fish oil sample		EPA and DHA Standard		Mineral Oil		Final	
	μL	mg	μL	mg	μL	mg	μL	mg
A	50	45.05	0	0	200	168.15	250	213.20
B	50	44.92	50	46.50	150	126.36	250	217.78
C	50	45.11	100	90.24	100	83.00	250	218.35
D	50	45.52	150	136.59	50	42.23	250	224.34
E	50	44.99	200	185.18	0	0	250	230.17
-	-	Avg. 45.12	-	-	-	-	-	Avg. 220.77
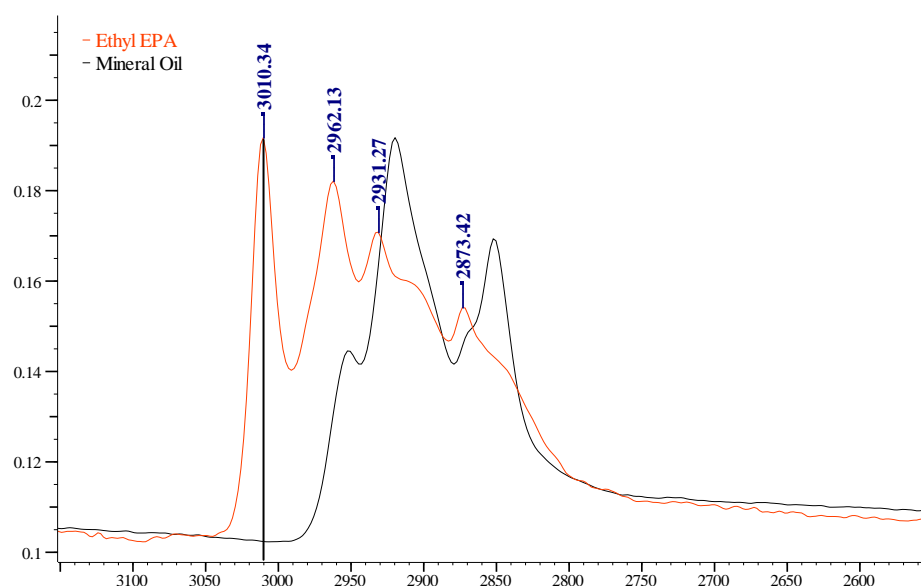
Figure 3-33   Overlay of IR spectra of ethyl EPA and mineral oil

The ATR-FTIR spectrum of each sample preparation was obtained using the same

procedures summarized in section 3.5.2. Manually measured the IR absorbance at 3012

cm^{-1} and 3040 cm^{-1} (for baseline correction) using the KnowItAll software. The

absorbance results are summarized in Table 3-13. After plotting the added standard

concentration of EPA and DHA in mg/mg vs. the IR absorbance at 3012 cm^{-1} (baseline corrrected), the concentration of EPA and DHA was obtained where the line crosses the x axis. The calibration plot is shown in Figure 3-34.

The correlation coefficient (R^2) of the calibration plot was found to be 0.999, which demonstrated very good linearity. The equation of the line is:

$$y = 0.0819x + 0.0059 \qquad\qquad (3\text{-}4)$$

Then the EPA and DHA concentration in the diluted in-house blended fish oil sample is:

$$x = \frac{y\ intercept}{slope} = \frac{0.0059}{0.0819} = 0.072\ mg/mg$$

Therefore, the EPA and DHA concentration (%wt/wt) in in-house blended fish oil

sample is: *%wt/wt = (220.77 x 0.072) x100/45.12 = 35.2*

The total EPA and DHA in the in-house made fish oil analyzed using the standard addition method is 35.2% (wt/wt) and whereas the actual concentration is 36.7% (as indicated in Table 3-9. The absolute difference between actual and measured is 1.5% and the relative difference is - 4.1% ((35.2 – 36.7)*100/36.7). The relative difference is within the typical IR quantitative analysis accuracy range (~5 %). The results demonstrated that the standard addition approach is suitable for a rapid analysis of EPA and DHA in the in-house blended fish oil sample using the IR band at 3012 cm^{-1}.

Table 3-13   Absorbance Results of Each Sample Preparation (in-house made)

Sample Preparation #	Added EPA/DHA Concentration mg/mg	Absorbance at 3012 cm^{-1}	Baseline Absorbance at 3040 cm^{-1}	Baseline corrected absorbance
A	0.0000	0.1232	0.1179	0.0053
B	0.2135	0.1438	0.1199	0.0239
C	0.4133	0.1632	0.1234	0.0398
D	0.6089	0.1820	0.1255	0.0565
E	0.8045	0.2001	0.1291	0.0711
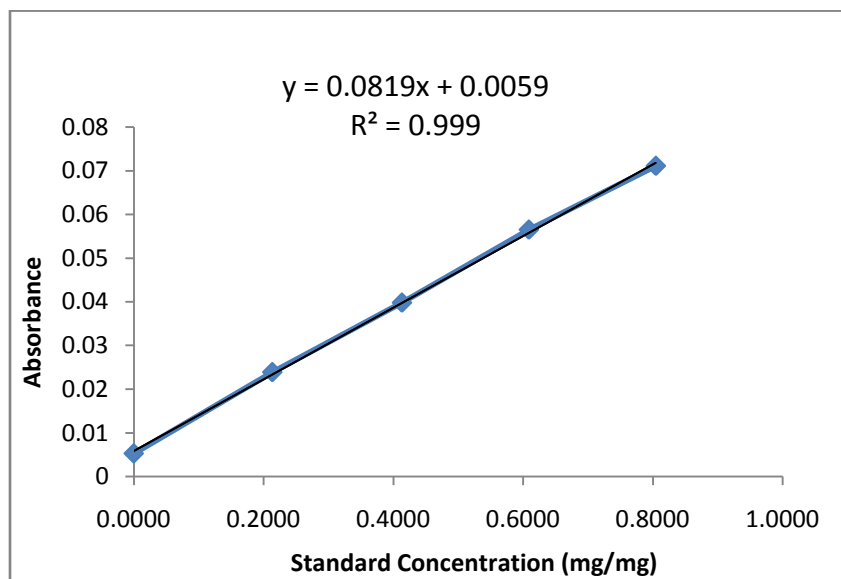
Figure 3-34   Standard addition calibration plot (In-house made sample analysis)

2.   Natural MaxEPA Sample Analysis:

One of fish oil dietary supplements, Natural MaxEPA, which contains natural

form (triglyceride) of EPA (180 mg) and DHA (120 mg) in 1000 mg fish oil concentrates

manufactured by Solgar, was analyzed using the standard addition method. Since the

ratio of EPA to DHA in this product is 1.5, a mixture of 350 µL (336.34 mg) triglyceride

EPA and 250 µL (225.11 mg) triglyceride DHA reference material was prepared to be

used for standard addition. Each sample was prepared and measured following the

similar procedures described in section 1 above (in-house made fish oil sample analysis).

The details of the each sample preparation are listed in Table 3-14. The IR absorbance

results are listed in Table 3-15. The plot of the added standard concentration in mg/mg

vs. the absorbance at 3012 cm^{-1} (baseline corrected at 3040 cm^{-1}) is shown in Figure 3-

35.

The correlation coefficient (R^2) of the calibration plot was found to be 0.999, which also demonstrated very good linearity. The equation of the line is:

$$y = 0.0878x + 0.0074 \tag{3-5}$$

Then the EPA and DHA concentration in the diluted Natural MaxEPA sample is:

$$x = \frac{y\ intercept}{slope} = \frac{0.0074}{0.0878} = 0.084\ mg/mg$$

Therefore, the total EPA and DHA concentration (%wt/wt) in Natural MaxEPA sample

is: *%wt/wt = (227.01 x 0.084) x100/45.74 = 41.7*

The total EPA and DHA in Natural MaxEPA analyzed using the standard addition method is 41.7% (wt/wt), and whereas the label claimed concentration 30%, the absolute difference is 11.7%. The analysis result is much higher than the label claim. This may be due to either the label claim is not accurate or the standard addition approach is not accurate for the quantitation of total EPA and DHA in some of the commercial fish oil supplements when the exact formulation composition is not available for a complete evaluation of the method.

Table 3-14   Details of Standard Addition Sample Preparations (MaxEPA)

Sample Preparation #	Natural MaxEPA		EPA/DHA Standard		Mineral Oil		Final	
	μL	mg	μL	mg	μL	mg	μL	mg
A	50	45.83	0	0	200	170.42	250	216.25
B	50	45.54	50	48.09	150	126.11	250	219.74
C	50	45.79	100	97.32	100	85.49	250	228.60
D	50	45.58	150	143.17	50	44.84	250	233.59
E	50	45.95	200	190.94	0	0	250	236.89
-	-	Avg. 45.74	-	-	-	-	-	Avg. 227.01

Table 3-15   Absorbance Results of Each Sample Preparation (MaxEPA)

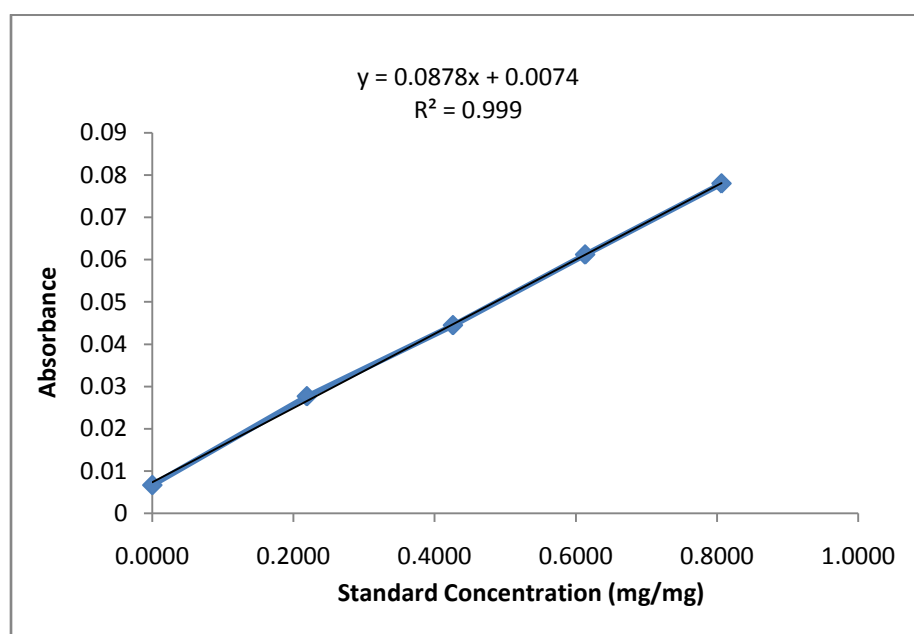| Sample Preparation #	Added EPA/DHA Concentration mg/mg	Absorbance at 3012 cm⁻¹	Baseline Absorbance at 3040 cm⁻¹	Baseline corrected absorbance
A	0.0000	0.0803	0.0736	0.0067
B	0.2188	0.1042	0.0765	0.0277
C	0.4257	0.1273	0.0828	0.0445
D	0.6129	0.1473	0.0861	0.0612
E	0.8060	0.1689	0.0909	0.0780

Figure 3-35   Standard addition calibration plot (MaxEPA sample analysis)

3.   Omacor Sample Analysis:

Omarcor (now Lovaza) is the first and only prescription omega-3 medication. Contents on the label claims 465 mg EPA ethyl esters and 375 mg DHA ethyl esters in each 1 gram capsule (84% EPA+DHA), and other omega-3 acids 80 mg (8%).

The Omarcor sample first was diluted to about 50% with ethyl palmitate pure material (276.06 mg of Omarcor + 261.87 mg of ethyl palmitate), then the diluted sample was used for standard addition analysis. Since the ratio of EPA to DHA in Omarcor is about 1.2, a mixture of 375 µL (341.10 mg) ethyl EPA and 320 µL (283.86 mg) ethyl DHA reference material was prepared to be used for standard addition. Each sample was prepared and measured following the similar procedures described in section 1 above (in-house blended fish oil sample). The details of the sample preparation are listed in Table 3-16. The IR absorbance results are listed in Table 3-17. The plot of the added standard concentration in mg/mg vs. the absorbance at 3012 cm^{-1} (baseline corrected) is shown in Figure 3-36.

The correlation coefficient (R^2) of the calibration plot was found to be 0.998, which also demonstrated very good linearity. The equation of the line is:

$$y = 0.0896x + 0.0090 \tag{3-6}$$

then the EPA and DHA concentration in the diluted Omarcor sample is:

$$x = \frac{y\ intercept}{slope} = \frac{0.0090}{0.0896} = 0.101\ mg/mg$$

Therefore, the total EPA and DHA concentration (%wt/wt) in Omarcor sample is:

%wt/wt = (220.55 x 0.101) x100/(44.54 x 0.513) = 97.4

The total EPA and DHA in Omacor sample analyzed using the standard addition method is 97% (wt/wt), and the label claimed concentration is 84% (90% total omega-3 fatty acids). Again, the analysis result is rather higher than the label claim. Since the exact formulation composition is not available to fully evaluate whether the standard addition approach is suitable for the analysis of EPA and DHA in particular samples, plus

the accuracy of the label claim is unknown, it is difficult to understand why the result

calculated from standard addition method is high.

Table 3-16   Details of Standard Addition Sample Preparations (Omarcor)

Sample Preparation #	Diluted Omarcor		EPA and DHA Standard		Mineral Oil		Final	
	μL	mg	μL	mg	μL	mg	μL	mg
A	50	44.33	0	0	200	169.74	250	214.07
B	50	44.33	50	48.59	150	123.04	250	215.96
C	50	45.13	100	91.69	100	83.54	250	220.36
D	50	44.44	150	140.82	50	40.01	250	225.27
E	50	44.48	200	182.60	0	0	250	227.08
-	-	Avg. 44.54	-	-	-	-	-	Avg. 220.55

Table 3-17   Absorbance Results of Each Sample Preparation (Omarcor)

Sample Preparation #	Added EPA and DHA Concentration mg/mg	Absorbance at 3012 cm^{-1}	Baseline Absorbance at 3040 cm^{-1}	Baseline corrected absorbance
A	0.0000	0.0966	0.0884	0.0082
B	0.2250	0.1216	0.0916	0.0299
C	0.4161	0.1434	0.0961	0.0472
D	0.6251	0.1650	0.0986	0.0665
E	0.8041	0.1846	0.1048	0.0798
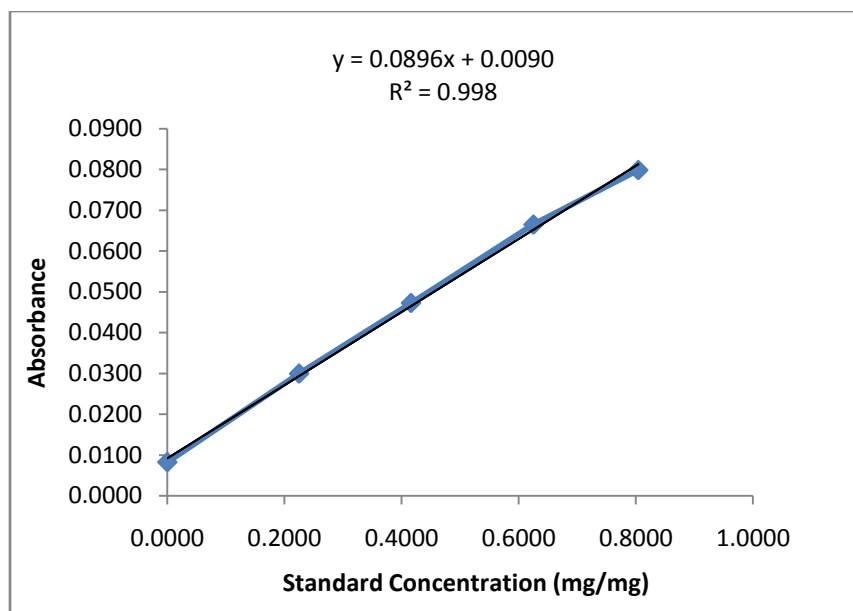
Figure 3-36   Standard addition calibration plot (Omarcor sample analysis)

3.5.6   Summary

The proposed standard addition method using the IR 3012 cm^{-1} band to analyze total EPA and DHA concentration in fish oil supplements was evaluated on an in-house made fish oil sample, a dietary supplement Natural MaxEPA, and a prescription drug Omarcor.

The analysis result (35.2%) of total EPA and DHA in the in-house made fish oil sample agreed well with the actual concentration (36.7%), and this demonstrated that the standard addition approach is suitable for a rapid analysis of EPA and DHA in the in-house blended fish oil sample. This sample is a simple mixture if a few fatty acid ethyl eaters. The only ingredient which exhibits absorbance at 3012 cm^{-1} is oleic acid ester (C18:1) besides EPA and DHA. The response factor of oleic acid ethyl ester may be quite different from that of EPA and DHA, therefore, the standard addition method works very well to eliminate the matrix interference and produce correct results.

However, the analysis result 41.7% of total EPA and DHA concentration in Natural MaxEPA and 97.4% in Omarcor were much higher than the label claims 30% in Natural MaxEPA and 84% in Omarcor. Since the exact formulation compositions of these two products are not available to evaluate whether the standard addition approach is proper for analyzing EPA and DHA, in addition the accuracy of the label claims is unknown, it is not easy to fully understand why the results were high. If some of other ingredients in the formulation have similar response factors to that of EPA and DHA, then the standard addition method may not be able to correct the matrix effect and generate accurate results. Typically, a product formulation list should be evaluated for a quantitative analytical method development.

3.6   Two-Dimensional FTIR Spectral Correlation Analysis of Qmega-3 Fatty Acids (EPA Esters)

3.6.1   Objective

This study is to evaluate for the first time the temperature-dependent FTIR spectral characteristics of the active ingredients such as ethyl ester of EPA and triglyceride EPA in fish oil supplements using two dimensional (2D) IR correlation analyses.

3.6.2   Materials

Ethyl ester EPA, Lot # U-99E-A29-S, Purity >99%, and triglyceride EPA, Lot # T-325-N18-P, Purity >99%, were both purchased from Nu-Chek-Prep, Inc. (Elysian, MN) and used as is without any treatment.

3.6.3   Instrumentation and Data Acquisition

A SensIR IlluminATR micro ATR-FTIR spectrometer (Smiths Detection, Danbury, CT) fitted with a diamond ATR and equipped with a mercury cadmium telluride (MCT) detector was used to measure the spectra. The spectrometer is attached to a Rensishaw System 1,000 (Renishaw Inc., Hoffman Estates, IL) micro Raman spectrometer. Two-hundred co-added scans were taken at a resolution of 4 cm^{-1} between 4000 - 650 cm^{-1} using the 100-μm slit mask. A background spectrum was collected before each sample measurement.

An aluminum heating block that was designed and built in-house and controlled by a digital temperature controller was used for sustaining sample temperature. A schematic of the temperature-controlled heating stage is shown in Figure 3-31. The sample liquid (50 uL) was placed on a small indentation in the aluminum block and then the ATR diamond objective was lowered into the sample to acquire the spectra as shown in Figure 3-37. The spectra of the samples were collected in the temperature range of 10 - 150°C (10°C, 20°C, 40°C, 60°C, 80°C, 100°C, 120°C, 140°C, 150°C, and return to 20°C). The sample was kept at the each temperature for about 10 minutes before every measurement to allow the sample to reach a stable homogenous temperature. The temperature stability was better than ± 0.2^{o}C.
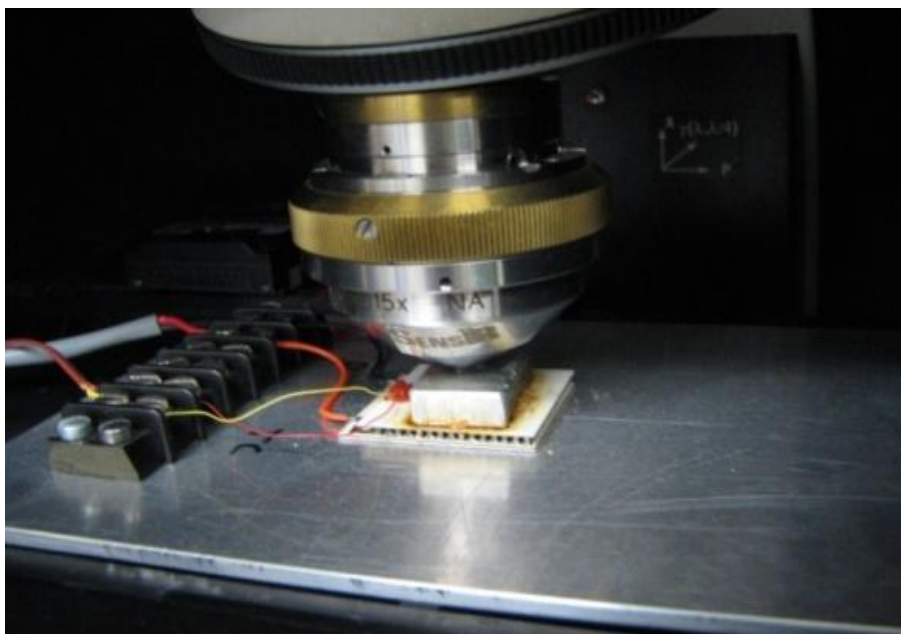
Figure 3-37   Spectra measurement of sample placed on the Al heating block

3.6.4   *2D Correlation Analysis*

As discussed in the section 1.2, generalized 2D correlation can obtain two kinds of spectra, namely synchronous and asynchronous spectra. The peaks generated on the diagonal line in synchronous spectra are referred to as autopeaks representing the changes in intensities of observed spectral bands under the external perturbation. By spreading peaks along the second dimension, the spectral resolution is enhanced, and seemingly complicated spectra have often been simplified. The cross peaks which lie in asynchronous spectra determine the sequential order of intensity changes of bands.

Thermal treatment has been chosen in this study as perturbation to monitor the infrared behaviors of two essential omega-3 fatty acids EPA and DHA in ethyl ester and triglyceride forms, and also Omarcor prescription drug product sample. Synchronous and asynchronous correlation intensities were computed for the FTIR spectra at different

temperature by applying the generalized 2D correlation algorithm of Noda[42]. Before 2D

calculation, each spectrum was cut off region (chose $800 - 3200 \text{ cm}^{-1}$), smoothed and

baseline corrected using ACD curve manager software. 2D-IR correlation spectra were

obtained by the treatment of the series of dynamic spectra with *2Dshige* (version 1.3)

software, which was developed by Shigeaki Morita in professor Yukihiro Ozaki's group

at Kwansei-Gakuin University.

As a result of the symmetric and antisymmetric properties of the cross correlation

peaks with respect to the diagonal line in the 2D plots, only peaks below the diagonal are

discussed. Peaks are identifies as $(X, Y) \text{ cm}^{-1}$, where *X* and *Y* represent the frequencies

marked on the *x*- and *y*-axes, respectively. Throughout this study, red and blue peaks in

the 2D plots denote positive and negative correlation peaks, respectively. According to

the rules proposed by Noda[43], the positive peak in the asynchronous map indicated that

the spectral intensity change at *X* occurs at a lower temperature than that at *Y* if the

corresponding synchronous peak at (X, Y) is also positive. On the other hand, if the

synchronous peak at (X, Y) is negative, the spectral intensity change at *X* occurs at higher

temperature than that at *Y*. A negative peak in the asynchronous map is interpreted in a

similar manner; i.e., *X* changes at higher (lower) temperature if the synchronous (X, Y)

peak is positive (negative).

3.6.5 Results and discussion

1). 1D IR spectral analysis of Ethyl Ester and Triglyceride of EPA

Figure 3-38 shows the overlay IR spectra (smoothed and baseline corrected) of

ethyl EPA (a) and triglyceride EPA (b), which were collected at the temperatures of 10°

C, 20°C, 40°C, 60°C, 80°C, 100°C, 120°C, 140°C, 150°C, and return to 20°C. By

comparing the spectra with eyes, it appears that the intensities of most of bands decreases with the increasing of temperature, and baseline also became noisier at higher temperatures. The spectrum of the sample at returned 20° C is similar to that at 150°C, and this indicates that the sample chemical configuration might be altered at high temperature such as 150°C.

The spectra of ethyl EPA and triglyceride EPA at different temperatures were also analyzed with PCA, and the scores plots are shown in Figure 3-39 (a) and (b), respectively. The PCA scores plots indicated that the sample spectra at 10°C, 20°C, 40°C, 60°C, and 80°C were at the similar region of PC1, but the spectra were spread along PC1 for the samples at 100°C and higher temperatures. The PC1 factor of the spectrum at returned 20°C was very different from that of the spectrum at initial 20°C, but similar to that at 150°C. This further confirmed that the sample chemical configuration may change at a higher temperature. The corresponding loading plot indicated that the C=O band (ester) intensity was possibly the major variable that contributed to the spectra distribution along the PC1 in PCA scores plots.
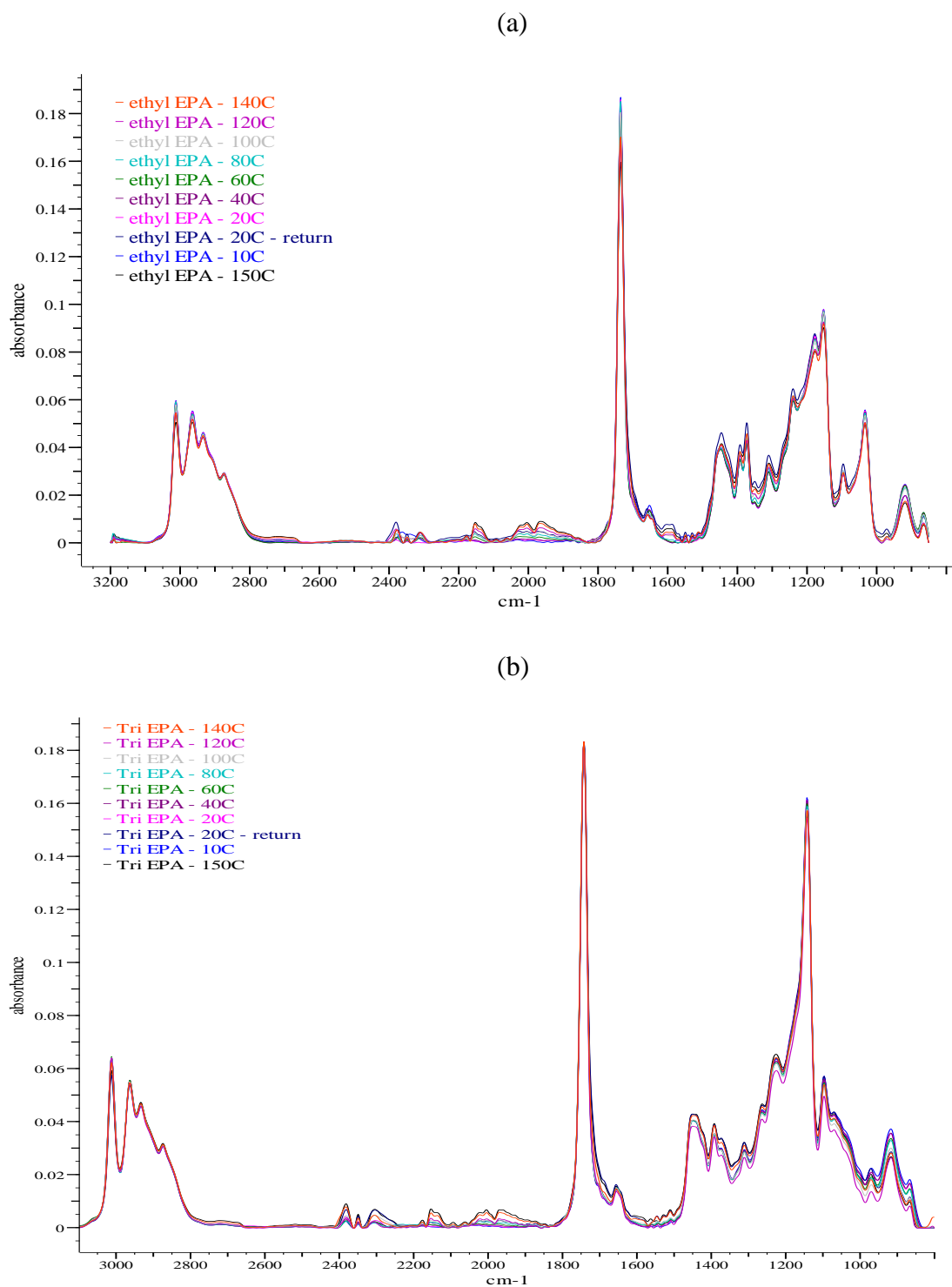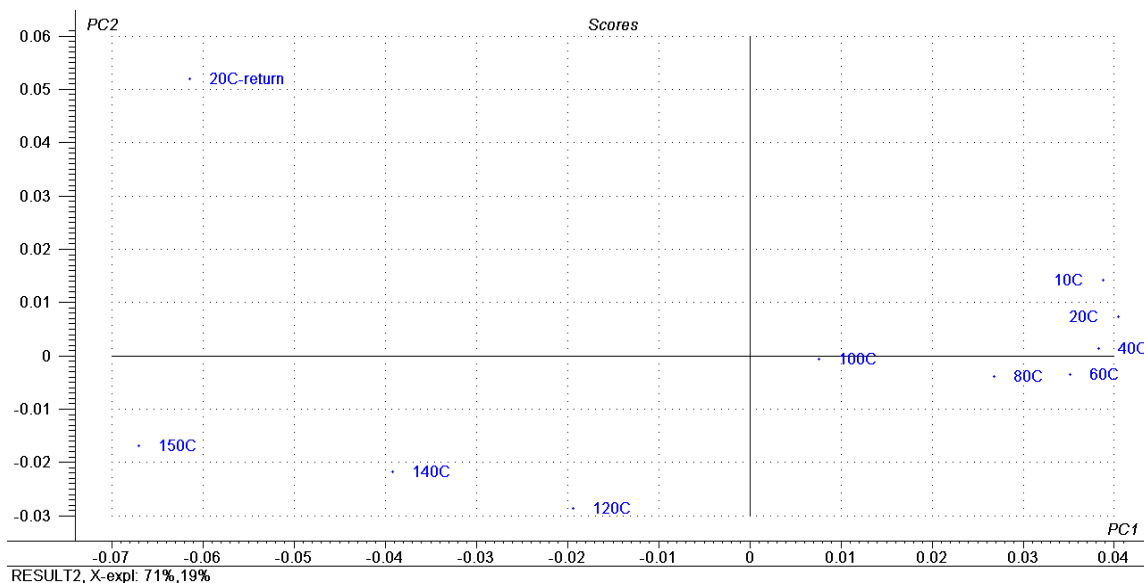
(a)

(b)

Figure 3-38   FTIR spectra overlay of ethyl EPA (a), and triglyceride EPA (b), at temperatures ranging from 10^0C to 150^0C
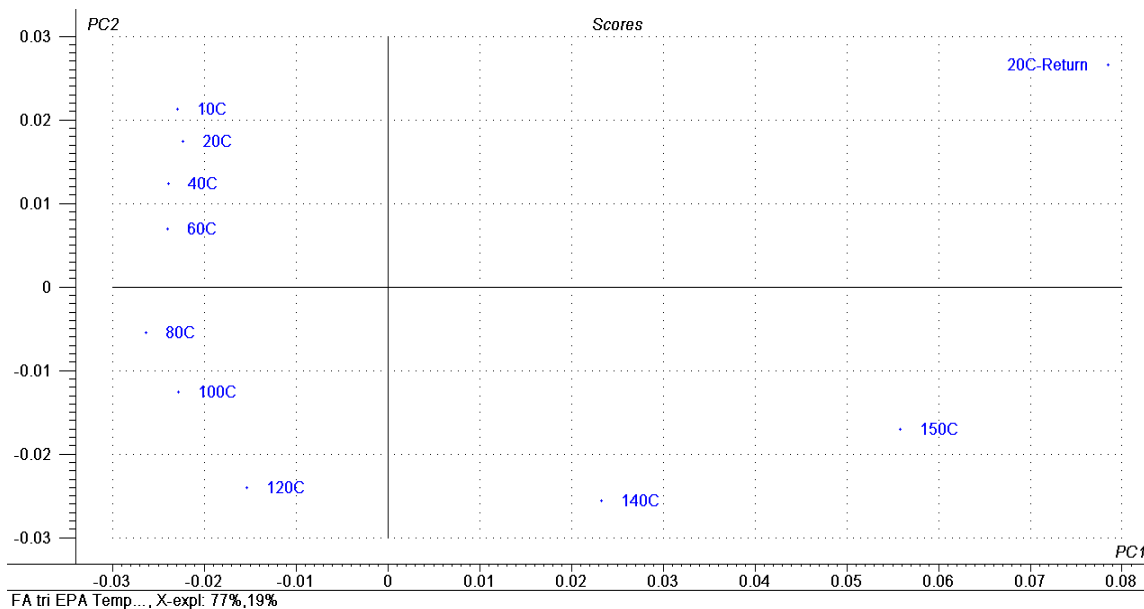
(a)

(b)

Figure 3-39   PCA scores plot of ethyl EPA IR spectra (a), and PCA scores plot of

triglyceride EPA IR spectra (b), at different temperatures

2).   2D IR Correlation Analysis of Ethyl Ester of EPA

Usually 2D IR correlation is performed on a relatively narrow wavelength ranges (not full spectrum range such as 4000 to 600 cm^{-1}) due to software calculation limitation and 2D map complexity. In this study, 2D IR correlation was examined in the wavenumber ranges of 3080 - 2760 cm^{-1}, 1830 - 1620 cm^{-1}, 1280 - 1135 cm^{-1}, and 1120 - 850 cm^{-1}. The 2D IR correlation was not examined in the range of 1500 - 1280 cm^{-1} due to the complexity of 2D maps. The 2D spectra represent the coordinated temperature-dependent spectral intensity variations in this region from 10°C to 150°C.

- 3080 - 2760 cm^{-1} region

Figure 3-40 shows (a) overlay 1D IR spectra of ethyl EPA from 10°C to 150°C, (b) 2D FTIR synchronous spectrum, and (c) 2D IR asynchronous spectrum, of ethyl EPA in the 3080 - 2760 cm^{-1}.

In the synchronous map (Figure 3-40 (b)), two autopeaks are observed around 3012 cm^{-1} (due to =C-H cis stretching) and 2965 cm^{-1} (due to –C-H (CH$_3$) asym. stretching). This indicates that the intensities of these two bands change with increasing temperature. There are no autopeaks observed for at 2874 cm^{-1} (due to –C-H (CH$_2$) sym. stretching) and 2934 cm^{-1} (due to –C-H (CH$_2$) asym. stretching), and this indicates that intensity changes are very minor for these two bands when the temperature increases. The major cross peak in the synchronous map is at (2965, 3012) cm^{-1}. The signs of the cross peaks is positive (red color), indicating that the temperature-induced changes in the spectral intensities are in the same direction. This result is in agreement with the observation in Figure 3-34 (a) that the intensities of these IR bands decrease with increasing temperature.

A number of cross peaks are observed in the asynchronous spectrum as shown in Figure 3-40 (c). Since the major cross peak at (2964, 3012) cm^{-1} is positive in the asynchronous map, and is also positive in the synchronous map, the band intensity changes (decreases) at 2964 cm^{-1} occur faster than that at 3012 cm^{-1} with increasing temperature.
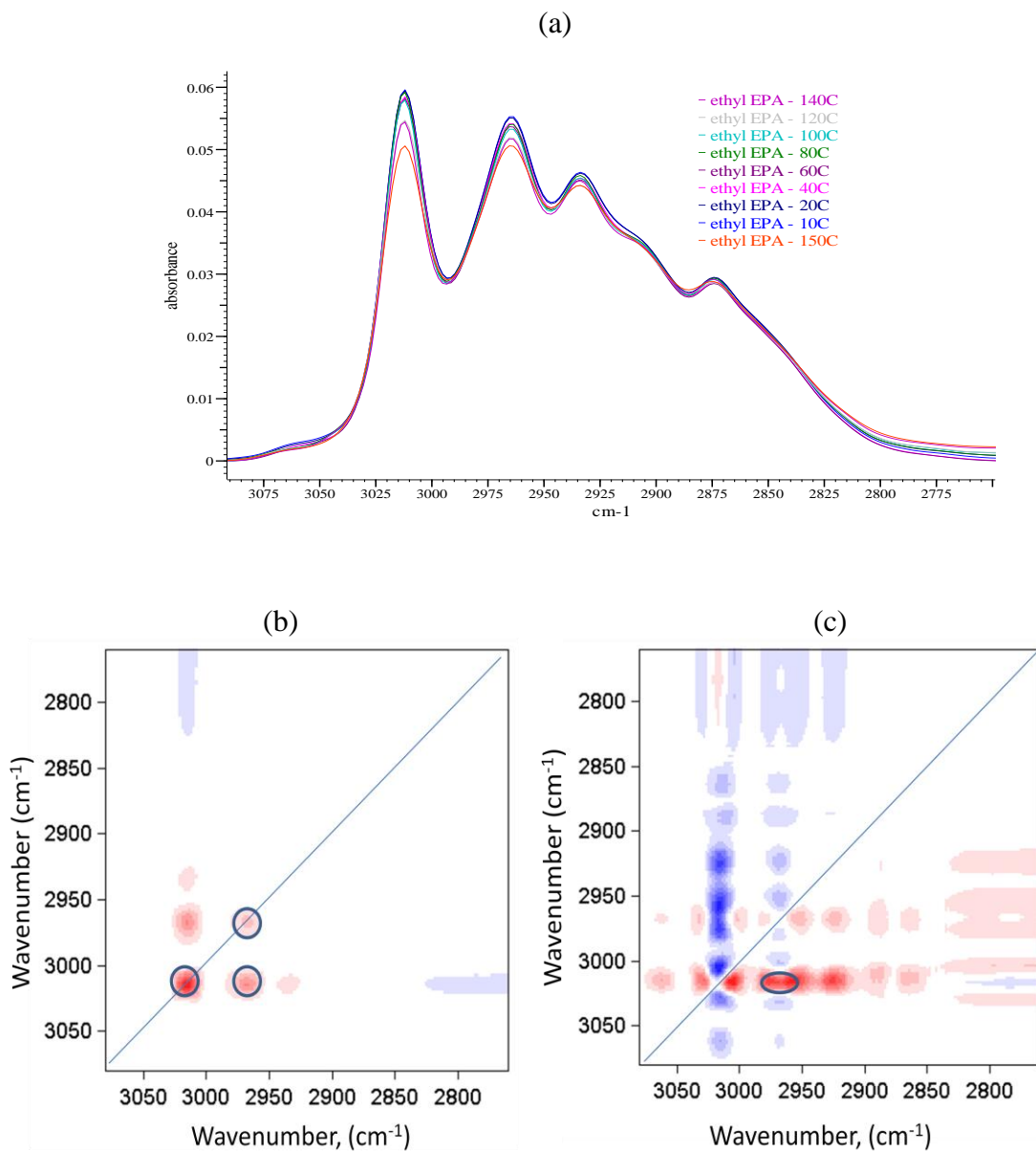
(a)

(b)   (c)

Figure 3-40   1D IR (a), 2D IR Synchronous (b), and 2D IR Asynchronous (c), spectra of ethyl EPA in 3080 - 2760 cm^{-1} region

- 1830 - 1620 cm^{-1} region

Figure 3-41 shows (a) overlay 1D IR spectra of ethyl EPA from 10°C to 150°C, (b) 2D FTIR synchronous spectrum, and (c) 2D IR asynchronous spectrum, of ethyl EPA in the 1830 - 1620 cm^{-1} region.

In the synchronous map (Figure 3-41 (b)), two autopeaks (along the diagonal) centered at 1735 cm^{-1} (due to C=O ester stretching) and 1716 cm^{-1} (due to C=O acid stretching) are observed, indicating that the relative intensities of these two bands change with increasing temperature. There was no autopeak observed at 1650 cm^{-1} (due C=C cis stretching), and this indicates that the band intensity change of this band is minor when the temperature increases. The major cross peak observed in the synchronous spectrum is at (1716, 1735) cm^{-1}. The sign of the cross peak is negative (blue color), indicating that the temperature-induced changes in the spectral intensities of the two bands are in opposite direction. This result is in agreement with the observation in Figure 3-41 (a) which shows that the intensity of band at 1735 cm^{-1} decreases and intensity of the band around 1716 cm^{-1} increases with increasing temperature. In addition, one minor cross peak is observed in the synchronous map at (1735, 1751) cm^{-1}, and the sign is negative, which means the intensity of the band at 1735 cm^{-1} decreases while the intensity of the band around 1751 cm^{-1} increases with increasing temperature.

The intensity increasing of bands at ~ 1716 cm^{-1} and ~ 1750 cm^{-1}, and decreasing of band at 1735 cm^{-1} indicate that the C=O (ester stretching) band gets broaden and less intense when the temperature increases. Unusually strong temperature broadening of the C=O band is interpreted to be caused by thermal population of a very flexible excited conformational configuration. The hypothesis is that at high temperature there is a wider

distribution of conformations that will produce a broadening of both these spectral marker bands. As temperature decreases, the functional group relaxes to lower energy states, and the band should narrow.

A strong cross peak observed in the asynchronous 2D correlation map (Figure 3-41 (c)) is at (1716, 1735) cm^{-1}, and it is positive. Since this peak is negative in the synchronous map, the band intensity changes (decrease) at 1735 cm^{-1} occur faster than the band intensity increase at 1716 cm^{-1} with increasing temperature. The band around 1716 cm^{-1} is a typical free fatty acid (FFA) C=O band. FFA are common fatty acid ester hydrolysis products in crude oils and are formed to some extent in refined oils as a results of oxidation or degradation during oil refining processes mostly at high temperatures. In this study, the increase of band intensity at 1716 cm^{-1} with temperature may be an indication of a small increase in the amount of free fatty acid at high temperatures due to oxidation. Figure 3-42 shows the overlap spectra of ethyl EPA at 20°C and 20°C - return (return to 20°C after ethyl EPA was heated to 150 ^{o}C). The C=O band is more broaden and band intensity is higher around 1705 cm^{-1} to 1720 cm^{-1} at 20°C – return, and this confirmed that the increase of band intensity at 1716 cm^{-1} with temperature is not only a temperature effect, but also due to chemical structure change (a small increase in the amount of free fatty acid at high temperatures due to oxidation). Owing to the overlap of this band with the very strong ester carbonyl absorption at 1735 cm^{-1}, there is no resolution between these two bands in 1D IR spectral. However, it is very clear that 2D correlation spreads these two bands over two dimensions and thus enhances the band resolution.
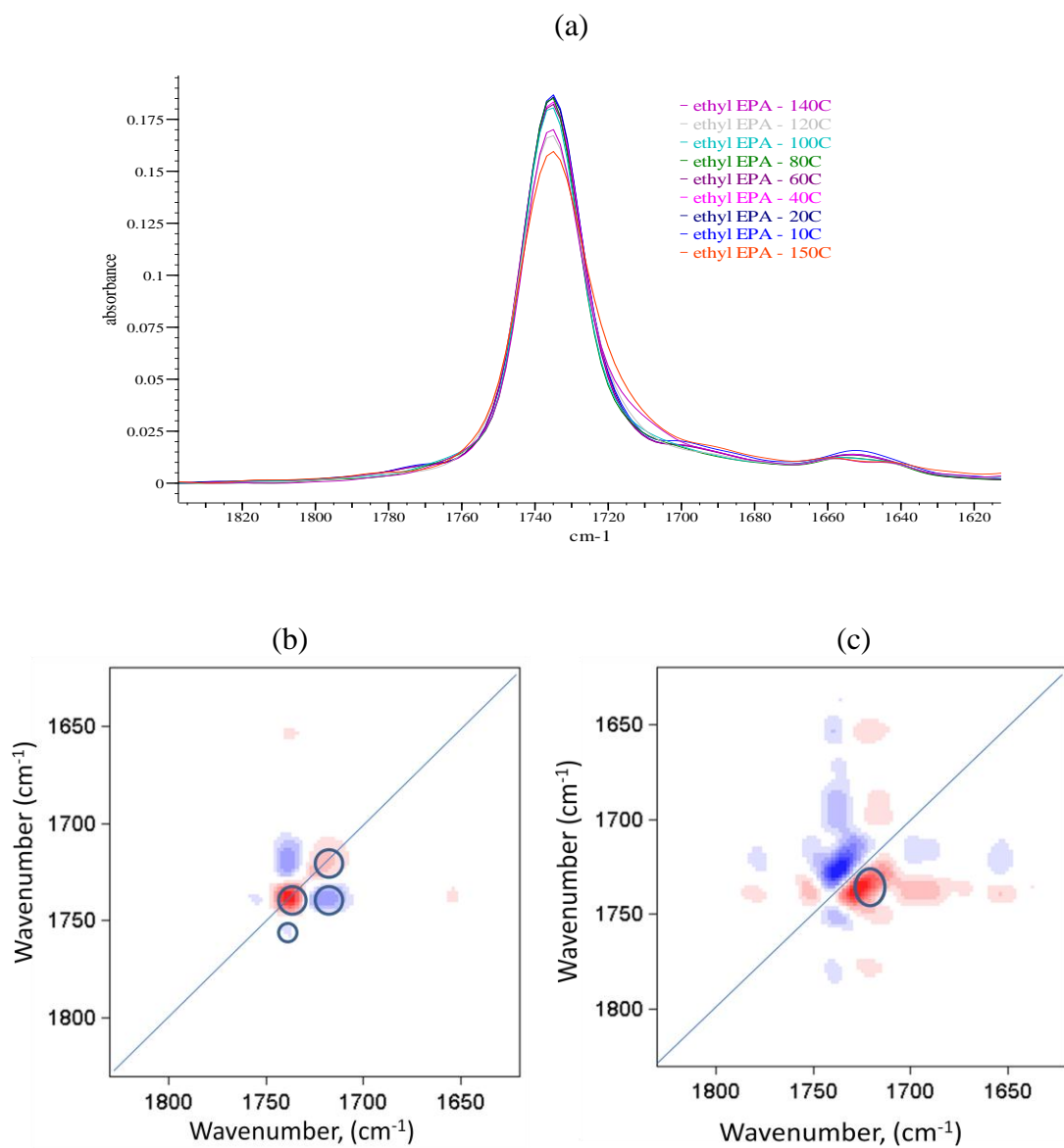
(a)

(b)

(c)

Figure 3-41   1D IR (a), 2D IR Synchronous (b), and 2D IR Asynchronous (c), spectra of ethyl EPA in 1830 - 1620 cm^{-1} region
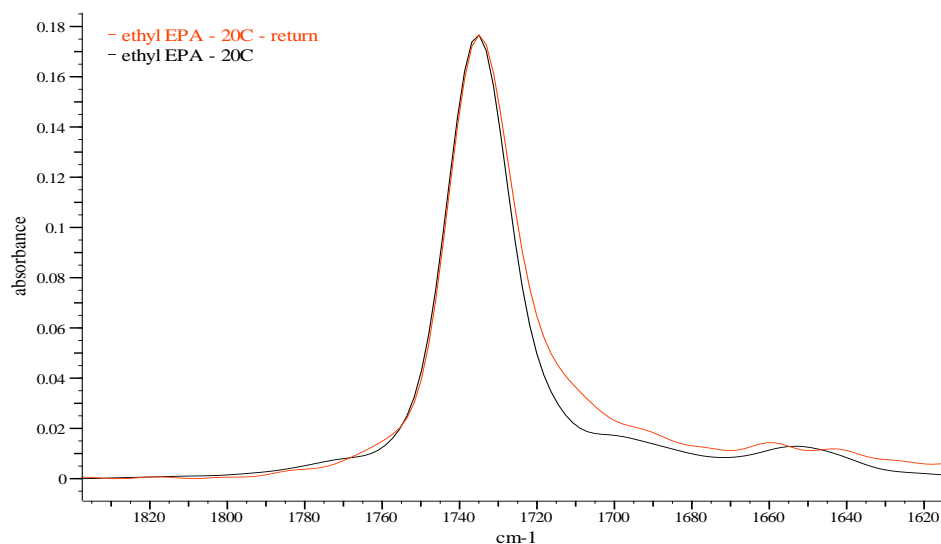
Figure 3-42   Overlap spectra of ethyl EPA at 20^{0}C and 20^{0}C - return

- 1120 - 850 cm^{-1} region

Figure 3-43 shows (a) overlay 1D IR spectra of ethyl EPA from 10°C to 150°C,

(b) 2D FTIR synchronous spectrum, and (c) 2D IR asynchronous spectrum, of ethyl EPA

in 1120 - 850 cm^{-1} region.

In the synchronous map (Figure 3-43(b)), three autopeaks (along the diagonal)

centered at 1033 cm^{-1} (due to C-O stretching), 919 cm^{-1} (due to =C-H cis out of plane

bending), and 866 cm^{-1} are observed, indicating that the relative intensities of these three

bands change with increasing temperature. There were no autopeaks observed at ~ 975

cm^{-1} (due =C-H trans out of plane bending) and 1096 cm^{-1} (due to C-O stretching), and

this indicates that intensity changes of these bands were minor with increasing

temperature. There are three positive cross peaks observed in the synchronous spectrum

at (919, 1033) cm^{-1}, (866, 1033) cm^{-1}, and (866, 919) cm^{-1}, indicating that the

temperature-induced changes in the spectral intensities of the three bands at 1033 cm^{-1},

919 cm^{-1}, and 866 cm^{-1} are in the same direction (decreasing). The results are in agreement with the observation in Figure 3-43 (a) that the intensity of these bands decreases with the increasing temperature. In addition, there is one negative cross peaks observed at (919, 975) cm^{-1}, indicating the intensity of the band at 919 cm^{-1} decreases while the intensity of the band at 975 cm^{-1} increases with increasing temperature. In fact at high temperature, a small percentage of cis C=C bond could change to trans configuration, so the band intensity at ~ 975 cm^{-1}, which is due to =C-H trans out of plane bending, were observed increasing.

In the asynchronous map (Figure 3-43(c)), two positive cross peaks were observed at (975, 1033) cm^{-1} and (866, 919) cm^{-1}. Since the peak (975, 1033) cm^{-1} is negative and the peak (866, 919) cm^{-1} is positive in synchronous map, the band intensity changes (decrease) at 1033 cm^{-1} occur faster than the band intensity increase at 975 cm^{-1} and the band intensity changes at 866 cm^{-1} occur faster than that at 919 cm^{-1} with the increasing of temperature. There were four major negative cross peaks observed at (919, 1033) cm^{-1}, (919, 975) cm^{-1}, (866, 1033) cm^{-1}, and (866, 975) cm^{-1}, combined with the existence of the positive or negative of the same peak at synchronous map, these results indicate that the change at 1033 cm^{-1} occurs prior to that of 919 cm^{-1} and 866 cm^{-1}, the change at 919 cm^{-1} occurs prior to that of 975 cm^{-1}, and the change at 866 cm^{-1} occurs prior to that of 975 cm^{-1}. Therefore, the overall sequence of intensity change in ascending order of temperature as follows: 1033 cm^{-1} > 866 cm^{-1} > 919 cm^{-1} > 975 cm^{-1}.
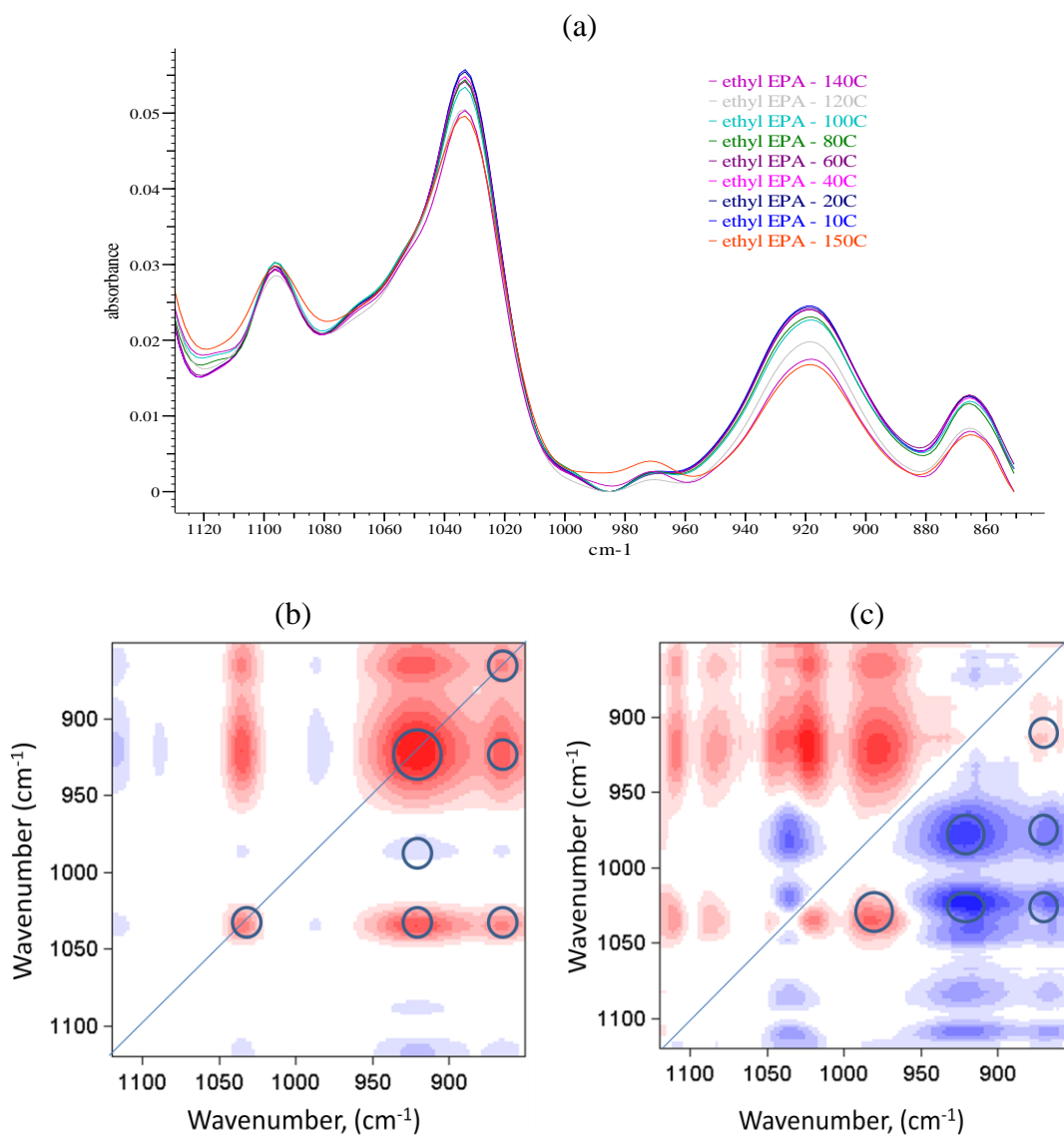
Figure 3-43   1D IR (a), 2D IR Synchronous (b), and 2D IR Asynchronous (c), spectra of ethyl EPA in 1120 - 850 cm^{-1} region

- 1280 - 1135 cm^{-1} region

Figure 3-44 shows (a) overlay 1D IR spectra of ethyl EPA from 10°C to 150°C, (b) 2D FTIR synchronous spectrum, and (c) 2D IR asynchronous spectrum, of ethyl EPA in 1280 - 1135 cm^{-1} region.

In the synchronous map (Figure 3-44 (b)), four autopeaks at 1152 cm^{-1} (due to C-O stretching), 1178 cm^{-1} (due to C-O stretching, -CH2- bending), 1240 (-CH2- bending), and 1265 cm^{-1} are observed, indicating that the relative intensities of these bands change with increasing temperature. There is one positive cross peak observed at (1152, 1178) cm^{-1}, indicating that the temperature-induced changes in the spectral intensities of the bands at 1152 cm^{-1} and 1178 cm^{-1} are in the same direction (decreasing). There are four negative cross peaks observed at (1178, 1240) cm^{-1}, (1152, 1240) cm^{-1}, (1178, 1265) cm^{-1}, and (1152, 1265) cm^{-1}, indicating the intensity of each pair of bands change in opposite direction with increasing temperature. The band intensity decreases at 1152 cm^{-1} and 1178 cm^{-1} while it increases at 1240 cm^{-1} and 1265 cm^{-1}. This also indicated that bands 1152 cm^{-1} and 1178 cm^{-1} may be from the same origin such as C-O stretching and 1240 cm^{-1} and 1265 cm^{-1} are from other origin such as –CH$_2$- bending.

In the asynchronous map (Figure 3-44 (c)), two positive cross peaks were observed at (1152, 1240) cm^{-1} and (1178, 1240) cm^{-1}. Since the peaks are negative in synchronous map, the band changes (increase) at 1240 cm^{-1} occur faster than the band intensity decrease at 1152 cm^{-1} and 1178 cm^{-1}. There is a major negative cross peaks at (1152, 1178) cm^{-1}, combined with the existence of the positive peak at synchronous map, the result indicates that the change at 1178 cm^{-1} occurs prior to that of 1152 cm^{-1}. Therefore, the overall sequence of intensity change in ascending order of temperature is as follows: 1240 cm^{-1} > 1178 cm^{-1} > 1152 cm^{-1}.

(a)

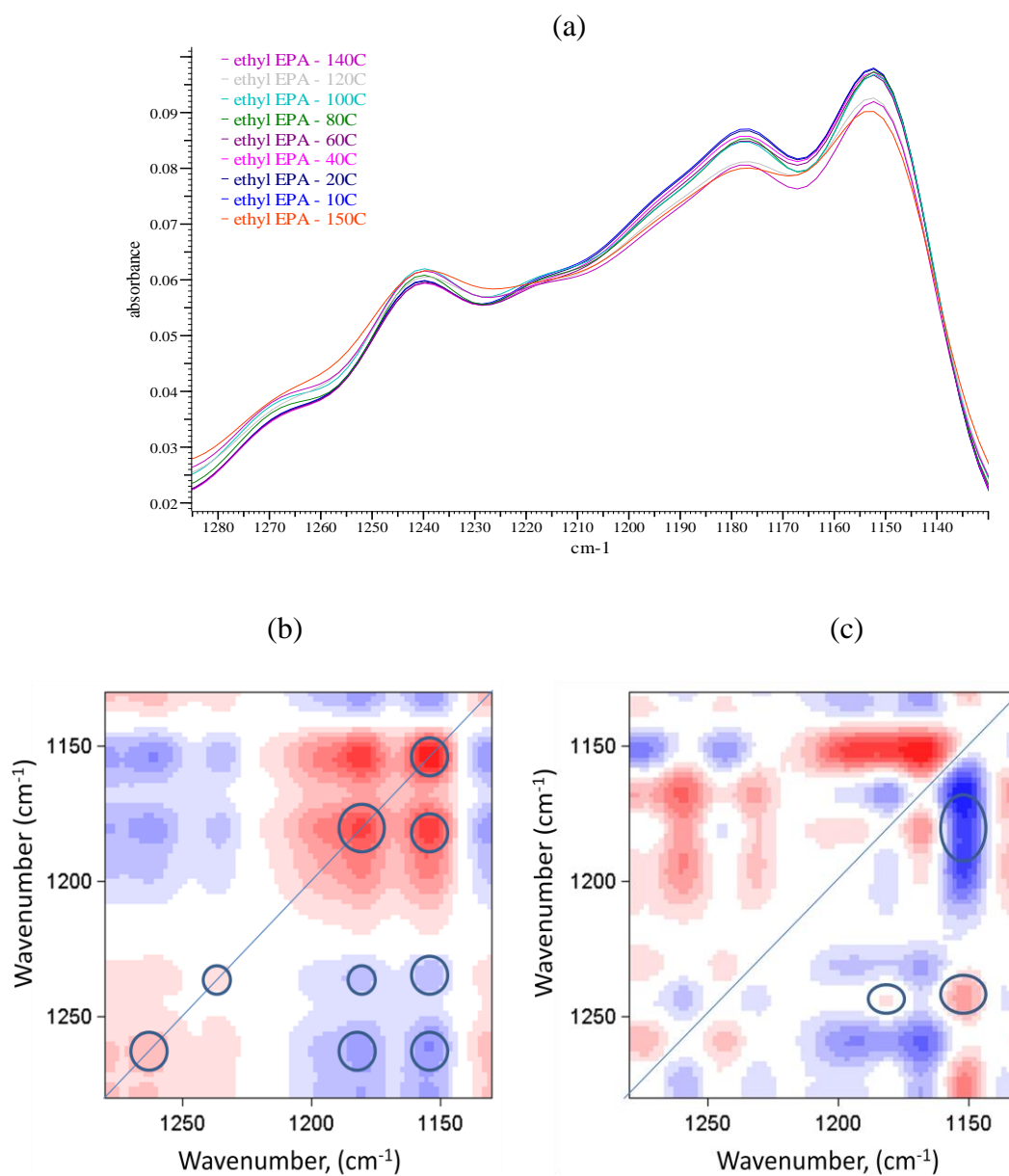(b)   (c)

Figure 3-44   1D IR (a), 2D IR Synchronous (b), and 2D IR Asynchronous (c),
spectra of ethyl EPA in 850 – 1120 cm^{-1} region

3).   2D IR Correlation Analysis of Triglyceride of EPA

Similar to the study of ethyl EPA, 2D IR correlation was also performed on

triglyceride EPA in the wavenumber ranges of 3080 - 2760 cm^{-1}, 1830 - 1620 cm^{-1}, and

$1280 - 840$ cm^{-1}. The 2D spectra represent the coordinated temperature-dependent spectral intensity variations in this region from 10°C to 150°C.

- $3080 - 2760$ cm^{-1} region

Figure 3-45 shows (a) overlay 1D IR spectra of triglyceride EPA from 10°C to 150°C, (b) 2D FTIR synchronous spectrum, and (c) 2D IR asynchronous spectrum, of triglyceride EPA in the $3080 - 2760$ cm^{-1} region.

In the synchronous map (Figure 3-45 (b)), two autopeaks are observed around 3012 cm^{-1} (due to =C-H cis stretching) and 2964 cm^{-1} (due to –C-H (CH$_3$) asym. stretching). This indicated that the intensities of these two bands changed with ascending temperature. There were no autopeaks observed for bands 2874 cm^{-1} (due to –C-H (CH$_2$) sym. stretching) and 2934 cm^{-1} (due to –C-H (CH$_2$) asym. stretching), indicating that there were no or very minor band intensity changes for these two bands. A major positive cross peak is at (2964, 3012) cm^{-1} and minor positive one is at (2934, 3012) cm^{-1}, indicating that the temperature-induced changes in the spectral intensities are all in the same direction. The intensities of these IR bands decrease with increasing temperature.

Two positive cross peaks were observed in the asynchronous map (Figure 3-45 (c)) at (2964, 3012) cm^{-1} and (2934, 3012) cm^{-1} and since this peak is also positive in the synchronous map, the band intensity changes (decrease) at 2964 cm^{-1} and 2934 cm^{-1}occur faster than that at 3012 cm^{-1} with increasing temperature.
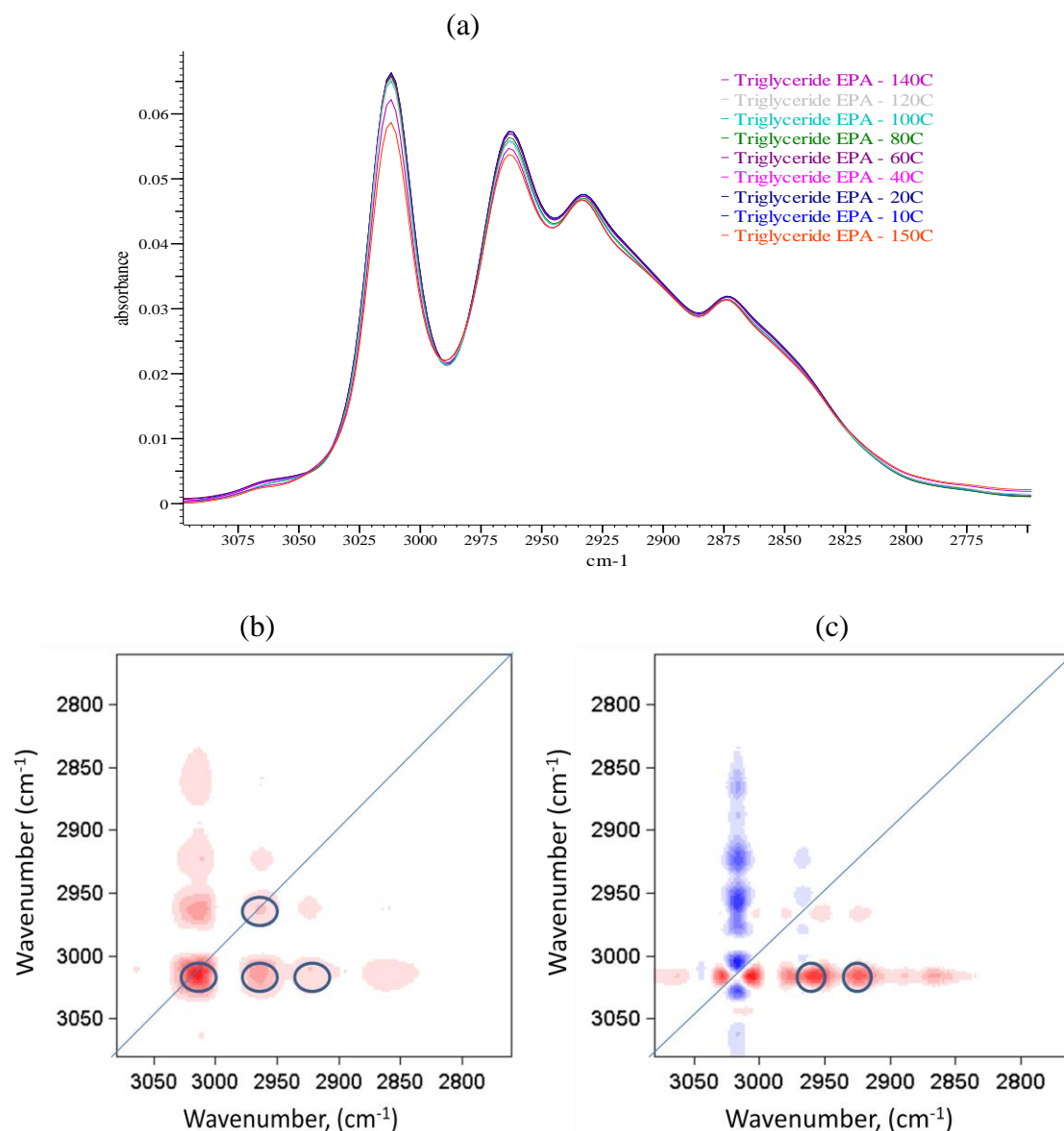
Figure 3-45   1D IR (a), 2D IR Synchronous (b), and 2D IR Asynchronous (c) spectra of triglyceride EPA in 3080 - 2760 cm^{-1} region

- 1830 - 1620 cm^{-1} region

Figure 3-46 shows (a) overlay 1D IR spectra of triglyceride EPA from 10°C to 150°C, (b) 2D IR synchronous spectrum, and (c) 2D IR asynchronous spectrum, of triglyceride EPA in the 1830 - 1620 cm^{-1} region.

In the synchronous map (Figure 3-46 (b)), two autopeaks centered at 1742 cm^{-1} (due to C=O ester stretching) and 1716 cm^{-1} (due to C=O acid stretching) are observed, indicating that the relative intensities of these two bands change with increasing of temperature. There was no autopeak observed at 1650 cm^{-1} (due C=C cis stretching), and this indicated that band intensity change of this band was insignificant. A major negative cross peak observed in the synchronous spectrum is at (1716, 1742) cm^{-1}, indicating that the temperature-induced changes in the spectral intensities of these two bands are in opposite direction. This result is in agreement with the observation in Figure 3-46 (a) which shows that the intensity of the band at 1742 cm^{-1} decreases whiles the intensity of the band around 1716 cm^{-1} increases with increasing temperature. In addition, there are a number of minor cross peaks observed in the synchronous map. Two positive peaks at (1690, 1716) cm^{-1} and (1716, 1775) cm^{-1}, and the other one is negative at (1690, 1742) cm^{-1} which shows the intensity of the band at 1742 cm^{-1} decreases while the intensities of the band around 1690 cm^{-1}, 1716 cm^{-1} and 1775 cm^{-1} increase with the increasing of temperature. The intensity increasing of these bands indicates that the C=O ester band gets broaden and less intense when the temperature increases. Again, this may be due to a wider distribution of conformations that will produce a broadening of both these spectral marker bands at high temperature.

A strong positive cross peak observed in the asynchronous 2D correlation map (Figure 3-46 (c)) is at (1716, 1742) cm^{-1}. Since this peak is negative in the synchronous map, the band intensity decreases at 1742 cm^{-1} occur faster than the band intensity increases at 1716 cm^{-1} with increasing temperature. As discussed in early section for ethyl EPA, the band around 1716 cm^{-1} is a typical free fatty acid (FFA) C=O band. The

band intensity increasing at 1716 cm^{-1} may be an indication of a increasing of a small amount of free fatty acid at high temperature due to oxidation. Owing to the overlap of this band with the very strong ester carbonyl absorption at 1742 cm^{-1}, there is no resolution between these two bands in 1D IR spectral. However, it is clear that 2D correlation enhances the band resolution.
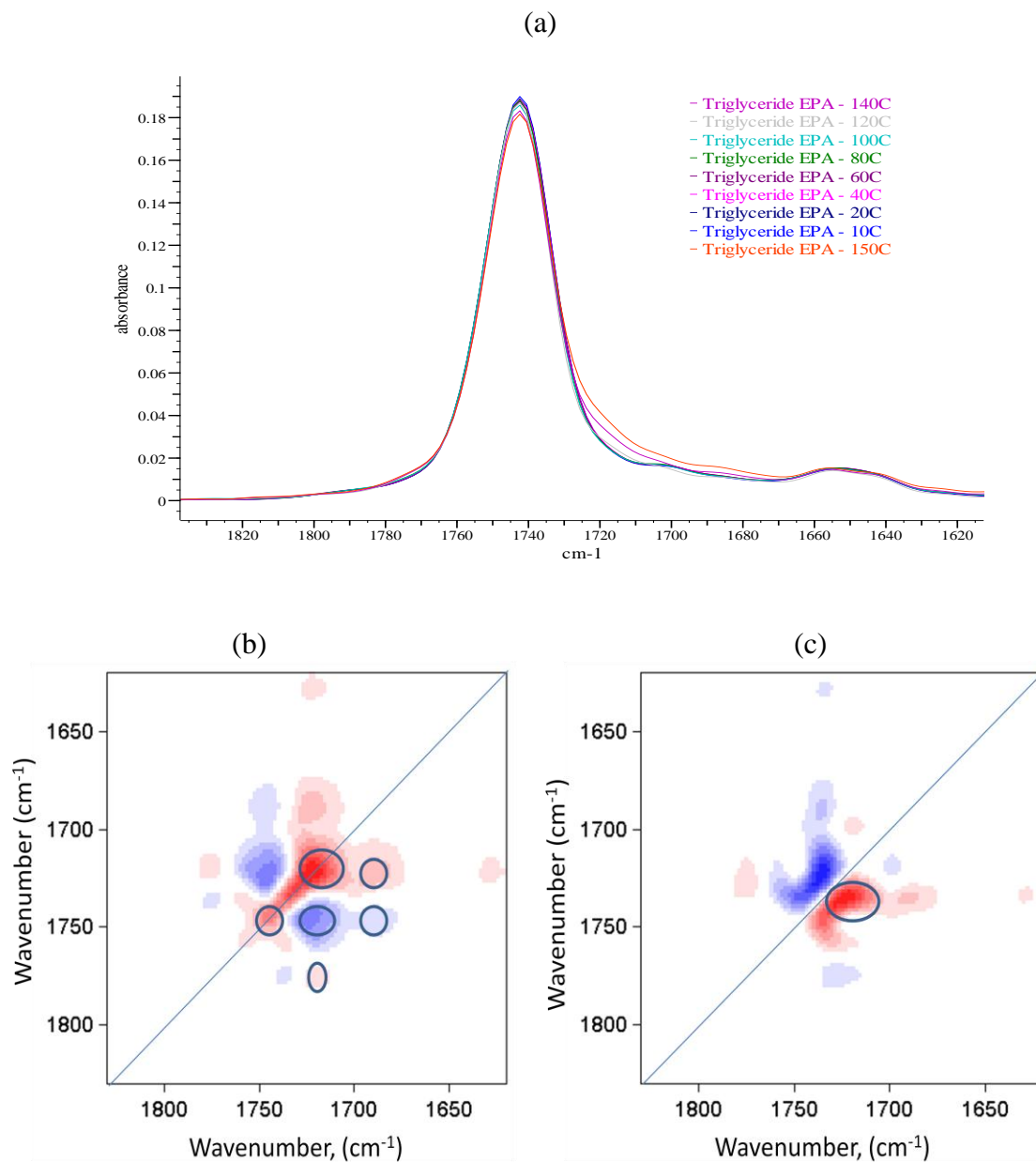
(a)

(b)   (c)

Figure 3-46   1D IR (a), 2D IR Synchronous (b), and 2D IR Asynchronous (c), spectra of triglyceride EPA in 1830 - 1620 cm^{-1} region

- 1280 - 840 cm^{-1} region

Figure 3-47 shows (a) overlay 1D IR spectra of triglyceride EPA from 10°C to 150°C, (b) 2D FTIR synchronous spectrum, and (c) 2D IR asynchronous spectrum, of triglyceride EPA in the 1280 - 840 cm^{-1} region.

In the synchronous map (Figure 3-47 (b)), four autopeaks at 919 cm^{-1} (due to =C-H *cis* out of plane bending), 975 cm^{-1} (due to =C-H *trans* out of plane bending),1115 cm^{-1} (not a band, at valley) and 1143 cm^{-1} (due to C-O stretching) are observed, indicating that the relative intensity changes of these bands with increasing temperature. There is a positive cross peaks observed in the synchronous spectrum at (919, 1143) cm^{-1}, indicating that the temperature-induced changes in the spectral intensities of the bands at 1143 cm^{-1}and 919 cm^{-1} are in the same direction (decreasing). There are negative cross peaks observed at (975, 1143) cm^{-1} and (919, 975) cm^{-1}, indicating the intensity of the band at 975 cm^{-1} increases while the intensity of the band at 919 cm^{-1} and 1143 cm^{-1} increases with increasing temperature. At high temperature, a small percentage of *cis* C=C bond might change to *trans* configuration, so the band intensity at ~ 975 cm^{-1} (due to =C-H *trans* out of plane bending) was observed increasing.

In the asynchronous map (Figure 3-47 (c)), two major negative cross peaks were observed at (919, 975) cm^{-1} and (919, 1143) cm^{-1}. Combined with the negative/positive peaks in synchronous map, the band intensity decreases at 1143 cm^{-1} occur faster than the band intensity decrease at 919 cm^{-1}, and band intensity decrease at 919 cm^{-1} occur faster than the band intensity increase at 975 cm^{-1}. There is a positive cross peak observed at (975, 1143) cm^{-1}, together with the negative peak in synchronous map, this indicates that band intensity decreases at 1143 cm^{-1} occur faster than the band intensity increase at 975

cm-1. Therefore, the overall sequence of intensity change in ascending order of

temperature is as follows: $1143 \text{ cm}^{-1} > 919 \text{ cm}^{-1} > 975 \text{ cm}^{-1}$.
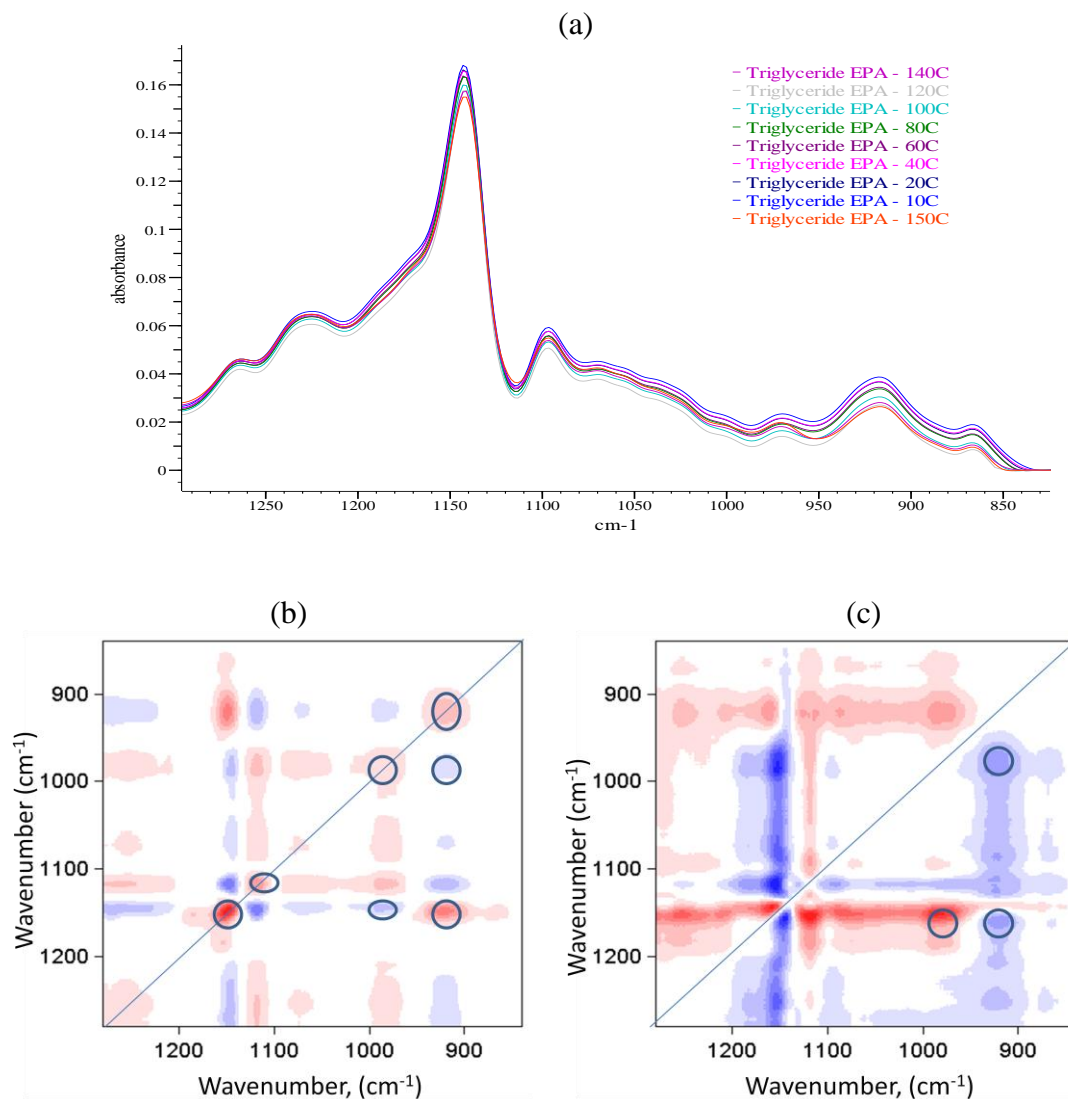
Figure 3-47   1D IR (a), 2D IR Synchronous (b), and 2D IR Asynchronous (c) spectra of triglyceride EPA in $1280 - 840 \text{ cm}^{-1}$ region

4).   Summary of 2D IR Correlation Analysis

The results of 2D correlation analysis for ethyl EPA and triglyceride EPA are

very similar. Generally, for the bands at 3012 cm^{-1}(=C-H *cis* stretching), 2964 cm^{-1} (–C-

H (CH$_3$) asym. stretching), $1735 - 1742 \text{ cm}^{-1}$ (C=O ester stretching), 1178 cm^{-1} (C-O

stretching), 1152 cm^{-1} (C-O stretching), 1143 cm^{-1} (C-O stretching), and 919 cm^{-1} (=C-H

cis out of plane bending), the band intensities decrease with the ascending of temperature.

For the bands at ~1716 cm^{-1} (C=O acid stretching) and ~ 975 cm^{-1} (=C-H *trans*

stretching), the intensities increase with increasing temperature. The band intensity

increasing at 1716 cm^{-1} may be an indication of a increasing of small amount of free fatty

acid at high temperature due to oxidation, and band intensity increasing at 975 cm^{-1} may

be due to *cis* C=C bond convert to *trans* configuration at high temperature. Two

dimensional IR correlation clearly shows better resolution separating these two increasing

bands comparing to 1D IR spectra.

Within each wavenumber range, such as 3080 - 2760 cm^{-1}, 1830 - 1620 cm^{-1},

1280 - 850 cm^{-1}, the sequence of major band intensity changes with increasing

temperature were suggested by analyzing asynchronous map.

For the bands from 1280 to 1500 cm^{-1} such as ~1310 cm^{-1}, ~1372 cm^{-1}, ~1392

cm^{-1}, ~1446 cm^{-1}, which mostly due to –C-H- bending/scissoring, the band intensities

appear increasing slightly with increasing temperature by examining the 1D IR spectra.

Two dimentional correlation was not evaluated for this region because of the complexity

of the 2D maps.

In fact, other fatty acids such as ethyl DHA, triglyceride DHA, and Omarcor, etc.

fish oil products were also studied using temperature-dependent 2D IR correlation, and

the results are very similar to those of ethyl EPA and triglyceride EPA presented above.

Therefore, these study results are not included in this thesis.

3.7   Conclusion

- Fish oil supplements labels are misleading and the products do not contain the free acids EPA and DHA active ingredients.

- ATR-FTIR can quickly and easily distinguish between the ethyl ester and the triglyceride forms of fatty acids using the carbonyl band position.

- Principal component analysis (PCA) grouped the FTIR and Raman spectra of fish oil supplements successfully. The fish oil supplements are clearly clustered into groups:

  - Fish oil supplements containing fatty acids in ethyl ester form, the total EPA and DHA concentration is about $50 - 70\%$.

  - Fish oil supplements containing fatty acids in triglyceride form, the total EPA and DHA concentration is more than 50%.

  - Fish oil supplements containing omega 3, 6, and 9 fatty acids in triglyceride form, the total EPA and DHA concentration is less than 20%.

  - Fish oil supplements containing fatty acids in triglyceride form, the total EPA and DHA concentration is about 30%.

  PCA can be used to screen these products and to identify the products that may be made by the same manufacturers with the same quality, but sold with different prices.

- A fish oil spectral library was created for rapid searching and product comparison.

- Standard addition method using bands at 3012 cm-1 may be used for rapid quantitative analysis of total EPA and DHA in fish oil supplements.

- 2D-IR correlation spectroscopy can be used to study the temperature-dependent spectral variations of polyunsaturated omega-3 fatty acid esters.

Chapter 3 References

1. W.S Harris, *American Journal of Clinical Nutrition* (The American Society for Nutrition), 65 (5 Supplement): 1645S–1654S (1997).

2. H.M Roche, M.J. Gibney, *European Journal of Clinical Nutrition,* **50** (9): 617–624 (1996).

3. T.A.B. Sanders, F.R Oakley, G.J. Miller, K.A. Mitropoulos, D Crook, and M.F. Oliver, *Arteriosclerosis, Thrombosis, and Vascular Biology,* **17** (12): 3449–3460 (1997).

4. M.H. Davidson, E.A. Stein, H.E. Bays, K.C. Maki, R.T. Doyle, etl. *Clinical Therapeutic,* 29 (7): 1354–1367(2007).

5. H.C. Bucher, P. Hengstler, C. Schindler, G. Meier, *The American Journal of Medicine,* **112** (4): 298–304(2002).

6. M.L. Burr, P.M. Sweetham, A.M. Fehily, *European Heart Journal* , **15** (8): 1152–1153 (1994).

7. W.C. Willett, M.J Stampfer, G.A.Colditz, F.E. Speizer, B.A. Rosner, C.H. Hennekens, *The Lancet* , 341 (8845): 581–585 (1993).

8. N.J. Stone, *Circulation* (American Heart Association), **94**: 2337–2340 (1996).

9. K.P. Su, S.Y. Huang, C.C. Chiub, W.W. Shenc, *European Neuropsychopharmacology* 13 (4): 267–271 (2003).

10. K. Naliwaiko, R.L. Araújo, R.V. da Fonseca, J.C. Castilho, R. Andreatini, etl. *Nutritional Neuroscience* , **7** (2): 91–99(2004).

11. P.R. Fortin, R.A. Lew, M.H. Liang, etl. *Journal of Clinical Epidemiology* , **48** (11): 1379–1390 (1995).

12. J.M. Kremer, J. Bigauoette, A.V. Michalek, etl. *The Lancet* (Elsevier), **1** (8422): 184–187 (1985).

13. Ref. www.equazen.com.

14. L.D. Lawson, B.G. Hughes, *Biochem Biophys Res Commun.* 156(2), 960-3 (1988).

15. B. Beckermann, M. Beneke, I. Seitz, *Arzneimittel-Forschung,* 40 (6): 700–704 (1990).

16. K.E. Krokan, K.S. Bjerve, E. Mork, *Biochim Biophys Acta.* 1168(1), 59-67 (1993).

17. A. Nordoy, L. Barstad, W.E. Connor, L. Hatcher, *Am J Clin Nutr.* 53(5), 1185-90 (1991).

18. Van de Voort F.R., A.A. Ismail, and J. Sedman., *Ibid.*, 72, 873-880 (1995).

19. Fatty Acid Composition by GLC: Marine Oils, in *Official Methods and Recommended Practices of the American Oil Chemists' Society*, 4th edn., AOCS Press, 1993 (reapproved 1997), Official Method Ce 16-89.

20. T. Takagi, M. Kaneniwa, and Y. Itabashi, *Lipids 21*:430 (1986).

21. R.G. Ackman, Fatty Acids, in *Marine Biogenic Lipids, Fats and Oils* (edited by R.G. Ackman), CRC Press Inc., Boca Raton, Vol. 1, pp. 103–138 (1989).

22. T. Kajishima, S. Aoki, Y. Nishimoto, E. Hasegawa, E. Moriyoshi, and H. Nagayama, *J. Jpn. Oil. Chem. Soc.45*:335 (1996).

23. I. Medina, S. Aubourg, J.M. Gallardo, and R. Perez-Martin, *Int. J. Food Sci.Technol. 27*:597 (1992).

24. A.A. Ismail, F.R. van de Voort, G. Emo and J. Sedman, *J. Am.Oil Chem. Soc.*, 70:335 (1993).

25. M.M. Mossoba, J.K.G. Kramer, J. Fritsche, M.P. Yurawecz, K.D. Eulitz, Y. Ku, and J.I. Rader, *J. Am.Oil Chem. Soc.*, 78:631- 634 (2001).

26. M.M. Mossoba, M..P. Yurawecz, and R.E. McDonald, *J. Am. Oil Chem. Soc., 73*:1003–1009 (1996).

27. M. Safar, D. Bertrand, P. Robert, M.F Devaux and C. Genot, *J. Am.Oil Chem. Soc.*, 71:371-377 (1994).

28. A. Al-Alawi, F.R. van de Voort, and J. Sedman, *J. Am. Oil Chem. Soc., 81*:441-446 (2004).

29. Y.W. Lai, E.K. Kemsley, and R.H. Wilson, *J. Agric. Food Chem.* 42:1154-1159 (1994)

30. A. Flatten, E.A. Bryhni, A. Kokler, B. Egelandsdal, and T. Isakaaon, *Meat Science*, 69: 433-440 (2005).

31. S. Yoshida and H. Yoshida, *Biopolymers (Biospectroscopy),* 70: 604-613 (2003).

32. H. Sadeghi-jorabchi, R.H. Wilson, P.S. Belton, et al., *Spectrochim. Acta,* Part A, 47:1449 (1991).

33. M. Meurens, V. Baeten, S.H. Yan, E. Mignolet, and Y. Larondelle, *J. Agric. Food Chem.* 53, 5831 (2005).

34. V. Baeten, P. Hourant, M.T. Morales, R.Aparicio, *J. Agric. Food Chem.* 46, 2638 (1998).

35. J.R. Beattie, S.E.J. Bell, C. Borgaad, A.M. Fearon, B.W. Moss, *Lipid*, 39, 897 (2004).

36. N.K. Afseth, J.P. Wold, and V.H. Segtnan, *Analytica Chim. Acta*, 572, 85-92 (2006).

37. M. D. Guillén, A. Ruiz, *J. Sci. Food Agric.* 83**,** 338-346 (2003).

38. L. Broadhurst, W.F. Schmidit, M.A. Crawford, Y. Wang, and R. Li, *J. Agric. Food Chem. 52,* 4250-4255 (2004).

39. M. Aursand, I.B. Standal, and D.E. Axelson, *J. Agric. Food Chem.* 55, 38-47 (2007).

40. M. D. Guillén and N. Cabo, *J. Agric. Food Chem.* 46, 1788-1793 (1998).

41. J.R. Beattie, S.E.J. Bell, C. and B.W. Moss, *Lipid*, 39, 407-419 (2004).

42. I. Noda, *J. Am. Chem. Soc.*, 111, 8116-8118 (1989).

43. I. Noda, A.E. Dowrey, C. Marcott, and G.M. Story, *Applied Spectroscopy*, 54, 236A-248A (2000).

44. T. Igarashi, M. Aursand, Y. Hirata et al., *J. Am. Oil Chem. Soc.,* 77:737-747 (2000).

Chapter 4:   Summary

The research results outlined in the project I demonstrated that the unique IR method developed for simultaneous quantitation of dimethicone and cyclomethicone using two simultaneous absorbance – concentration equations at two fixed wavenumbers of 1258.50 cm^{-1} and 800.00 cm^{-1} (with baseline correction at 1325.00 cm^{-1} and 950.00 cm^{-1}, respectively) is applicable. The method has been successfully validated for the analysis of dimethicone and cyclomethicone in consumer products such as skin protective ointments. The method was shown to be linear, accurate, precise, and specific.

The research results outlined in the project II indicated that a fast qualitative ATR-FTIR method can be used to distinguish between the ethyl ester and triglyceride forms of fatty acids using the carbonyl band position. Principal Component Analysis (PCA) was used to classify fish oil supplements successfully by grouping the products into four groups based on the fatty acid chemical form and EPA and DHA concentrations. PCA was also demonstrated as a powerful tool to screen fish oil supplements that may be made by the same manufacturers with the same quality, but sold with different prices. A fish oil FTIR spectral library was also created for rapid searching and product comparison. In addition, an ATR-FTIR standard addition method was evaluated and shown to be suitable for the quantitative analysis of EPA and DHA esters in an in-house blended fish oil sample. However, the detail formulation information should be evaluated to determine whether this approach is applicable for other products. The temperature dependent spectral characteristics of EPA esters were successfully studied using two-dimensional FTIR correlation spectroscopy.

Curriculum Vitae

Jun Zhang

Education

1983 - 1987	Lanzhou University, Lanzhou, P.R. China B.S. in Chemistry, July 1987
1987 - 1990	Lanzhou University, Lanzhou, P.R. China M.S. in Polymer Chemistry, June 1990
1995 - 1997	Rutgers, The State University of New Jersey, New Brunswick, New Jersey M.S. in Chemistry, January 1997
2004 - 2009	Rutgers, The State University of New Jersey, New Brunswick, New Jersey Ph.D. in Analytical Chemistry, May 2009

Principle Occupation

1998 - Present	Staff Scientist Analytical Development**,** R&D Operations, J&J Group of Consumer Companies, Skillman, New Jersey
1997	Chemist Analytical R&D Department, Par Pharmaceutical Inc., Spring Valley, New York
1995 - 1996	Teaching Assistant and Research Assistant Chemistry and Psychology Department, Rutgers University, New Brunswick, New Jersey
1990 - 1994	Associate Research Scientist Lanzhou Chemistry Institute, Chinese Academy of Science, Lanzhou, P.R. China

Publication

Fang Ma, Jun Zhang and Chyan E. Lau., Determination of cocaine and its metabolites in serum microsamples by high- performance liquid chromatography and its application to pharmacokinetics in rats., *J. Chromatography B*, Vol. 693, No. 2(307-312), 1997.